공학석사 학위논문

Design of Slender Wall and Wall with Pilotis in Capacity Design of High-rise Residential Buildings

고층주거용건물의 성능설계 과정에서
세장한 벽체와 필로티가 있는 벽체의 설계

2017년 2월

서울대학교 대학원

건축학과

김 성 현

Design of Slender Wall and Wall with Pilotis in Capacity Design of High-rise Residential Buildings

지도 교수 박 홍 근

이 논문을 공학석사 학위논문으로 제출함

2017년 2월

서울대학교 대학원

건축학과

김 성 현

김성현의 공학석사 학위논문을 인준함

2017 년 2 월

위 원 장 _____ (인)

부위원장 _____ (인)

위 원 _____ (인)

Abstract

Design of Slender Wall and Wall with Pilotis in Capacity Design of High-rise Residential Buildings

Kim, Sung Hyun
Department of Architecture and Architectural Engineering
College of Engineering
Seoul National University

As the risk of earthquake in Korea increases, interest in seismic design increases and application of related design standard is strengthened. It is difficult to predict seismic load accurately by seismic design method based on conventional elastic analysis. Therefore, capacity design method can be used for seismic design of high-rise residential building to evaluate seismic load more accurately and obtain optimal design result. However, in order to apply the capacity design method in design of Korean high-rise residential buildings, some precautions due to characteristics of structural system should be considered. Therefore, in this study, among the considerations for capacity design of high-rise residential building, the shear demand distribution for the slender shear wall system and the design of transfer zone in the pilotis-wall system were studied.

Abstract

First, the problem that occurred in the capacity design of slender shear wall system was that shear demand of actual case is considerably amplified compared to that of design case. If the amplified shear demand is not considered in design, structural members can be under-designed, resulting structural unsafety of the building. Therefore, amplification effect of shear demand was investigated and some design factors reflecting it in the capacity design process were proposed.

By using Perform 3D, a nonlinear analysis program, nonlinear analysis modeling for each parameter were established and nonlinear dynamic analysis was carried out. Based on the analysis results, the factors affecting the shear demand amplification effect were analyzed and the base shear amplification factor for predicting the nonlinear shear demand was proposed. The proposed base shear amplification factor was determined by base over-strength factor and it can predict the nonlinear shear demand within the error range of 20%. Also, the story shear distribution model for nonlinear shear demand was suggested on the basis of average shear distribution of analysis results. The proposed story shear distribution model can predict the story shear demand more economically than conventional model which is suggested in Eurocode 8. The proposed base shear amplification factor and story shear distribution model can predict nonlinear shear demand of the wall more reasonably and secure the structural safety by preventing under-design.

Next, the design consideration of the capacity design of the pilotis-wall system was an economical design method for the transfer zone in which the pilotis and wall are connected. A system in which the transfer girder was eliminated was proposed and a reasonable capacity design method for this system is proposed. To evaluate the structural performance of proposed system and verify the design method, cyclic loading tests and compression test were carried out.

Based on principle of capacity design, the proposed pilotis-wall system without transfer girder was designed to prevent premature brittle failure in the transfer zone and pilotis and to induce ductile failure in the upper wall. Test results show that, in all the specimens, the premature brittle failure of the transfer zone and pilotis did not occurred, but in the upper wall, re-bars were yielded in the tensile side and concrete crushing occurred in the compressive side. The internal and external damage of the transfer zone and the pilotis were relatively limited. Through these results, it was confirmed that the preliminary design of the pilotis-wall system can be improved more economically without applying the special earthquake load and the presence of transfer girder.

Keywords : Capacity design, slender shear wall system, pilotis-wall system

Student Number : 2015-21099

Contents

List of Tables

List of Figures

List of Figures

List of Symbols

$A_{envelop}$: Lower area of the envelop curve

$A_{e\text{-}p}$: Lower area of the elasto-plastic curve

b : Breadth of member

Δ_y : Yield displacement

Δ_u : Maximum displacement

δ_i : Drift ratio of i th load step

δ_u : Yield drift ratio

δ_y : Maximum drift ratio

$f_{c'}$: Concrete strength

γ_{Rd} : Over-strength factor due to steel strain hardening

h : Thikcness of member

H : Height of member

h_n : Net height of the building

h_i, h_k : Height from the base to story level i or x

I_E : Occupancy importance factor

k_y : Yield stiffness

L : Length of member

M_{Ed} : Design bending moment at wall base

$M_{u,avg}$: Base average moment demand calculated by average response spectrum

$M_{n,0}$: Pure moment capacity with no axial force

$M_{n,x}$: Base moment capacity with the axial force ratio x %,

M_{Rd} : Design moment capacity at wall base

List of Symbols

n	:	Total number of stories
Ω	:	Base over-strength factor
Ω_0	:	Pure base over-strength factor
P_g	:	Vertical load acting on critical section, related to compression load
P_i , P_{i-1}	:	Lateral load of i th or i-1 th load step,
P_n	:	Nominal strength of each critical section
P_u	:	Compression load
P_v	:	Vertical load acting on critical section, related to lateral load
R	:	Response modification factor
$S_a(T)$	:	Spectral ordinate
T	:	Fundamental period of the building
T_{u1} , T_{u2}	:	Tensile force
V_a	:	Amplified shear
V_{base}	:	Base shear
V_{peak}	:	Lateral load of test result
V_u	:	Lateral load
$V_{u,avg}$	:	Base average shear demand by the average response spectrum
w_v	:	Base shear amplification factor

Chapter 1. Introduction

1.1 General

September 12, 2016, an earthquake of magnitude 5.8 occurred at Gyeongju. Due to the earthquake, although casualties did not happen, in some buildings walls and floors were cracked and windows were broken, which is shown in the Fig. 1-1.

Especially, it was the largest earthquake since the earthquake measuring began. Moreover, the aftershocks lasted for two month after the earthquake and total number of the aftershocks exceeded five hundreds. Recently, as shown in Fig. 1-2, the number of earthquake occurrence has been increased. This means that Korea is not anymore an earthquake safety zone and the safety measures of building for earthquake are required. In particular, if residential high-rise buildings which account for many of the buildings in densely populated metropolitan areas are damaged by the large earthquake, massive damage may occur.

Fig. 1-1 Damages of the earthquake in Gyengju

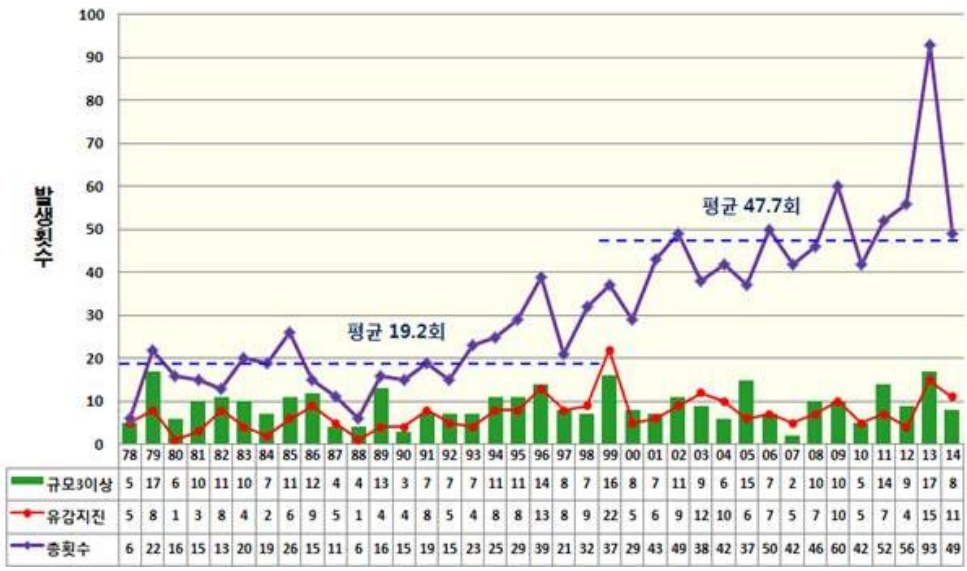

	78	79	80	81	82	83	84	85	86	87	88	89	90	91	92	93	94	95	96	97	98	99	00	01	02	03	04	05	06	07	08	09	10	11	12	13	14
규모3이상	5	17	6	10	11	10	7	11	12	4	4	13	3	7	7	7	11	11	14	8	7	16	8	7	11	9	6	15	7	2	10	10	5	14	9	17	8
유감지진	5	8	1	3	8	4	2	6	9	5	1	4	4	8	5	4	8	8	13	8	9	22	5	6	9	12	10	6	7	5	7	10	5	7	4	15	11
총횟수	6	22	16	15	13	20	19	26	15	11	6	16	15	19	15	23	25	29	39	21	32	37	29	43	49	38	42	37	50	42	46	60	42	52	56	93	49

Fig. 1-2 Earthquake records in Korea

In the conventional seismic design methods, the seismic loads were evaluated by the equivalent static analysis or response spectrum analysis on the assumption of elastic design. However, when using these elastic analysis methods the reliability of the design results could be decreased due to the limitation that it couldn't consider a characteristic of the buildings. In order to overcome the limitation and enable reliable design, analysis methods to evaluate the seismic loads accurately have been continuously studied.

Therefore, a capacity design method can be used for the design of high-rise residential buildings as a method to evaluate seismic load more accurately. In the capacity design method, the seismic load acting on the building is evaluated based on the actual capacity of the member, so it is possible to evaluate seismic load demand more accurately than the conventional elastic analysis method. Also, in this method, failure mode of structure is assumed by a designer and structural members are optimally designed so that the behavior of the entire building is

governed by the intended failure mode. Therefore, the capacity design method allows for economical design while at the same time having sufficient resistance to earthquake.

For high-rise residential buildings, the most important business goal is to secure economic efficiency. Therefore, the capacity design method which can evaluate the seismic load more accurately and obtain the optimum design result is applicable for these buildings. However, some precautions should be considered to apply this method to Korean high-rise residential buildings due to following reasons.

First, in the case of Korean high-rise residential buildings, a slender shear wall system is used as a major lateral load resistance system. In the case of the slender shear wall, by nonlinear dynamic characteristics, it has been reported that nonlinear shear demand is tend to be considerably amplified. Reason of this phenomenon is known to be caused by the effect of higher-order mode after yielding. As a result of shear amplification effect, in the case of capacity design of slender shear wall, it is possible that larger shear demand than predicted shear demand can be applied to the building. Since the shear demand is an important design parameter in the wall design, if the shear amplification effect is not considered, it is difficult to ensure the structural safety due to under-design. To solve this problem, additional design factors are needed to accurately consider the nonlinear shear demand of the wall and its vertical distribution.

Next, recently, in the case of Korean high-rise residential buildings, pilotis-wall system in which pilotis are placed in lower story of the buildings is frequently used due to architectural requirement. In this system, a deep transfer girder is placed to transfer load between pilotis and wall. Since the transfer girder has many

disadvantages, attempts have been made to use this system without transfer girder. However, in this system without transfer girder, due to the difference in stiffness between pilotis and wall, transfer zone is likely to be structurally vulnerable and entire structural behavior is governed by capacity of transfer zone. Therefore, in the capacity design of pilotis-wall system, especially in the case of the system without transfer girder, it is required to sufficiently consider the structural safety of the transfer zone. As a study for this purpose, it is necessary to propose a capacity design method for this part and to verify the design method through structural test.

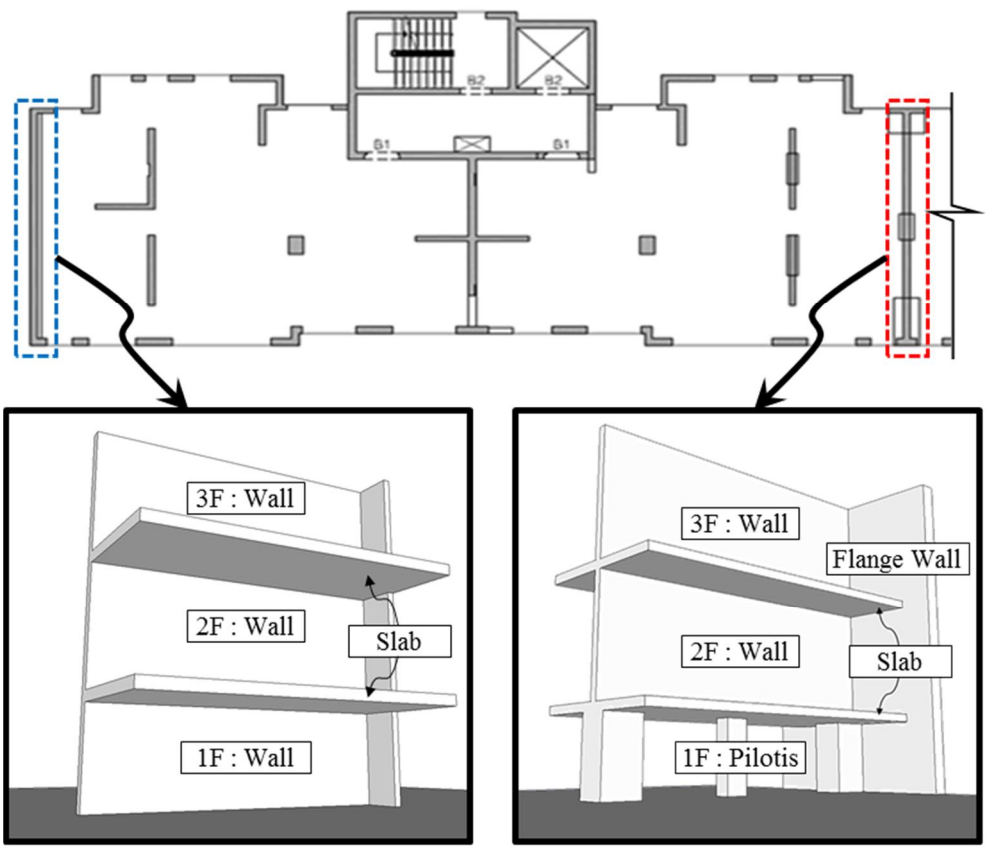

(a) Shear wall system (a) Piloti-wall system

Fig. 1-3 Structural plan of high-rise residential building

In addition to the design considerations for the transfer zone, it is require to consider the shear demand distribution due to placement of pilotis. Furthermore, as shown in Fig. 1-3, these two types of systems used in high-rise residential buildings are not used independently of each other in the entire structural system, but rather they are used in combination at the same time. Therefore, it is require to consider the change in the shear demand distribution of the slender wall and the wall with pilotis by interaction of two systems.

Fig. 1-4 shows summary of required studies for capacity design of high-rise residential buildings. Among these studies related with capacity design of high-rise residential buildings, in this study, a study for nonlinear shear demand distribution of slender shear wall system and a study for capacity design of transfer zone in the pilotis-wall system were preceded. As a study for slender shear wall system, amplification effect of nonlinear shear demand was analyzed for each parameters. Moreover, base shear amplification factor and story shear distribution model were proposed. As a study for pilotis-wall system without transfer girder, capacity design method for this system was proposed and in order to evaluate this system and verify the proposed method, cyclic loading tests and compression test were carried out.

Other studies for the capacity design of high-rise residential buildings, a study for nonlinear shear demand distribution of the wall with pilotis and a study for change of shear demand distribution due to interaction of two systems, can be carried out by a follow-up studies.

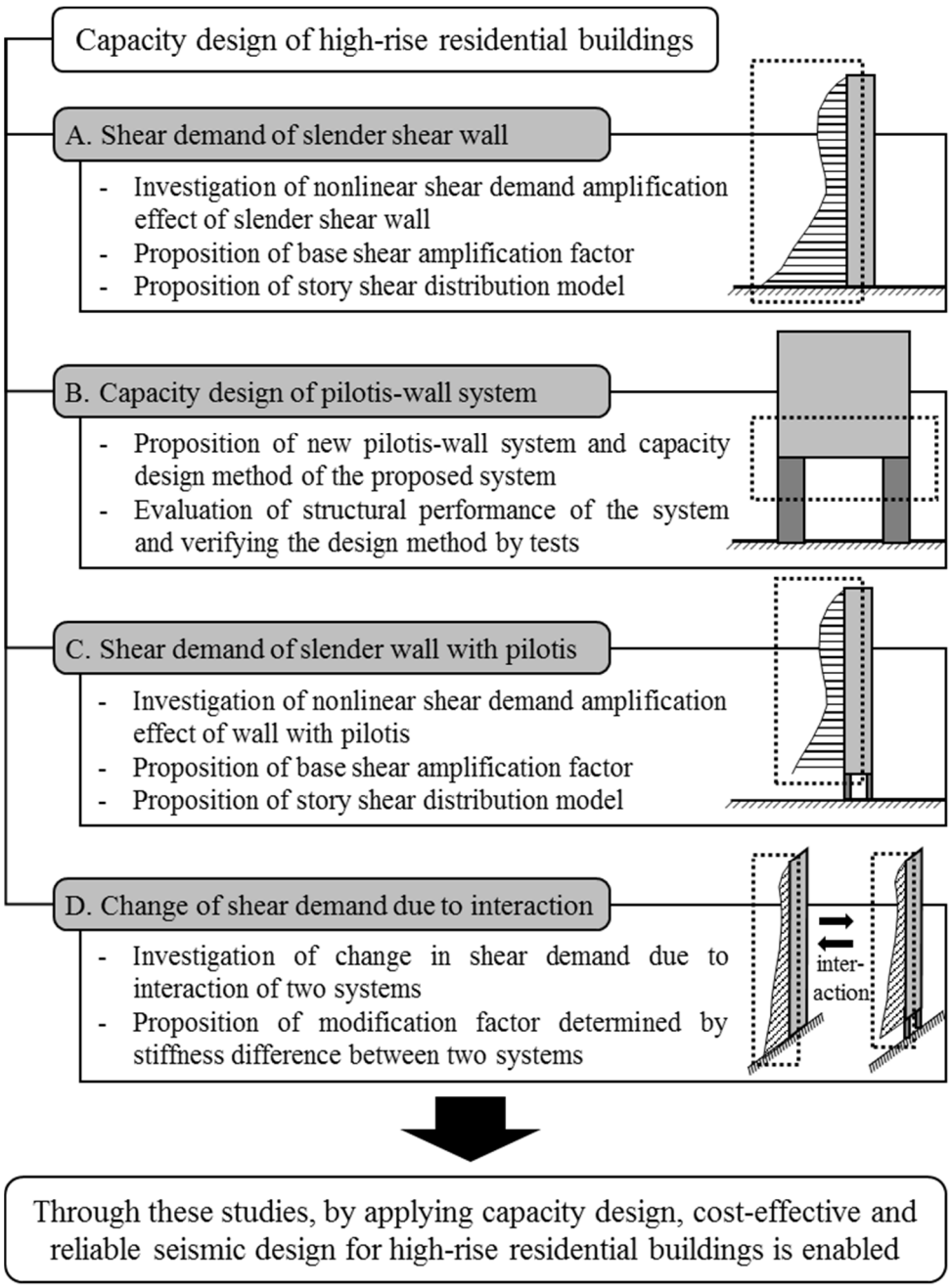

Fig. 1-4 Considerations for capacity design of hig-rise residential building

1.2 Scope and Objectives

The purpose of this study is to propose and verify considerations for capacity design of slender shear wall and wall with pilotis in the Korean high-rise residential buildings. Among the required studies already mentioned, as preceded studies, nonlinear shear demand of slender shear wall and capacity design of pilotis-wall system without transfer girder were carried out.

First, as a study of shear demand of slender shear wall system, the design factors were proposed to consider shear amplification effect in the capacity design. The causes of shear amplification effect occurring in nonlinear dynamic analysis in which the actual earthquake load is used for analysis were studied. By analyzing the analysis results for the parameters, the base shear amplification factor was proposed. Also, based on the vertical distribution of nonlinear shear demand, the story shear distribution model was proposed.

Next, as a study of capacity design of the pilotis-wall system without transfer girder, in order to design this system more economically, the new detail in which the wall was connected directly with the pilotis and the transfer girder was eliminated was proposed. Also, based on the capacity design concept, the method to design the system to prevent premature failure of pilotis and transfer zone was studied. In order to evaluate structural behavior of the system and verify the design method, the cyclic loading tests and the compression test were conducted.

1.3 Outline of the master's thesis

In the Chapter 2, review of capacity design method was conducted. Also, design codes and previous researches for shear amplification and story shear distribution model were investigated. Lastly, previous researches which had studied a method for designing pilotis-wall system economically were reviewed.

In the chapter 3, the shear amplification effect by the nonlinear dynamic analysis was studied. The wall in the dual system was assumed to be the target of the nonlinear dynamic analysis. Total five parameters were determined to evaluate the effect on the shear amplification. Total 173 modeling were analyzed. From the analysis results, the base shear amplification factor and the story shear distribution model were proposed.

In the chapter 4, a pilotis-wall system in which the transfer girder was eliminated was proposed and a method to design the system was studied. Total four scale reduction specimens, designed by the proposed method, were tested. Among the specimens, three were tested under the cyclic loading and the other one was tested under the uniaxial compression load. By analyzing the test results, the structural behavior of the proposed system was evaluated. Also, a validity of the proposed method was verified.

Finally, summary and conclusions presented in the chapter 5.

Chapter 2. Literature Review

2.1 Capacity design

Capacity design, first introduced in New Zealand, is a design method based on actual cpacity of members. In this method, a building is designed to provide ductile behavior for large earhquakes. Since it can accurately predict seismic loads and economically design buildings, it has been widely used in Europe and other countries.

Fig. 2-1 shows basic concept of the capacity design. Operating principle of the entire structural system based on the capacity design can be understood by a chain system. In the chain system, each link represents a member of the structural system. There are two possible failure mechanisms, brittle failure mechanism and ductile failure mechanism, which can occur when pulling both ends of the chain. If the brittle link is designed to have greater strength than the ductile link, it can be in elastic state during the ductile link yielding, which means that it can prevent brittle failure at brittle link and induce ductile failure at ductile link, which is more safe mechanism.

By the same principle, in the capacity design of a building, members are designed so that behavior of the entire building can be controlled by yielding of members having great ductility. Fig. 2-2 shows two types of failure mechanism of building. If behavior of building is controlled by column sway mechanism for earthquakes, strength of the building can be drastically reduced, leading to collapse. Thus, to prevent this mechanism, plastic hinges are induced in beams by securing

sufficient strength of columns and joints. For this, load demand is calculated based on flexural strength of beams, and other members and joints are designed to resist this load.

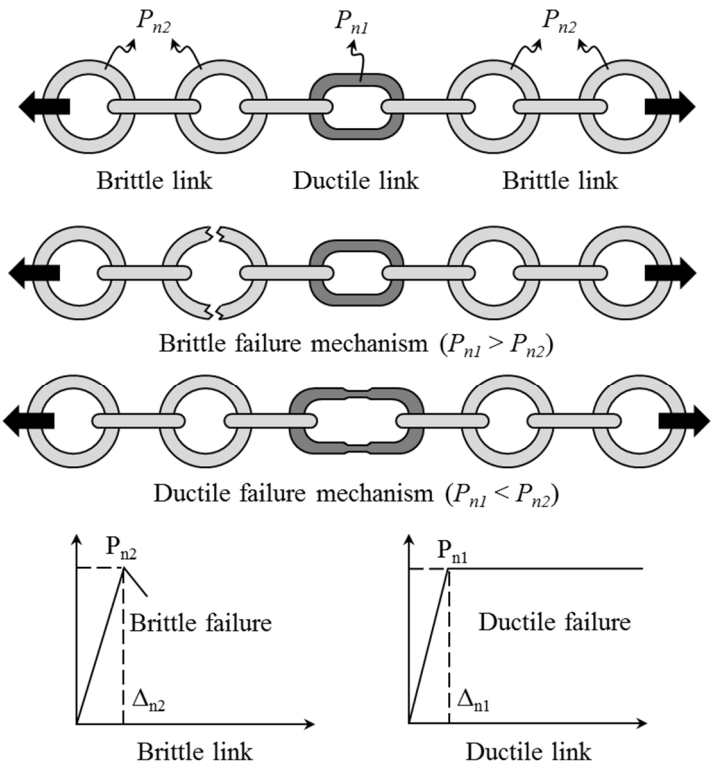

Fig. 2-1 Basic concept of capacity design

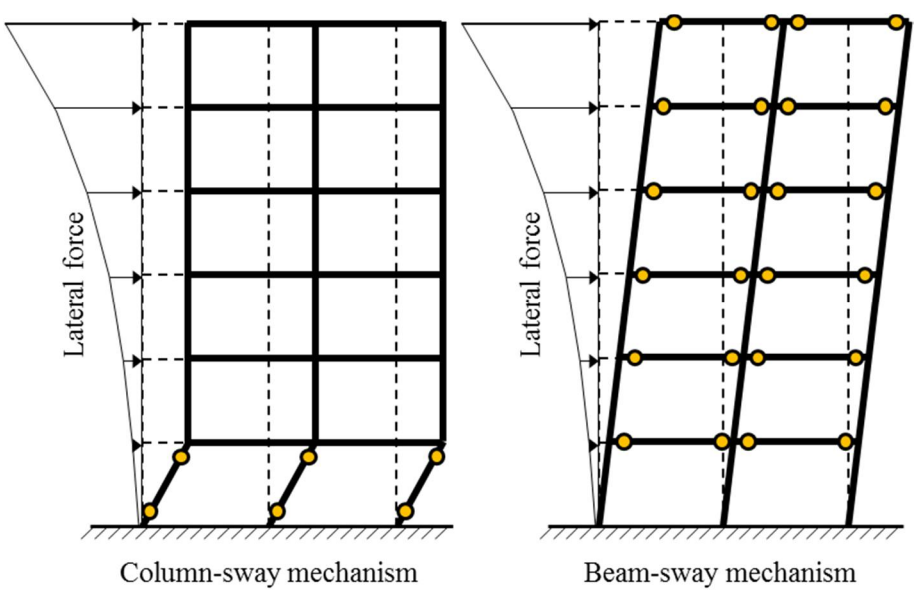

Fig. 2-2 Failure mechanisms of building

2.2 Shear amplification and the story shear distribution

2.2.1 Blakeley et al

Shear amplification effect was observed by New Zealand consulting engineers, which led to the 1975 pioneering paper by Blakeley et al.

In general, the cause of the shear amplification was known to be due to the higher mode. Fig. 2-3 shows principle of base shear amplification by higher mode. Despite yielding of wall, by the pined base mode, base shear could be increased continuously.

Based on this observation, in New Zealand seismic code and in European model code, base shear amplification factor was provided.

In these codes, the amplified shear V_a is calculated by following equations.

$$V_a = w_v V_{base} \tag{2-1}$$

In the New Zealand Code (NZS 1982, 1995, 2006)

$$w_v = \begin{cases} 0.9 + n/10 & n \leq 6 \\ 1.3 + n/30 \leq 1.8 & n > 6 \end{cases} \tag{2-2}$$

And in European model code (CEB 1980, 1983, 1985)

$$w_v = \begin{cases} 0.9 + n/10 & n \leq 5 \\ 1.2 + n/25 \leq 1.8 & n > 5 \end{cases} \tag{2-3}$$

Where the V_{base} is the base shear demand, w_v is the base shear amplification factor and the n is the total number of stories of building. However, in these codes,

the factor was only governed by the number of stories and upper bound was set 1.8.

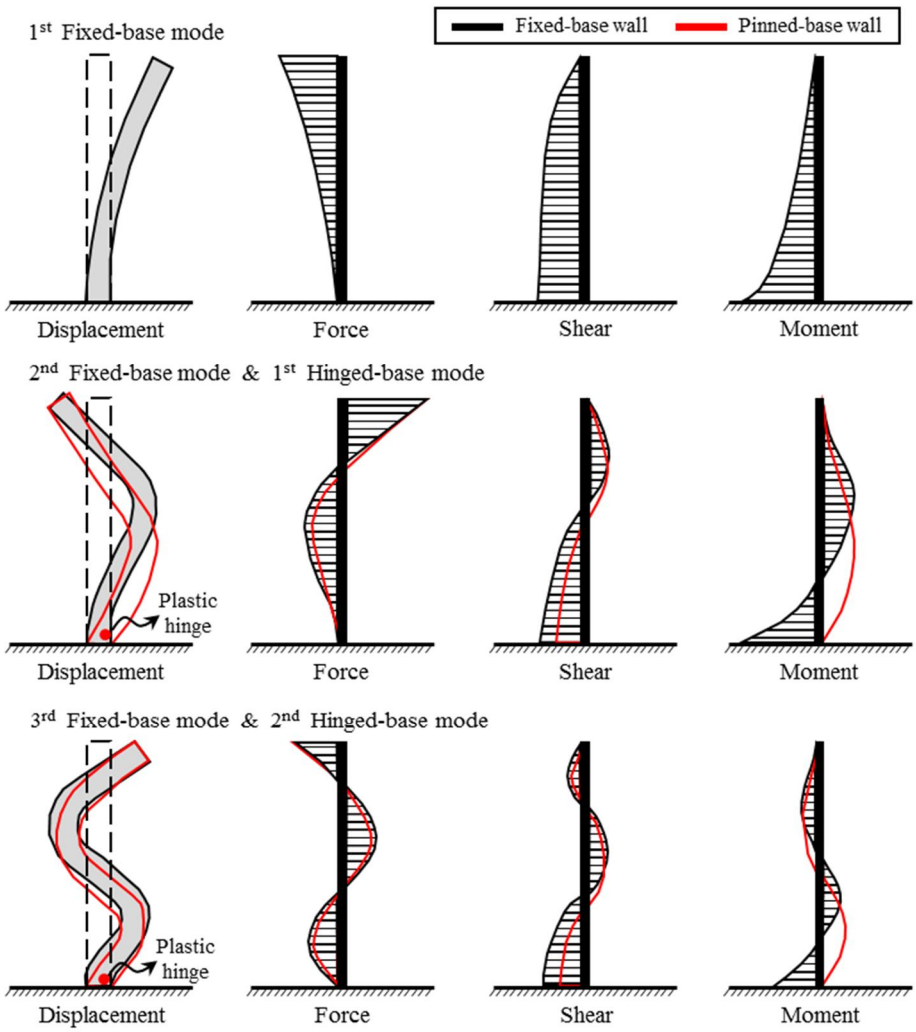

(a) Fixed base and hinged base cantilever mode shapes

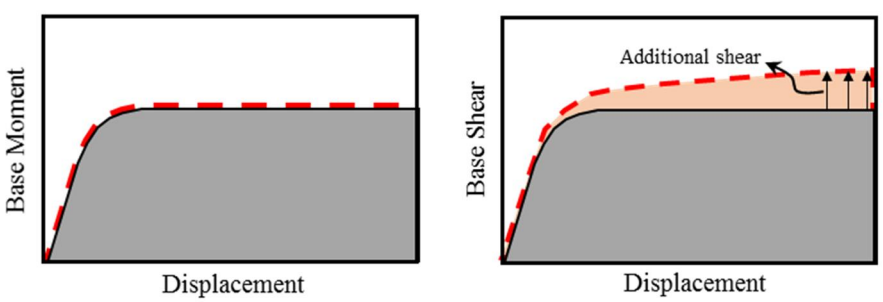

(b) Structural behavior at the base

Fig. 2-3 Principle of base shear amplification

2.2.2 Eibl and keintzel et al

Eibl and keintzel proposed base shear amplification factor by assuming that SRSS modal combination could also be applied in post-elastic range. They assumed that the 1st mode shear was limited by the moment capacity of the base wall and the higher modes respond linearly. Based on their study, following equation was provided into Eurocode 8 (CEN 1993, 2004)

$$w_v = R\sqrt{\left(\frac{\gamma_{Rd}}{R}\frac{M_{Rd}}{M_{Ed}}\right)^2 + 0.1\left(\frac{S_a(T_c)}{S_a(T)}\right)^2} \leq R \qquad (2\text{-}4)$$

Where the w_v is shear amplification factor, the R is response modification factor, the M_{Ed} is design bending moment at wall base, the M_{Rd} is design moment capacity at wall base, the γ_{Rd} is over-strength factor due to steel strain hardening, the T is fundamental period, the T_c is higher period corner of the constant acceleration plateau and the $S_a(T)$ is spectral ordinate.

This was a very useful equation because it could consider various parameters which are governing the shear amplification effect. However, when it was applied to high-rise building, this equation evaluated as too conservative.

2.2.3 Rutenberg and Nsieri

To advance the base shear demand of EC8 provisions, Rutenberg and Nsieri suggested revised equation governed by the fundamental period and the response modification factor.

$$w_v = [0.75 + 0.22\,(T + R + TR)] \qquad (2\text{-}5)$$

Where the w_v is shear amplification factor, the R is response modification factor and the T is fundamental period. Fig. 2-4 shows the comparison of EC8 provisions and proposed equation.

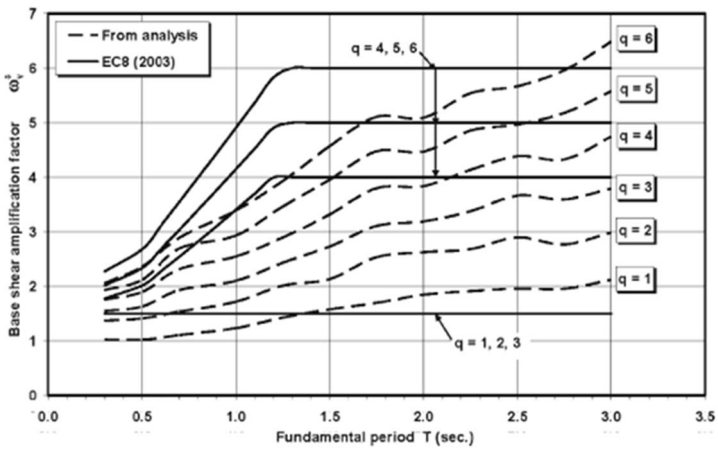

(a) Eurocode 8 provions

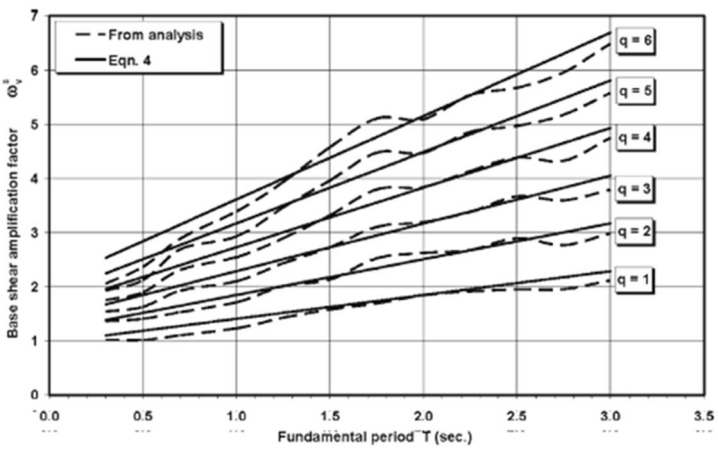

(a) Proposed equation

Fig. 2-4 Comparison of EC8 provisions and proposed equation

Also, they suggested the story shear distribution model by analyzing average dynamic story shear demand. Fig. 2-5 shows the story shear distribution normalized by the base shear. Fig. 2-6 shows the proposed story shear distribution

model.

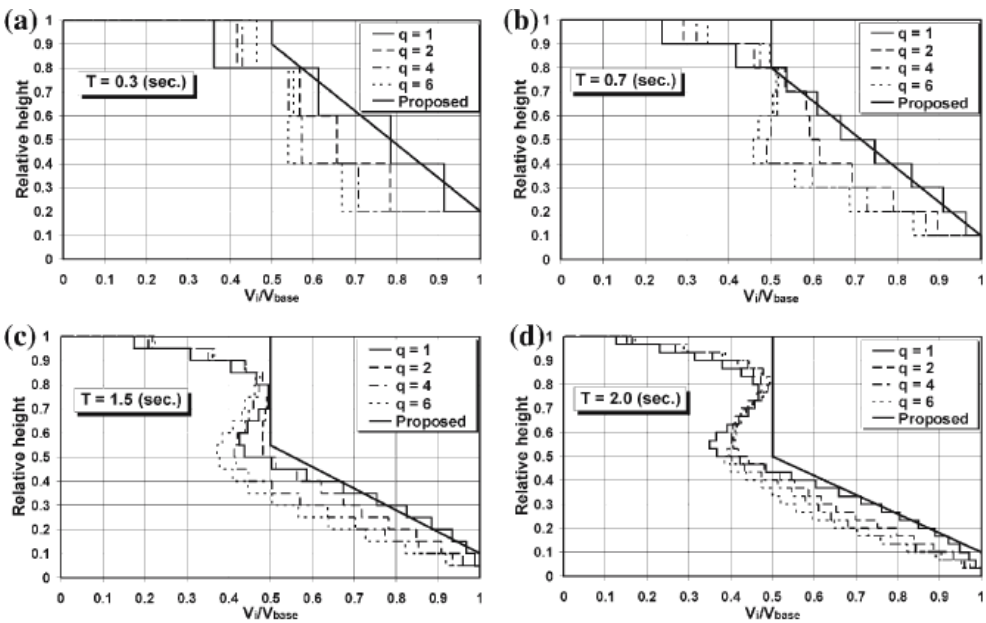

Fig. 2-5 Story shear distribution normalized by the base shear

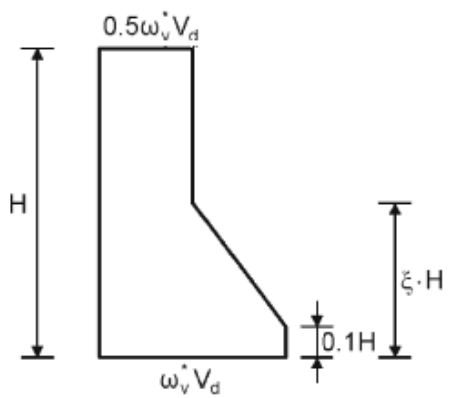

Fig. 2-6 Story shear distribution model.

In this model, ξ was calculated by following equation.

$$\xi = 1.0 - 0.3T > 0.5 \quad (2\text{-}6)$$

where the T is fundamental period.

2.3 Pilotis-wall system

There were some studies which tried to improve the pilotis-wall system by using arch system and hunch element.

2.3.1 Jung, Yoon, Hong and Kim

To improve inefficiency of the pilotis-wall system that unnecessary weight exists in the middle of the transfer girder, Jung, Yoon, Hong and Kim suggested the arch system. In their study, the behavior of the wall in the transfer zone was investigated. Fig. 2-7 shows the arch behavior of the wall in the transfer zone. The maximum vertical compressive stress was generated in the area where the wall and the transfer girder are joining. Also, the maximum horizontal tensile stress was generated in the middle of the transfer girder. When openings existed in the wall, both primary arch and secondary arch were generated.

Fig. 2-8 shows the analysis modeling in their study. The span length and the location of the openings were considered as analysis parameters. On the basis of the principal stress distribution, the height of the arch was determined to 60% of the span length.

Fig. 2-9 shows the comparison of the stress distribution of the original system and the arch system. In the case of the original system, the stress was concentrated on the bottom of the wall face. In the case of the arch system, the stress was concentrated on the bottom support of the arch. In the case of the original system with the opening, the stress was concentrated on the edge of the wall near the

opening. However, in the case of the arch system, the stress was concentrated on the edge of the wall far from the opening.

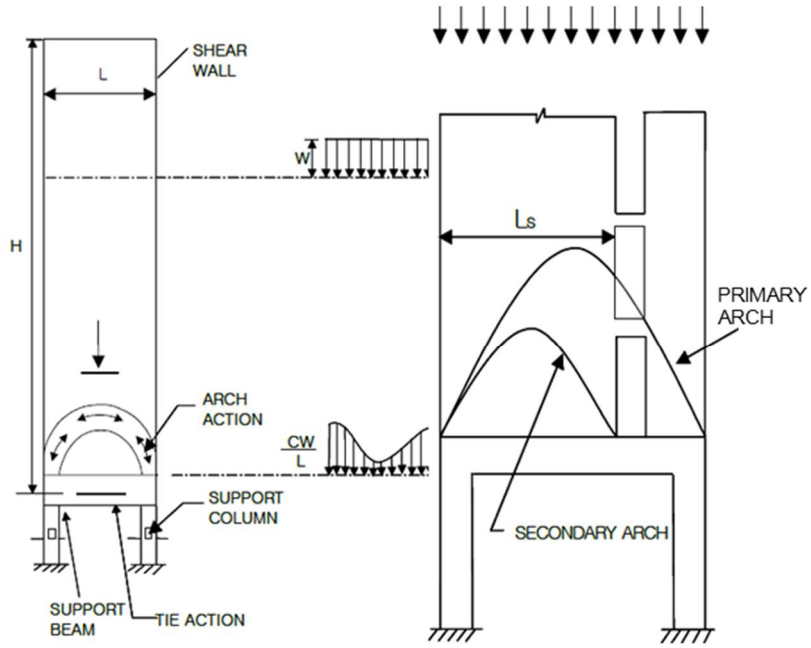

Fig. 2-7 Arch behavior of pilotis-wall system

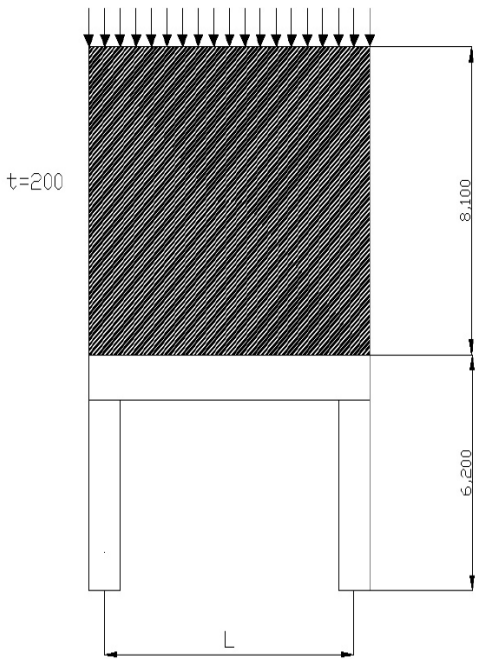

Fig. 2-8 Dimensions of Analysis modeling

Fig. 2-10 shows the comparison of the shear stress generated at the transfer girder. In the case of arch system, the shear stress was reduced, which meant that the volume of transfer girder could also be reduced.

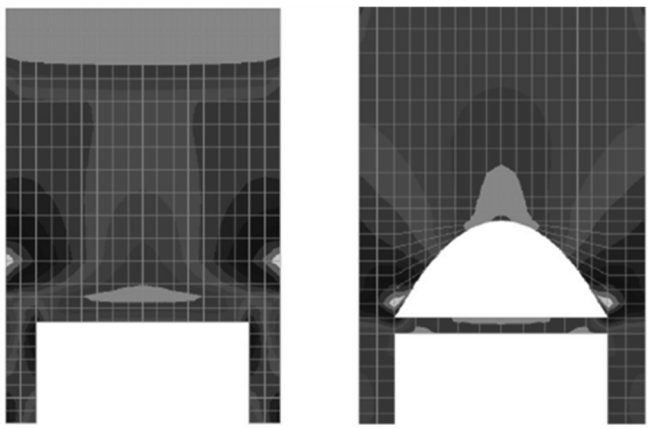

(a) Wall W/O opening

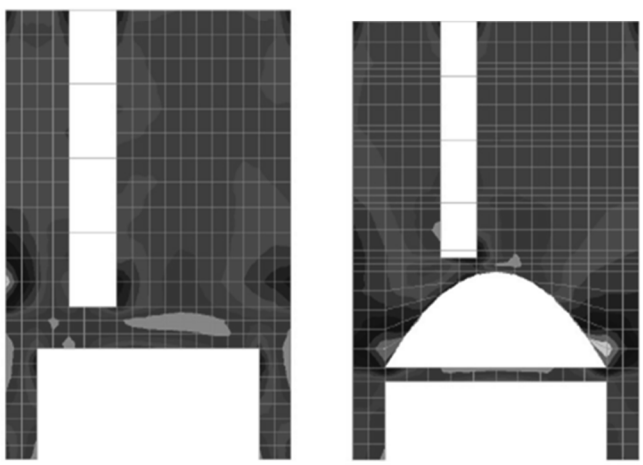

(b) Wall with opening

Fig. 2-9 Comparisons of stress distribution

Fig. 2-11 shows story seismic loads and moment demand of columns calculated by the equivalent static analysis. In the arch system, volume of the transfer girder was reduced so that the seismic load on the transfer zone was reduced. Moreover, in the arch system, moment demand was reduced than in the original system.

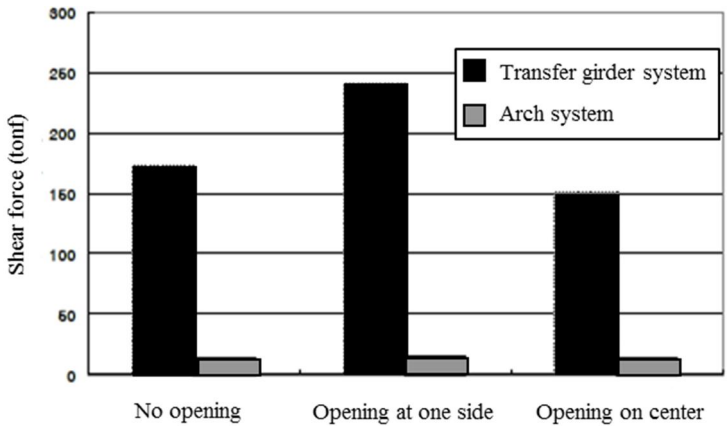

Fig. 2-10 Comparison of the shear stress

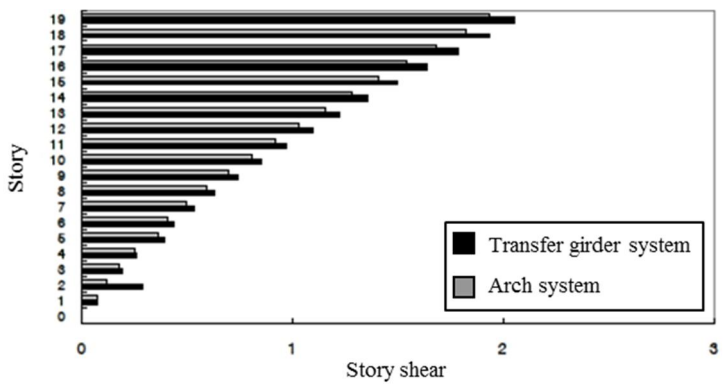

(a) Story shear

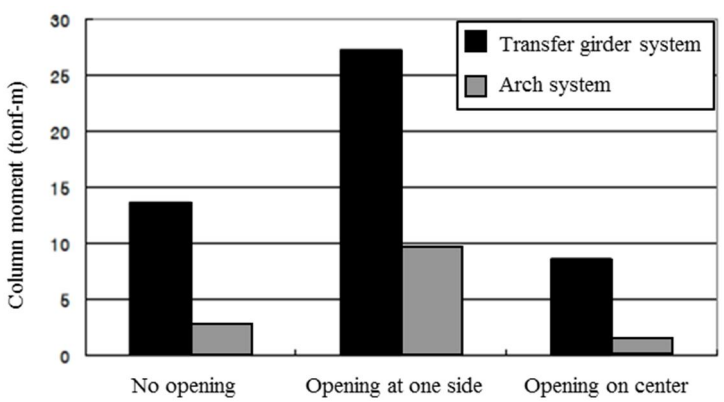

(b) Column moment

Fig. 2-11 Story seismic loads and moment demand of columns

2.3.2 Jang, Kim and Hong

To eliminate the transfer girder, Jang, Kim and Hong suggested to use the haunch element. By using simplified modeling of transfer zone, they investigated changes of arch behavior with the height of the transfer girder and the length of the supporting surface.

Fig. 2-12 shows the distribution of principal stress with the different height of the transfer girder. In the analysis modeling, height of the wall was fixed to 2,000 mm. When the height of the transfer girder was 1,200 mm, the inclination of the arch was decreased than in a height of 800 mm.

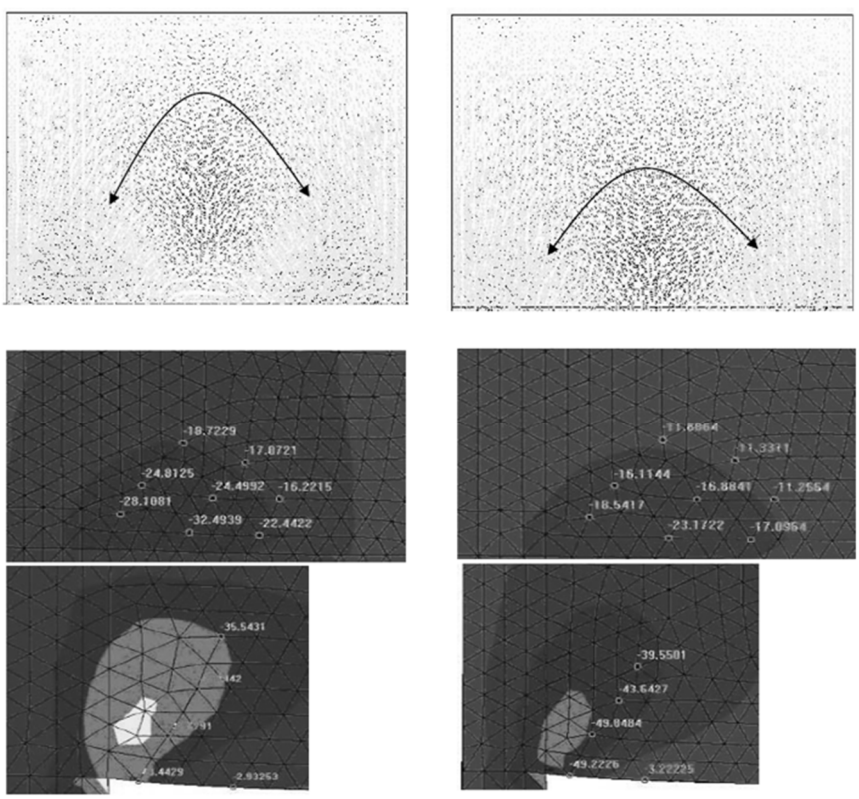

(a) Stress of 800mm T.G (b) Stress of 1200mm T.G

Fig. 2-12 Distribution of principal stress

Also, they found that the degree of stress concentration was able to be decreased when the length of the supporting surface was increased.

On the basis of these preceding analysis, optimal slope of the haunch was determined. Fig. 2-13 shows relationship between shear stress and length of the haunch. The height of the haunch was fixed to 300 mm. The shear stress was reduced as the length increased. However, after the length of the haunch became similar with height of the haunch, difference of maximum shear stress was not great. Therefore, optimal slope of the haunch was determined as 1:1 ratio that is the 45 degrees.

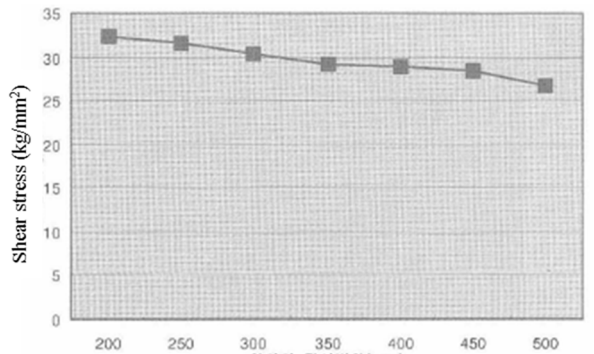

(a) Shear stress at wall

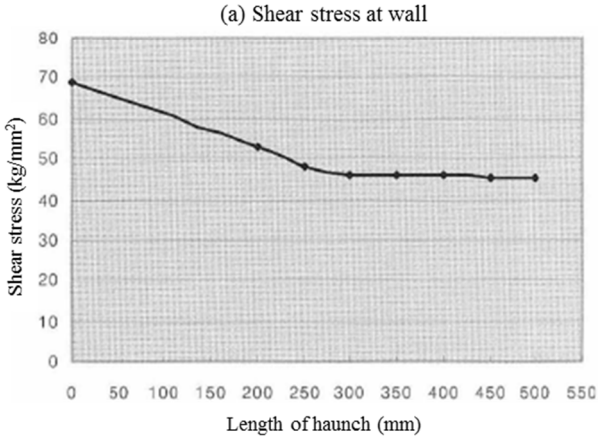

(b) Shear stress at transfer girder

Fig. 2-13 Relationship between shear stress and the length of haunch

Chapter 3. Capacity Design of Slender Shear Wall

3.1 Introduction

In the capacity design method, distribution of seismic loads is assumed by a designer and its size is determined by occurrence of plastic hinge in the wall under the assumed failure mode. By this method, it is possible to relatively accurately evaluate magnitude of seismic loads demand according to the actual capacity of members. However, in the case of shear demand distribution, by the shear

amplification effect due to characteristics of nonlinear dynamic behavior of the wall, shear demand of actual case can be considerably amplified compared with that of design case. One of the major cause of this phenomenon is that the shear demand is able to be increased by effect of higher mode despite of yielding in the wall at the base. After a plastic hinge occurs at the bottom of the wall, the shear demand can be increased continuously without increase of the bending moment at the bottom face.

If the difference between actual shear demand and design shear demand is not considered in design process, wall can be under-designed, which may lead to structural unsafety against earthquake. Therefore, in this chapter, to solve this problem, analytic study was conducted to propose design factors reflecting shear amplification effect. Analysis modeling were established for various parameters. To simulate earthquakes acting on buildings, nonlinear dynamic analysis was conducted for each modeling. The base shear from the analysis was compared to the design base shear. From these results, the base shear amplification factor was proposed. Additionally, the story shear demand distribution model was suggested. In the capacity design, they are able to be used to estimate actual shear demand.

3.2 Analysis model

3.2.1 Modeling concept

Fig. 3-1 shows the geometry and dimensions of analysis target building. In order to obtain evident tendency of analysis results, the shear demand which is applied on the wall should be maximized. Therefore, dual system was assumed as a building structural system of analysis modeling. As a result, 75% of total shear demand was distributed to the walls and the others was distributed to the columns.

Cross-sectional dimensions of the wall was determined to be 12 m x 240 mm. Story height was determined to be 2.8 m. The total height of the analysis modeling was determined by the total number of stories. Slabs were not modeled in the analysis modeling, however, to calculate the self-weight of slab, the thickness of slab was assumed to be 210 mm. The concrete strength was 21 MPa and the yield strength of re-bars was 400 MPa.

Table. 3-1 shows the assumption for the gravity load. For the gravity load, dead load and live load were considered. The dead load which included self-weight of the slab and superimposed dead load was assumed that 8 kN per unit square meters applied uniformly on the floor. The self-weight of the wall and columns were also considered separately. The live load was assumed that 2 kN per unit square meters applied uniformly.

Table. 3-2 shows the assumption for the seismic load. Ground condition was assumed to be ground of SB. From this assumption, velocity of shear wave was determined to be 760 m/s to 1500 m/s, which was used to select ground motions. Seismic use group was assumed to be level 1. From this assumption, importance factor was determined to be 1.2.

The building structural system was the dual system with ordinary reinforced concrete shear walls. Thus, the response modification factor was determined to be 5.5 and displacement amplification factor was determined to be 4.5.

In general case, to evaluate the seismic load, effective ground acceleration was determined to be 1.7 g or 2.2 g. However, in this study, in order to maximize the effect of the earthquake, 2.5 g, which was larger than general case, was used for the effective ground acceleration.

Table. 3-1 Assumption for the gravity load

Load case	DL (kN/m^2)	LL (kN/m_2)
Load value	8.0	2.0

Table. 3-2 Assumption for the seismic load

Assumption		Consideration
Ground condtion	S_B (Ordinary ground)	$760 \leq V_{s30} < 1500$ (Shear wave velocity at 30m depth)
Seismic use group	I	Importance factor $I_E = 1.2$
Building structural system	Dual system with RC Ordinary shear wall	R = 5.5 $C_d = 4.5$
Effective ground motion	0.25g (Larger than genral case)	$F_a = 1.0$, $F_v = 1.0$ (SB ground condition) $S_{DS} = 2.5 \times S \times F_a \times 2/3 = 0.4167g$ $S_{D1} = S \times Fv \times 2/3 = 0.1667g$

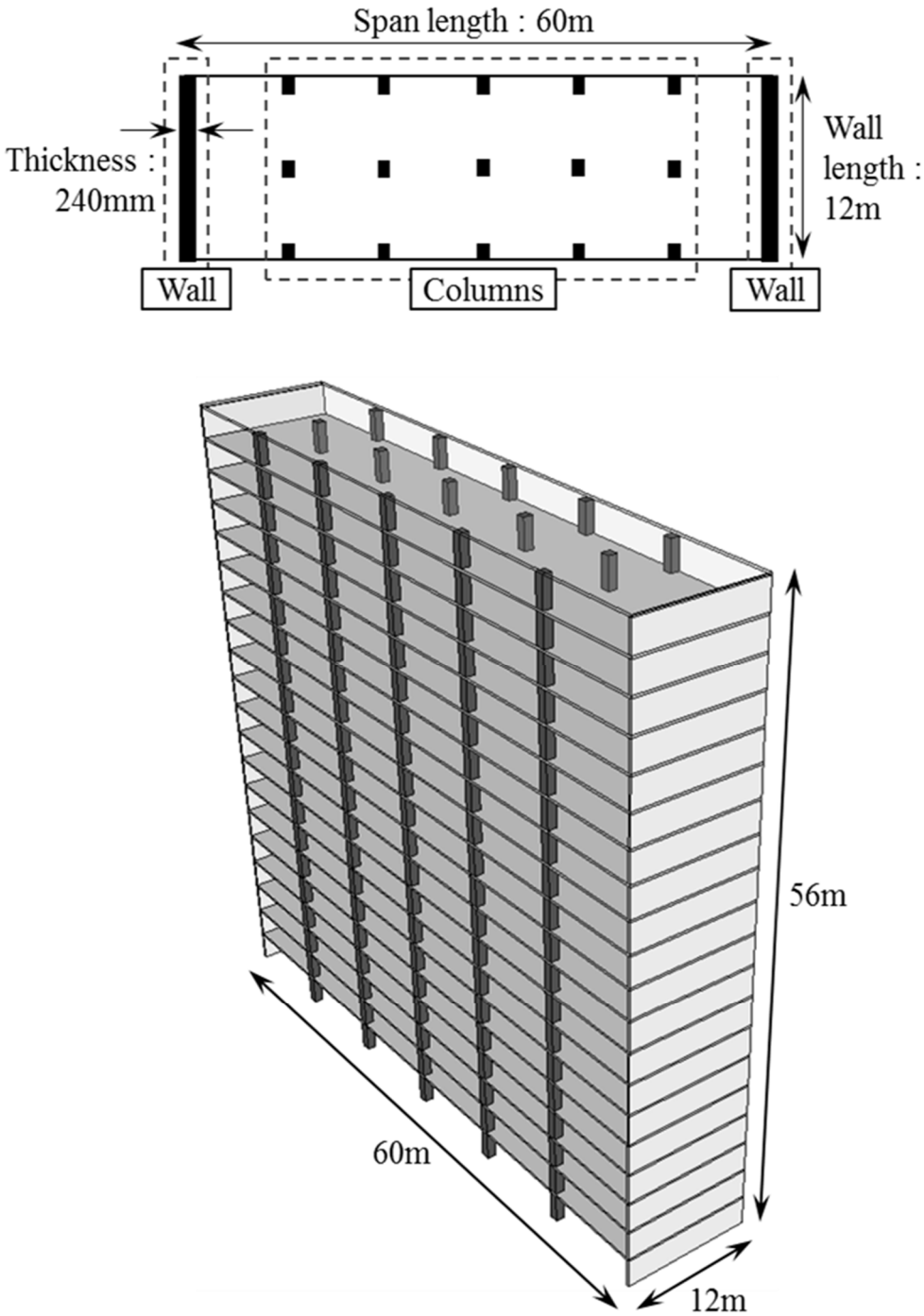

Fig. 3-1 Geometry and dimensions of target building

3.2.2 Modeling procedure

Fig. 3-2 shows procedures for establishing an analysis modeling. First step was determination of column size. By the assumption that 75% of total shear demand was distributed to the walls, column size was adjusted. In this procedure, iterative work was carried out until satisfying the assumption. For the convenience of iterative work, the columns were substitute to one lumped column. Table. 3-3 and Table. 3-4 show the story mass and modal analysis results after determination of column size.

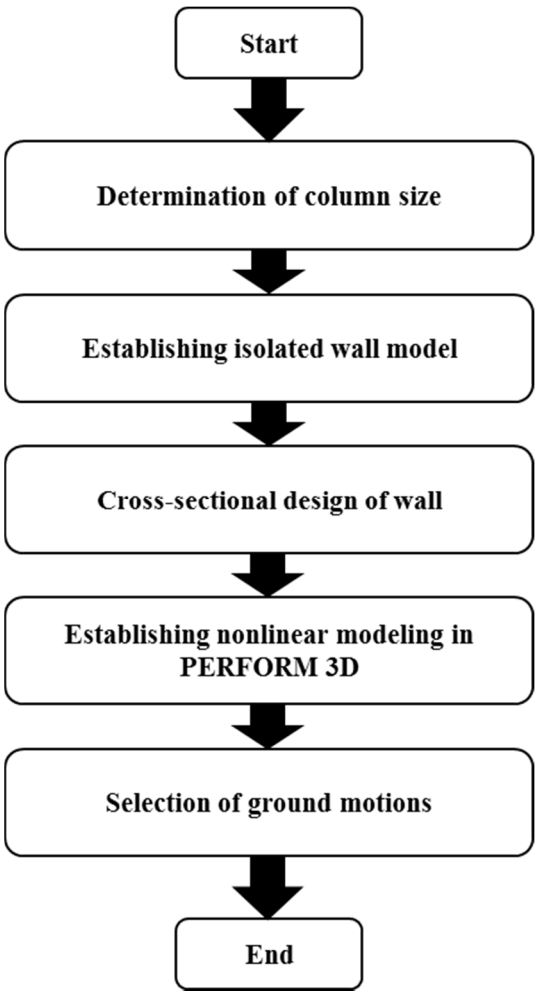

Fig. 3-2 Procedures for establishing an analysis modeling

Table. 3-3 Story mass

Story	Level (m)	Story mass (kN/g)
Roof	56	1694.937
20F	53.2	1724.527
19F	50.4	1724.527
18F	47.6	1724.527

17F	44.8	1724.527
16F	42	1724.527
15F	39.2	1724.527
14F	36.4	1724.527
13F	33.6	1724.527
12F	30.8	1724.527
11F	28	1724.527
10F	25.2	1724.527
9F	22.4	1724.527
8F	19.6	1724.527
7F	16.8	1724.527
6F	14	1724.527
5F	11.2	1724.527
4F	8.4	1724.527
3F	5.6	1724.527
2F	2.8	1724.527

Table. 3-4 Modal analysis results

Mode No.	Period (sec)	Modal Participation mass (%)
1	3.0465	63.75
2	0.5403	20.80
3	0.2202	7.13
4	0.1302	3.40
5	0.0910	1.82
6	0.0700	1.06
7	0.0572	0.66
8	0.0487	0.43
9	0.0427	0.29
10	0.0383	0.21
11	0.0349	0.15
12	0.0323	0.10
13	0.0303	0.07
14	0.0286	0.05
15	0.0274	0.04
16	0.0263	0.02
17	0.0256	0.01
18	0.0250	0.01
19	0.0246	0.00
20	0.0244	0.00

Next step was establishing of isolated wall modeling. If analysis modeling is established for the entire building, the shear amplification effect can be disturbed by behavior of column. Thus, in order to observe the shear amplification only by the walls, isolated wall modeling was established.

As the lumped column was eliminated, total story weight of the building was decreased. The story stiffness, however, was also decreased due to elimination of the lumped column. As a result, modal period of the isolated wall modeling was similar with that of the original entire building. Also, story shear demand of isolated wall modeling was similar with 75% of story shear demand of the original entire building, which shown in Fig. 3-3.

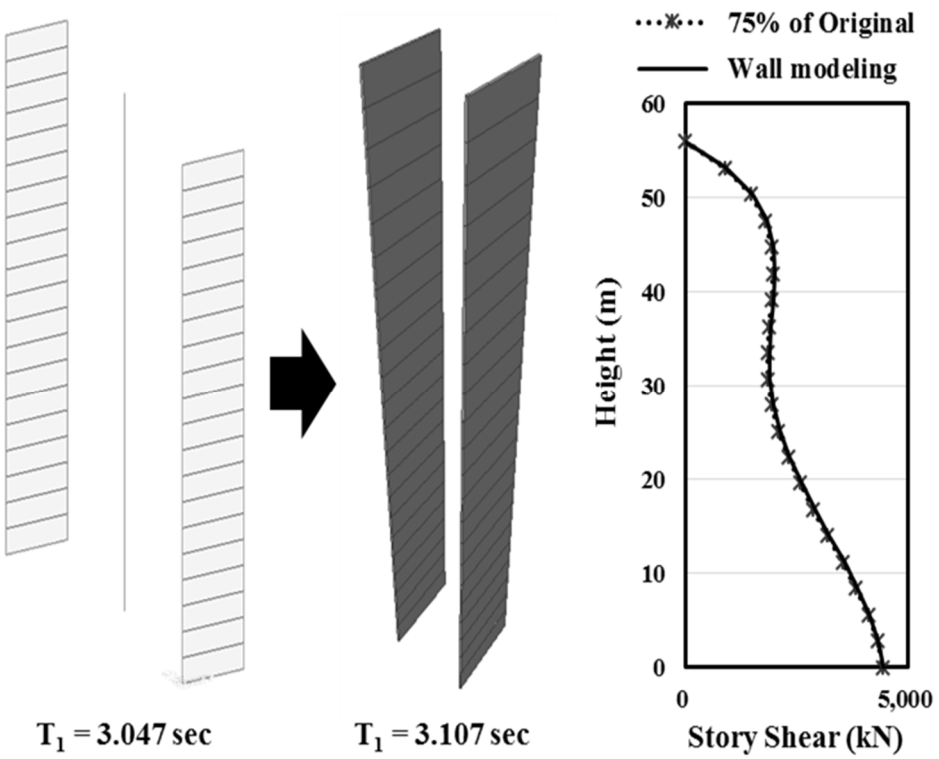

Fig. 3-3 Comparison of original and isolated wall modeling

Third step is cross-sectional design of the wall. The wall was designed by P-M ineraction diagram to resist both axial force and bending moment. Fig. 3-4 shows example of the wall design. Over-strength factor which was evaluated by dividing the moment capacity by the moment demand was designed to be minimized for optimal design.

Next, the analysis modeling was established in analysis program, Perform 3D. Wall elements were modeled by using fiber model. Nonlinear material models for concrete and re-bars were determined according to guidelines for performance-based seismic design of residential buildings, which shown in Fig. 3-5 and Fig. 3-6.

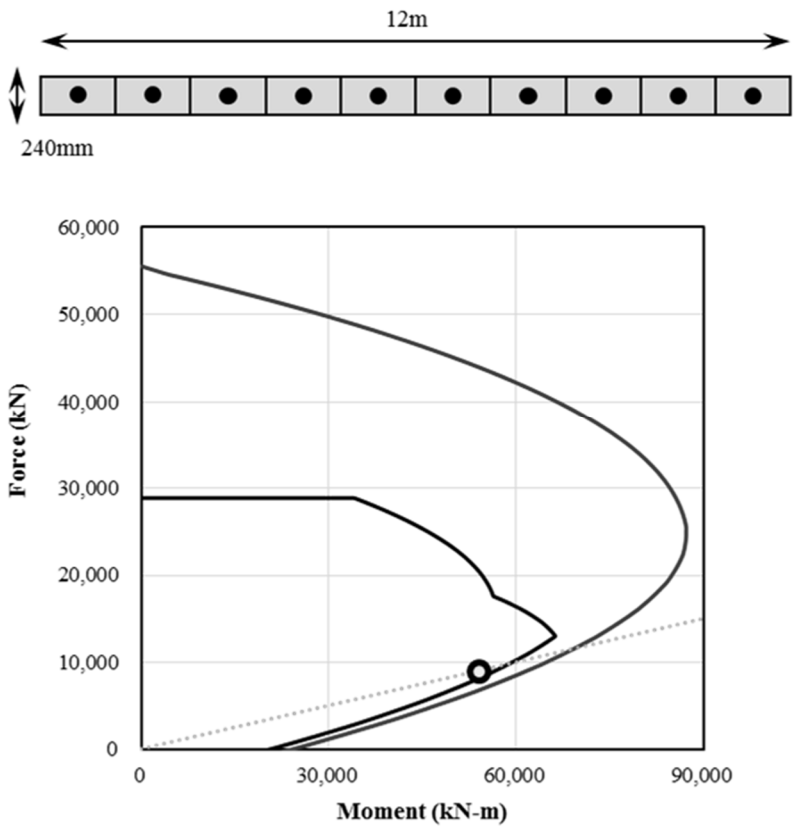

Fig. 3-4 Fiber model and P-M interaction diagram of the wall

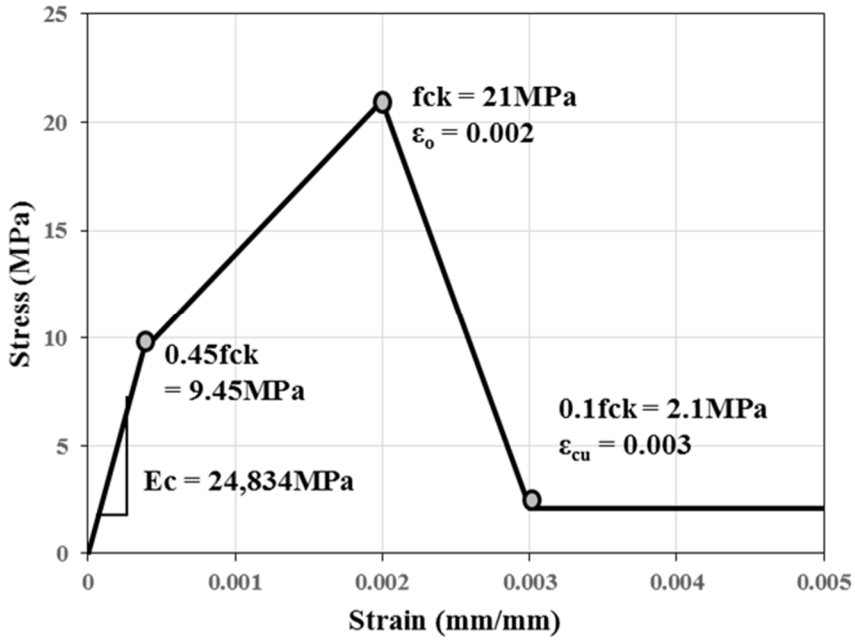

Fig. 3-5 Material model for concrete (C21)

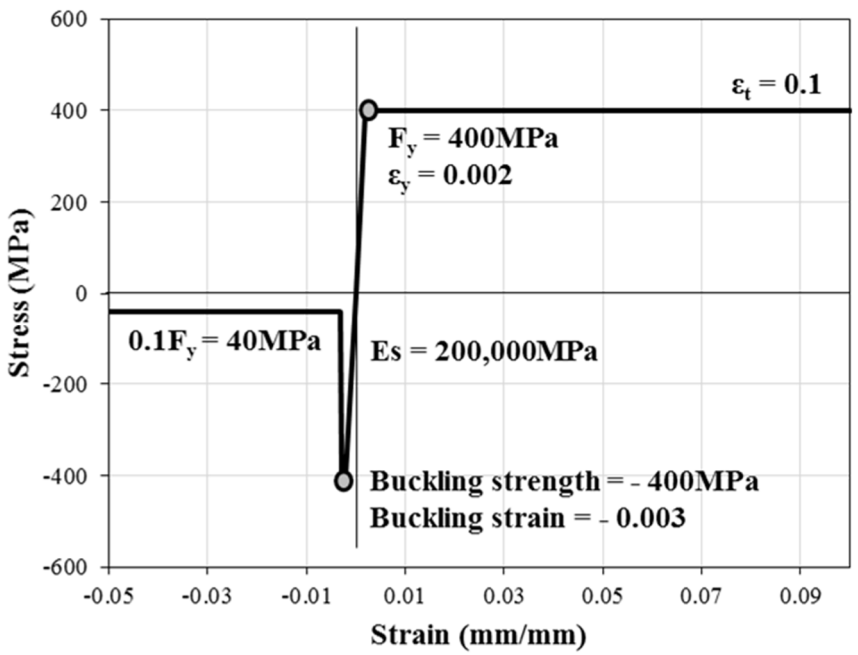

Fig. 3-6 Material model for re-bars (SD400)

In the Perform 3D, the concrete material model was limited to simplified tri-linear model. Since, it was assumed to have same area compared with concrete model suggested by Hognestad. Yield strength of concrete was defined to be 45% of concrete strength. Strain value responding to the concrete strength was determined to be 0.002. Residual stress was determined to be 10% of the concrete strength.

The material model for re-bars was assumed to be bi-linear model. Ultimate tensile strain was determined to be 0.1. In the compressive range, it was assumed that buckling occurred at the strain of 0.003. Residual stress after occurrence of buckling was determined to be 10% of the yield stress. Properties which included the geometry and dimensions, the gravity loads, the story mass and the boundary conditions was entered to be same with the elastic analysis modeling.

Lastly, seven pairs of ground motions for nonlinear dynamic analysis were selected. Ground motions were investigated through the PEER ground motion data base web site. Fig. 3-7 shows the searching conditions entered in the search-engine. First, target design response spectrum which had been evaluated according to KBC 2016 was uploaded. Next, searching conditions were set. Magnitude of the earthquake was set to be 5.0 to 7.0. Velocity of shear wave at the 30 m depth was set to be 760 to 1500 m/s. Scale factor was set to be 0.3 to 3.0.

Among the searched ground motions, seven pairs of the ground motions of different earthquakes were selected. The maximum acceleration response spectrum was determined for each ground motion. According to KBC 2016 the ground motions were scaled such that the average value of the 5% damped response spectra for the each ground motion is not less than design response spectrum of the

site for periods ranging from 0.2T to 1.5T seconds.

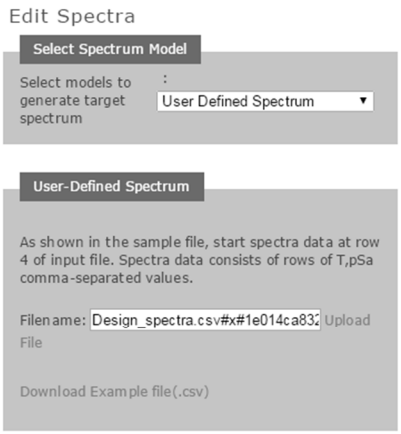

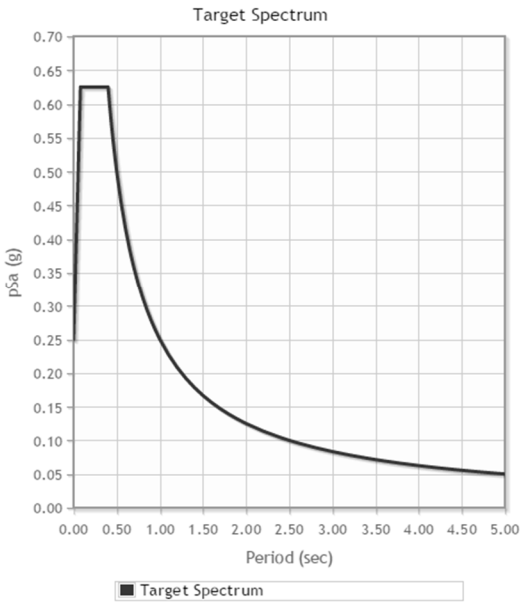

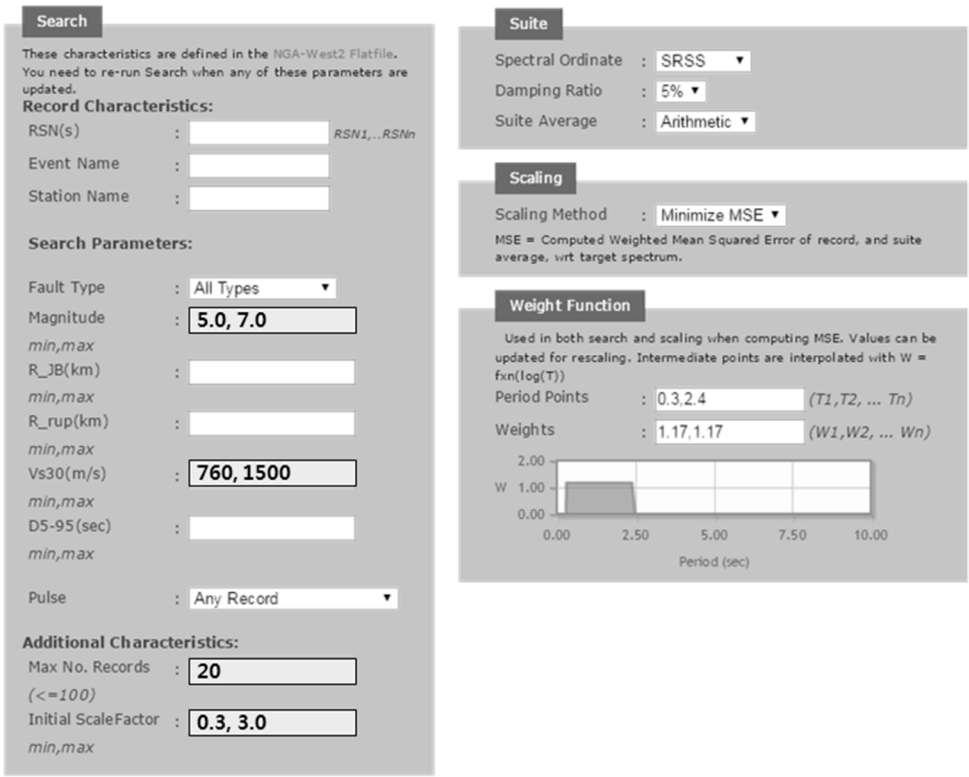

Fig. 3-7 Searching conditions entered in the PEER database

3.3 Analysis parameters

3.3.1 Parameter 1 : Axial force ratio

Since the shear amplification effect appears after yielding of the wall at the base, it is closely related with moment capacity of wall at the base. Since a wall resists both axial force and bending moment at the same time, by relationship between axial force and moment capacity of the wall, the shear amplification effect could become different. Fig. 3-8 shows the P-M interaction diagram of the wall. As the axial force ratio was increased up to a certain level, the moment capacity was increased, which meant that the over-strength factor was also increased. As a result, the amplification factor was expected to be increased. Therefore, to analyze effect

of axial force ratio, seven cases of axial force which changed from 10% to 40% were considered.

On the other hand, in the practical design, reinforcement is designed to be reduced to optimize over-strength factor. Fig. 3-9 shows the example of P-M interaction diagram of two cases designed by this method. To consider this case of constantly designed over-strength factor for different axial force ratio, the analysis modeling which had different cross-sectional design for each axial force ratio were added.

3.3.2 Parameter 2 : Response modification factor (R factor)

In the elastic analysis according to KBC 2016, the response modification factor is used for considering nonlinear behavior of seismic loads. Table. 3-5 shows the value of R factor with type of seismic resistance system of building. For example, in the case of dual system with ordinary reinforced concrete wall, which was assumed to be a structural system of analysis modeling, R factor is determined to be 5.5 and displacement amplification factor is determined to be 4.5.

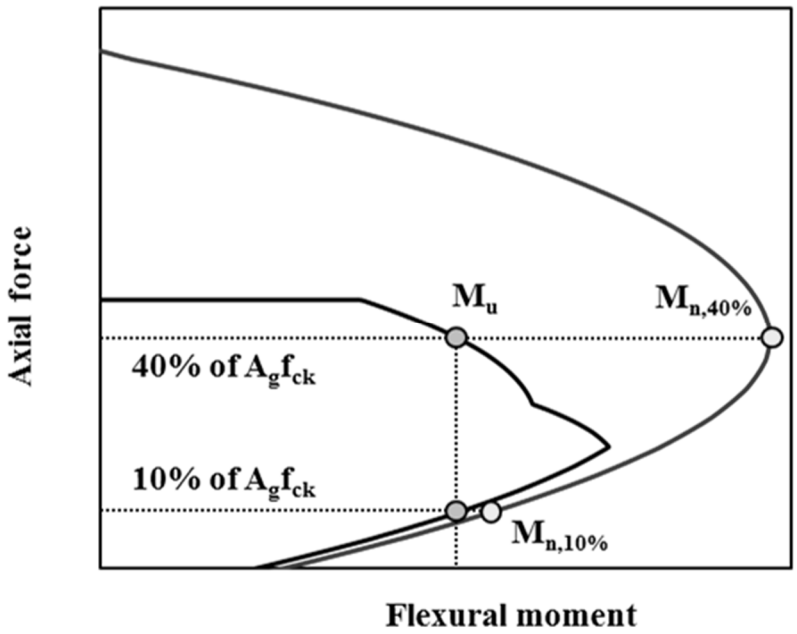

Fig. 3-8 P-M interaction diagram of designed wall

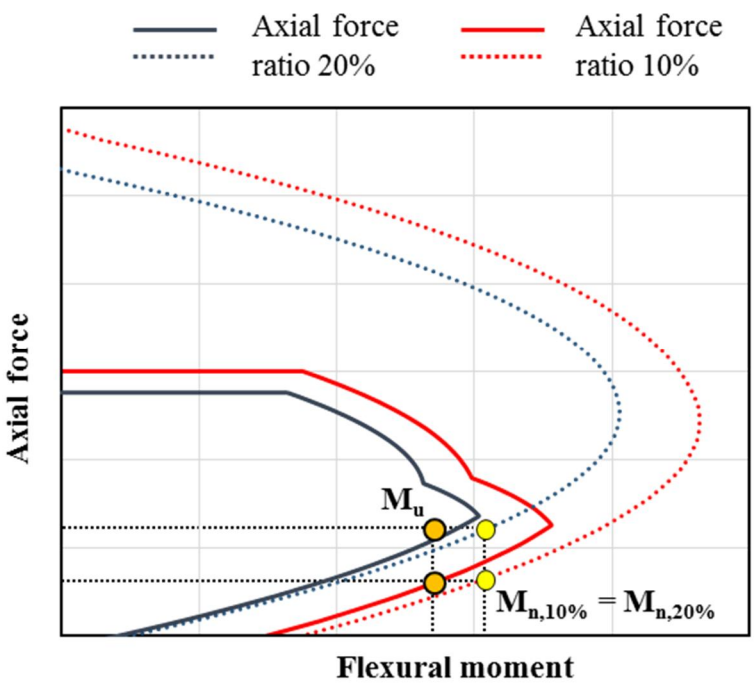

Fig. 3-9 P-M interaction diagram of wall in practical design

However, in the current design code, regardless of the originated properties of building such as geometry, dimensions and details, the R factor is only determined by type of building structural system. For this reason, the design based on elastic analysis cannot accurately consider actual nonlinear behavior of building, as a result, actual seismic loads obtained by nonlinear dynamic analysis can be largely different with design loads.

Therefore, in order to analyze effect of R factor, four cases of R factor which changed from 3.2 to 5.5 were considered. The value of R factor was obtained by reducing constantly from the value of 5.5 for dual system.

Table. 3-5 Design coefficients for seismic-force-resisting systems

Seismic-force-resisting system	Design coefficients			Limitations of height		
	Response modification coefficient R	System over strength factor Ω_0	Displacement amplification factor C_d	Seismic Design Category A or B	Seismic Design Category C	Seismic Design Category D
1. Bearing wall systems						
1-a. Special reinforced concrete shear walls	5	2.5	5	-	-	-
1-b. Ordinary reinforced concrete shear walls	4	2.5	4	-	-	60
1-c. Reinforced masonry shear walls	2.5	2.5	1.5	-	60	NP
1-d. Unreinforced masonry shear walls	1.5	2.5	1.5	-	NP	NP
2. Moment-resisting frame systems						
2-a. Special steel moment frames	8	3	5.5	-	-	-
2-b. Intermediate steel moment frames	4.5	3	4	-	-	-
2-c. Ordinary steel moment frames	3.5	3	3	-	-	-
2-d. Special composit moment frames	8	3	5.5	-	-	-
2-e. Intermediate composit moment frames	5	3	4.5	-	-	-
2-f. Ordinary composit moment frames	3	3	2.5	-	-	-
3. Dual systems with intermediate moment frames						
3-a. Special steel concentrically braced frames	6	2.5	5	-	-	-
3-b. Special reinforced concrete shear walls	6.5	2.5	5	-	-	-
3-c. Ordinary reinforced concrete shear walls	5.5	2.5	4.5	-	-	60
3-d. Reinforced masonry shear walls	3	3	2.5	-	60	NP

3.3.3 Parameter 3 : The number of stories designed identically

The basic principles in structural design is a safe and economical design. Based on these two principles, elements in the building is designed to resist required load for each floor. However, in the point of view of practical designer, as well as these principles, it is also important to shorten the construction time by enhancing workability. For this reason, in the practical design, in order to simplify the detail of design result, several floors were designed identically.

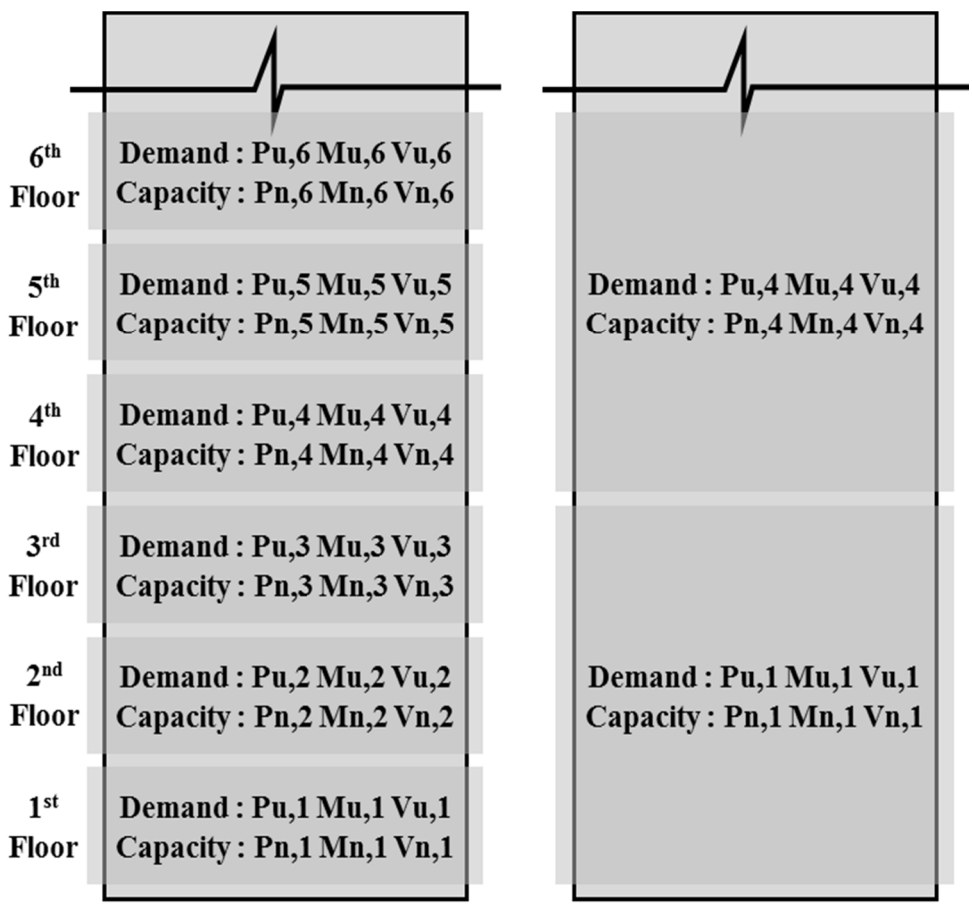

Fig. 3-10 Comparison of optimal and practical design

However, in the case of the building designed by this way, the element can be overdesigned than requirement in some floors. As a result, it is possible that the seismic loads increase than optimally designed case. Therefore, in order to analyze effect of the number of identically designed stories, three cases were considered, which included the case of designed for each story, the case of three stories identically designed and the case of six stories identically designed

3.3.4 Parameter 4 : Characteristics of selected ground motions

In the performance-based design, in order to conduct nonlinear dynamic analysis, actual ground motions should be scaled. According to KBC 2016, selected ground motions should be scaled such that the average value of the 5% damped response spectra for the each ground motion is not less than design response spectrum of the site for periods ranging from 0.2T to 1.5T seconds.

However, in the current design code, only lower bound for average response spectrum is provided. Because upper bound does not be limited, the average response spectrum depends on characteristics of selected ground motions. Fig Fig. 3-11 shows comparison of average response spectrum determined by two different set of selected ground motions. Both average response spectra satisfied the scaling criteria of KBC 2016. However, in the range of short period, average spectrum of case 2 was amplified more than that of case 1.

The shear amplification effect occurred due to effect of higher-order modes which generally have short period. Thus, when using the ground motions of case 2, the shear amplification effect can be larger than when using those of case 1. Therefore, in order to analyze effect of the characteristics of selected ground motions, using of different set of ground motions was considered in each analysis

modeling.

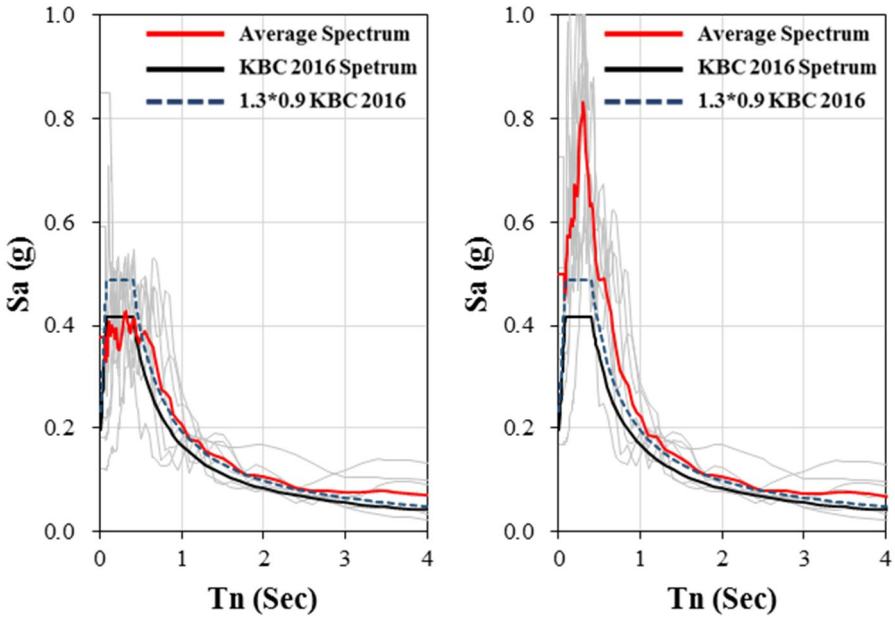

Fig. 3-11 Average spectrum determined by different ground motions

3.3.5 Parameter 5 : Detail of connection beam

In the plan of building structural system, type of arrangement of the wall is not only isolated type but also coupled type with connection beam. In the connection beam, large shear is applied due to coupling effect between two walls. Also, since aspect ratio of the connection beam usually less than 1:2, it is governed by brittle shear failure mode. For this reason, large amount of additional re-bars, such as diagonal re-bars, is required, which makes detail of the re-bars complicated and cases delaying of construction time.

In order to improve this problem, modified design for connection beam can be used. Fig. 3-12 and Fig. 3-13 shows comparison of cross-sectional properties and

structural behavior of original detail and proposed detail. In the proposed detail, the diagonal re-bars were eliminated. Instead, spacing of stirrups were decreased.

As a result, although the flexural strength was decreased, it could be not governed by brittle shear failure but ductile flexural failure. These behavior characteristics of proposed details were verified by test results, which had been conducted by Kwan and Zhao.

If this detail is used in the design of connection beam, the shear amplification can be decreased by reducing transferred shear. Therefore, in order to analyze effect of the detail of connection beam, two different case of detail were considered.

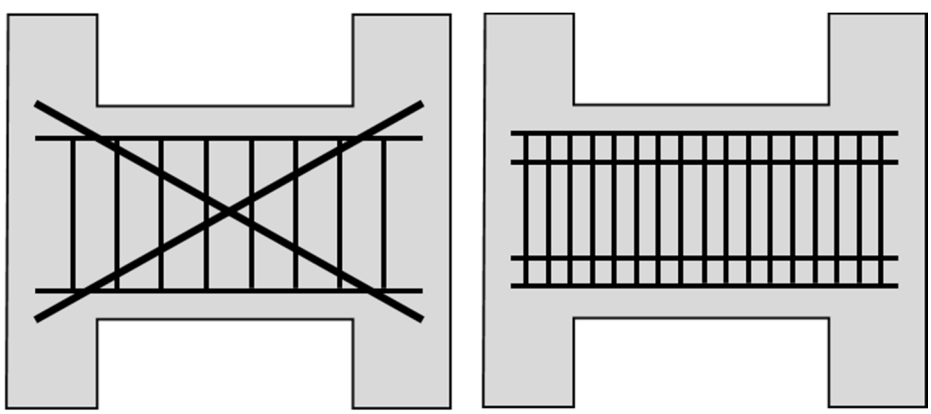

Fig. 3-12 Cross-sectional properties of two details

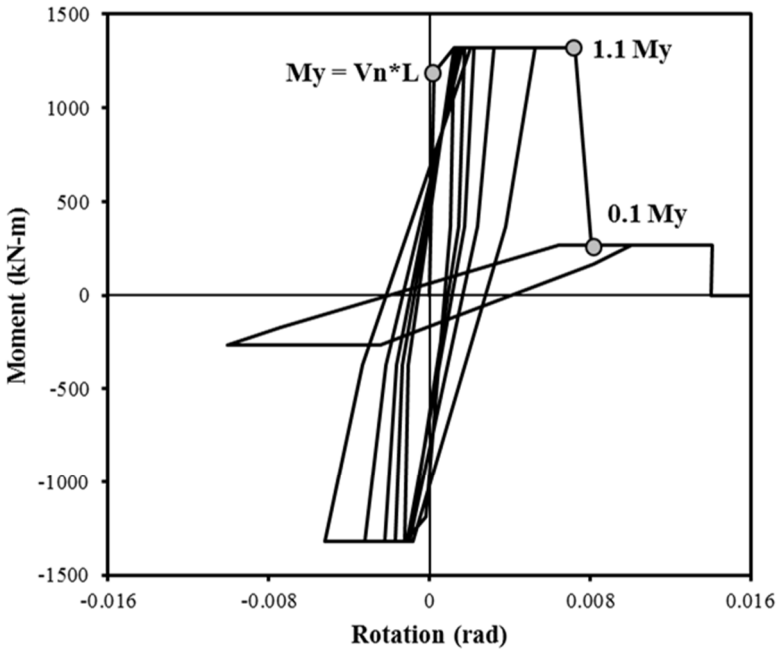

(a) Case 1

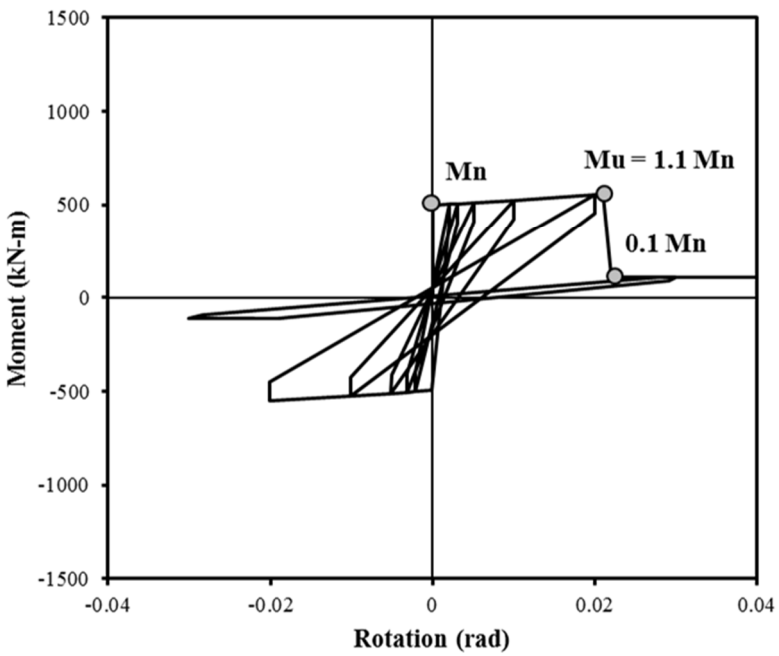

(b) Case 2

Fig. 3-13 Structural behavior of two details

3.4 Analysis results

3.4.1 Parameter 1 : Axial force ratio

Fig. 3-14 shows the analysis results for effect of the axial force ratio. Each case of modeling had different detail or different set of ground motions. X axis of the graph means axial force ratio and Y axis of the graph means base shear amplification factor. For each case of modeling, analysis was carried out as the axial force ratio increased. In the graph, data connected by continuous line belongs to same modeling.

As the axial force ratio increased, since the over-strength factor of bending moment was increased, the base shear amplification factor was also increased. Fig. 3-15 shows the normalized data of Fig. 3-14. Each data was normalized by dividing it by average value of each case. The normalized data was tend to linearly increase as the axial force increased.

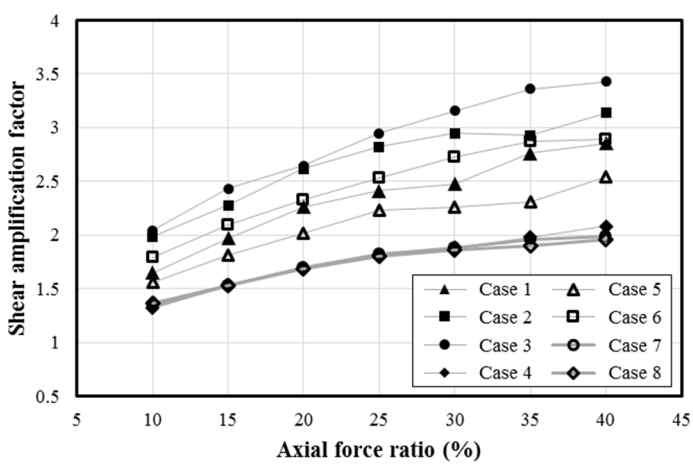

Fig. 3-14 Effect of the axial force ratio

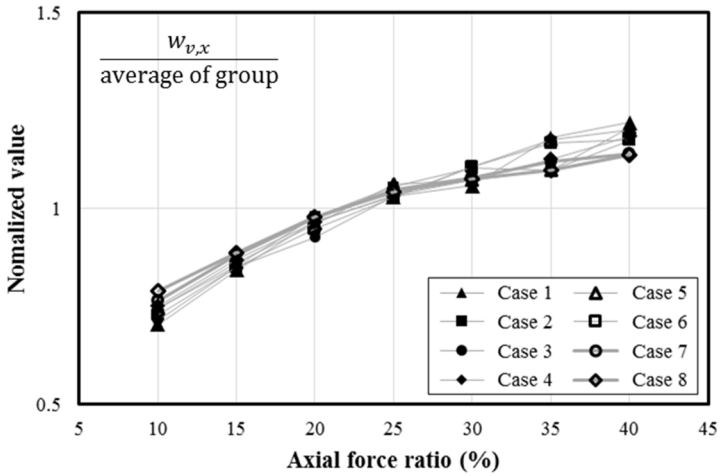

Fig. 3-15 Normalized data of Fig. 3-14

Fig. 3-16 shows the analysis results for the case that the reinforcement ratio was designed to be reduce in order to optimize over-strength factor. Although the over-strength factor was constant, the amplification factor was tend to be increased as the axial force increased. Through these results, it was found that another parameter which is related with axial force can affect the base shear amplification factor, as well as over-strength factor.

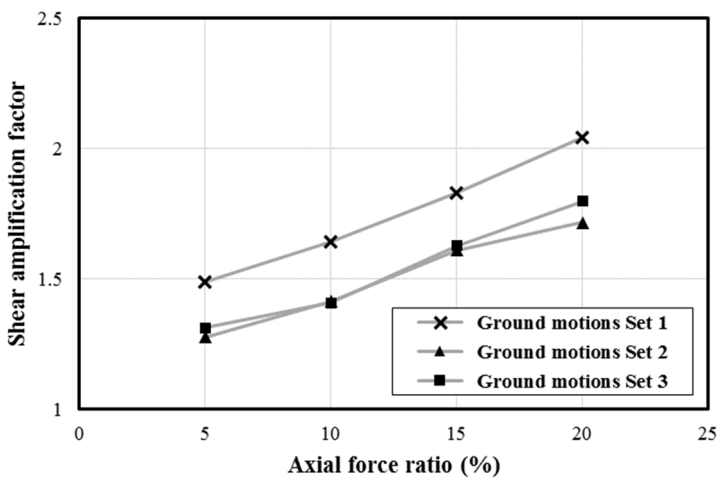

Fig. 3-16 Results of modeling designed optimize over-strength factor

3.4.2 Parameter 2 : Response modification factor (R factor)

Fig. 3-17 shows the analysis results for effect of the response modification factor. X axis of the graph means story shear divided by design base shear and Y axis of the graph means relative height. The base shear amplification factor was decreased as the smaller R factor was used to design.

In the modeling which was designed by smaller R factor, the shear and moment demand of the wall was increased, and more vertical re-bars were placed in the cross-section. As a result, the moment capacity of the wall at the base was increased and the absolute value of the dynamic base shear was also increased. However, due to nonlinear behavior, increment ratio of the dynamic base shear was not perfectly linear with respect to increment ratio of moment capacity. For this reason, since the increment ratio of dynamic shear was smaller than the increment ratio of base shear, the base shear amplification factor, calculated by dividing dynamic shear by design shear, was decreased.

From this results, it was found that the response modification factor suggested by current design codes could not accurately consider the actual characteristics of nonlinear behavior of the building. In order to overcome this limitation, in Eurocode 8, the R factor is evaluated by actual performance of the building. Therefore, in domestic structure code, it needs to review the method of evaluating the R factor for more accurate and reliable design.

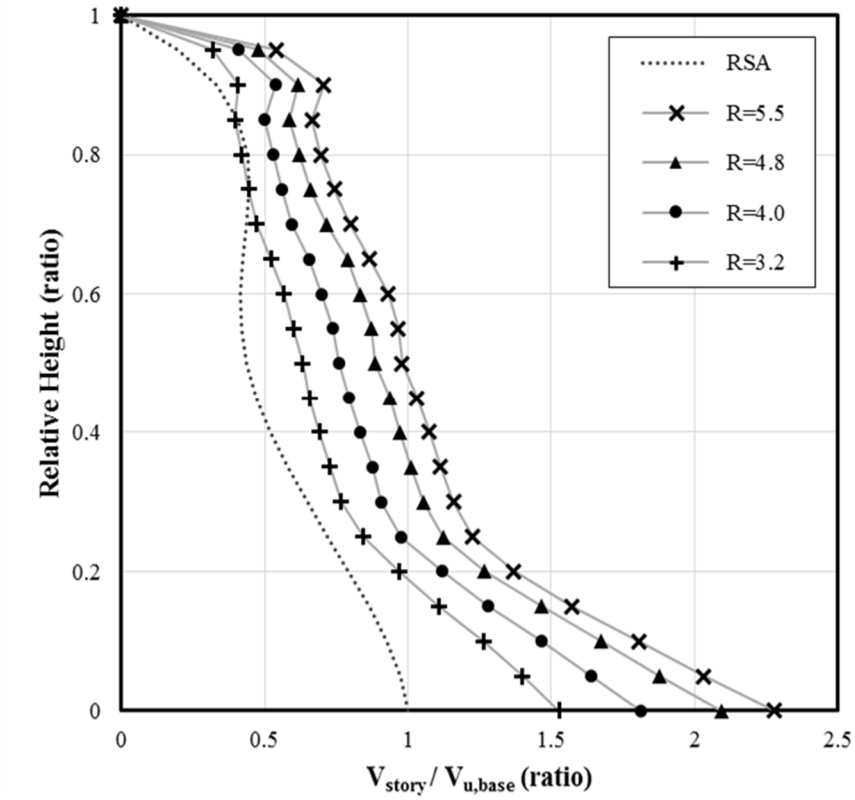

Fig. 3-17 Effect of the response modification factor

3.4.3 Parameter 3 : The number of stories designed identically

Fig. 3-18 shows the analysis results for effect of the number of stories designed identically. Each graph shows the result of modeling with 10, 15 and 20 stories. Each case in the graph represents the case of designed for each story, the case of three stories identically designed and the case of six stories identically designed. X axis of the graph means over-strength factor of the wall at the base and Y axis of the graph means the base shear amplification factor.

Difference in the number of stories designed identically did not significantly affect the base shear amplification factor. Rather, the base shear amplification factor was affected by the over-strength factor of the wall at the base.

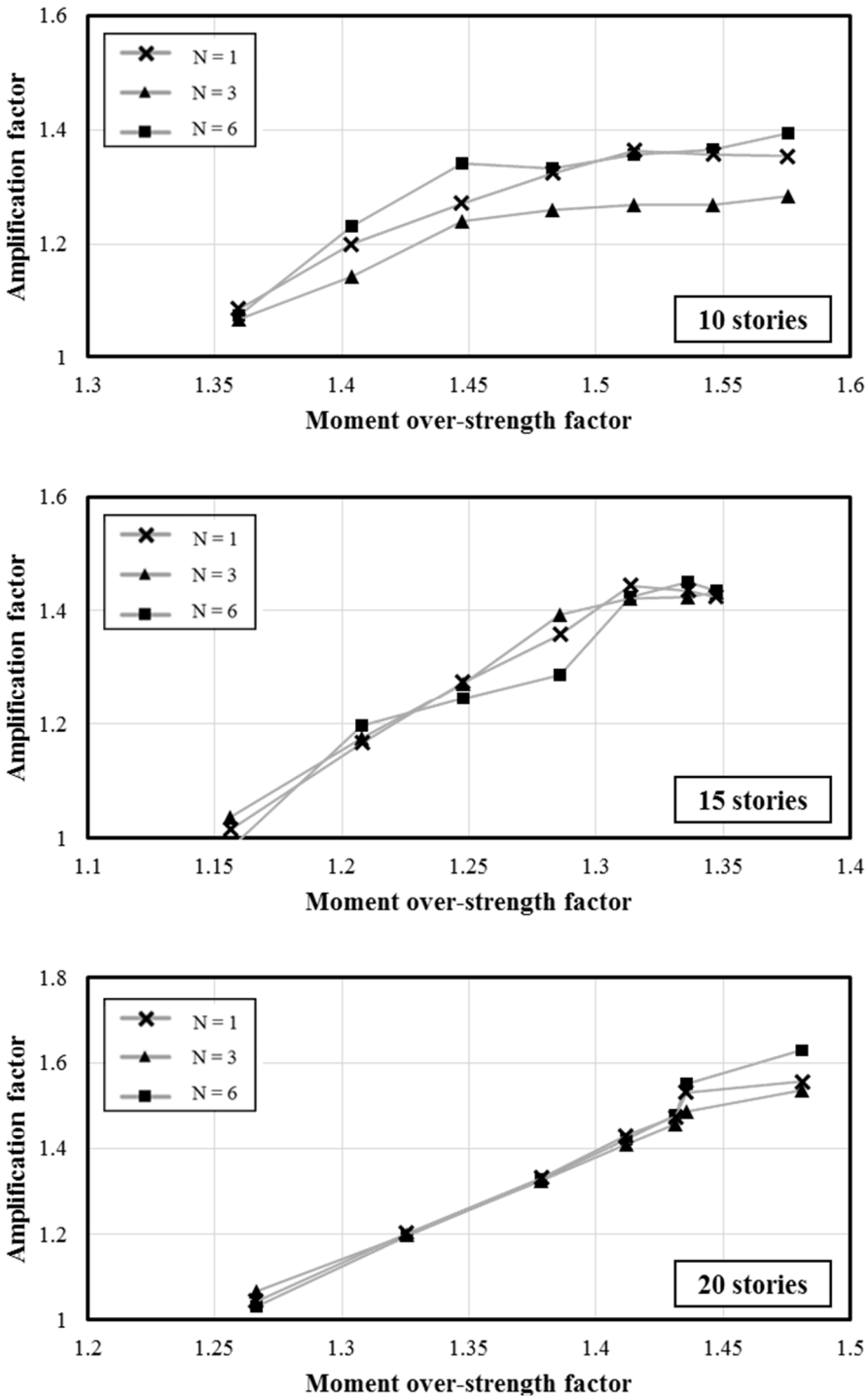

Fig. 3-18 Effect of the number of stories designed identically

3.4.4 Parameter 4 : Characteristics of selected ground motions

Fig. 3-19 shows the analysis results for effect of characteristics of selected ground motions. In the graph, the data marked with black point represent the results obtained by using ground motions of case 1 shown in Fig. 3-11. The others marked with red cross represent the results of case 2 shown in Fig. 3-11. X axis of the graph means over-strength factor of the wall at the base and Y axis of the graph means the base shear amplification factor.

The base shear amplification factor was greater in the case 2 than in the case 1. Because the average response spectrum of the case 2 was more amplified in the range of short period than that of the case 1. For this reason, modal seismic loads of higher-order modes were increased and the base shear was also increased.

In order to numerically consider this effect, the design shear demand for calculating the amplification factor was substituted to average shear demand obtained by the average response spectrum. Fig. 3-20 shows the data recalculated by using the average shear demand. By using the average shear demand, the tendency of both case 1 and case 2 became similar. Therefore, through these results, it was found that the average shear demand could be used to consider the characteristics of selected ground motions in the calculation of the base shear amplification factor.

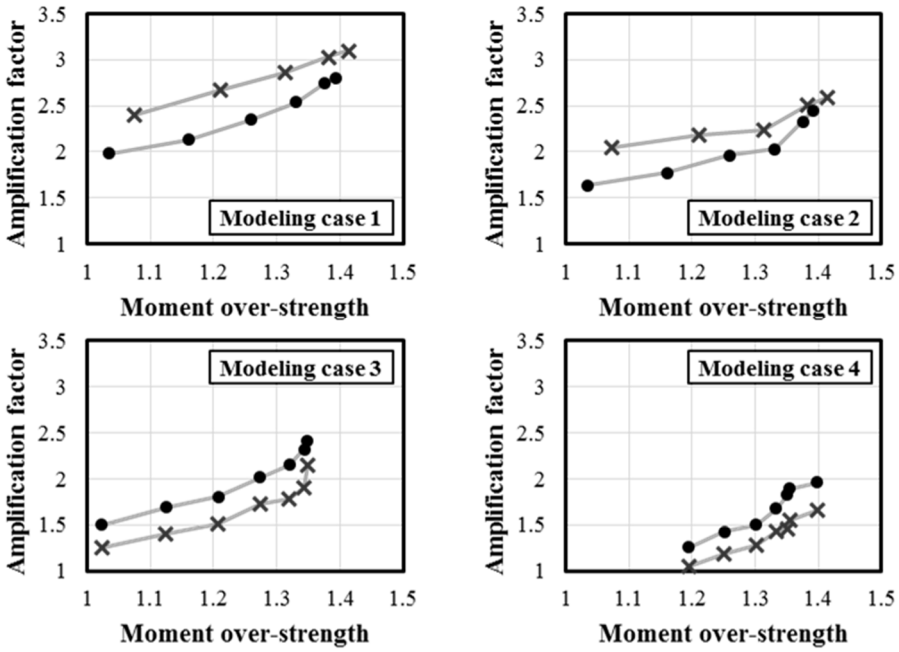

Fig. 3-19 Effect of characteristics of selected ground motions

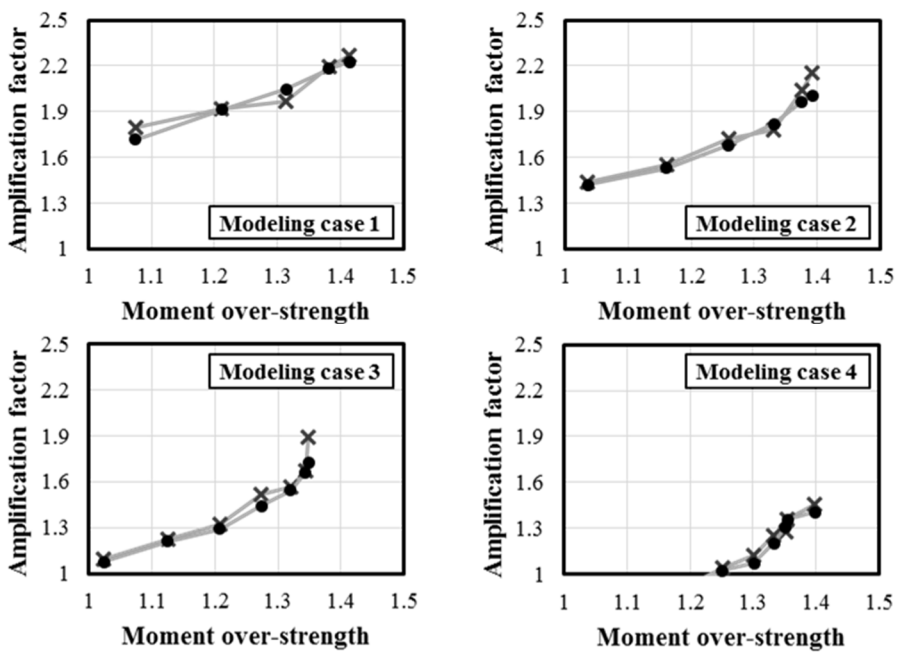

Fig. 3-20 Recalculated data by using the average shear demand

3.4.5 Parameter 5 : Detail of connection beam

Fig 4.23 shows the analysis results for effect of detail of connection beam. In the graph, the data marked with black point represent the results of modeling designed original detail. The others marked with red cross represent the results of modeling designed proposed detail. Each graph shows the result obtained by using different set of ground motions. X axis of the graph means axial force ratio at the base and Y axis of the graph means the base shear amplification factor. The base shear amplification factor was determined to be average value of both walls

In the case of modeling using proposed detail, the base shear amplification factor was significantly reduced. Since the connection beam with proposed detail was yielded in lower moment, the transferred shear between both walls was limited.

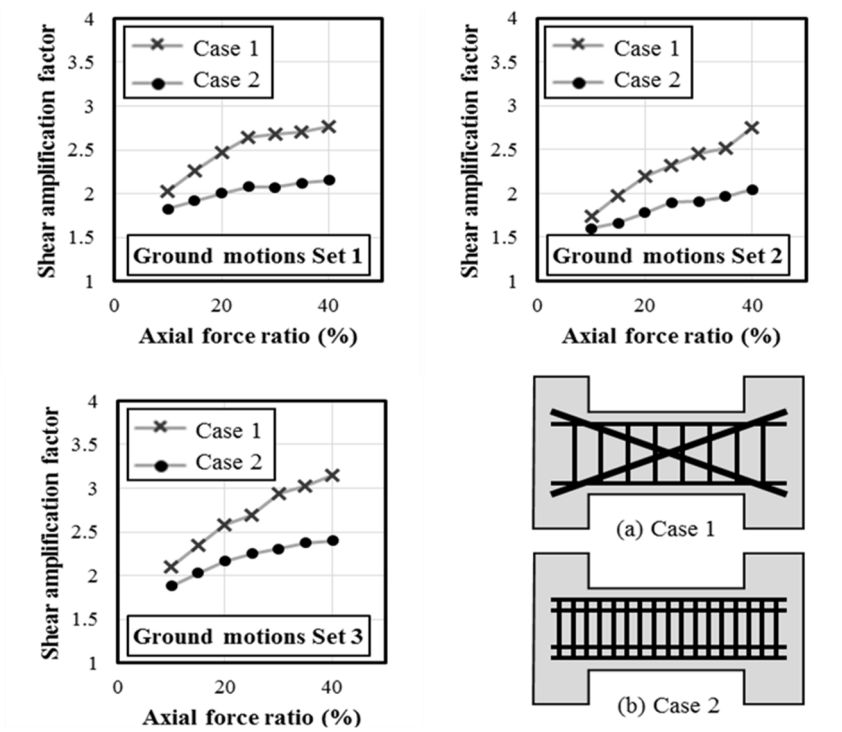

Fig. 3-21 Effect of detail of connection beam

3.5 Design of slender shear wall

3.5.1 Base shear amplification factor

Fig. 3-22 shows the all data corresponding to parameter 1 to 4. The data marked with red diamond correspond to 10 stories modeling. The data marked with black triangle correspond to 15 stories modeling. The data marked with blue cross correspond to 20 stories modeling. X axis represents the moment over-strength factor of the wall at the base, which was calculated by dividing the base moment capacity by the base average moment demand. The base moment capacity was determined at the base of the wall. And the base average moment was evaluated by the average response spectrum which calculated by selected ground motions. Through the distribution of the data, a certain regularity of the data was observed in order to derive a design equation for reasonably predicting the base shear amplification factor.

Fig. 3-23 shows separately the data of 20 stories modeling in the Fig. 3-22. The data marked with same color represent the data of same modeling. The data of same modeling shows linearly increasing tendency as the over-strength factor increases. The straight line colored same with the data represents approximately this tendency.

Since the straight lines had similar inclination, the data were able to be normalized to one group having a linear trend by following parallel translation.

$$\frac{M_{n,x}}{M_{u,avg}} \rightarrow \frac{M_{n,x}}{M_{u,avg}} - \frac{M_{n,0}}{M_{u,avg}} \left(= \frac{M_{n,x} - M_{n,0}}{M_{u,avg}} \right) \tag{3-1}$$

Where the $M_{n,x}$ is base moment capacity with the axial force ratio x %, the $M_{u,avg}$

is the base average moment demand calculated by the average response spectrum and the $M_{n,0}$ is pure moment capacity with no axial force.

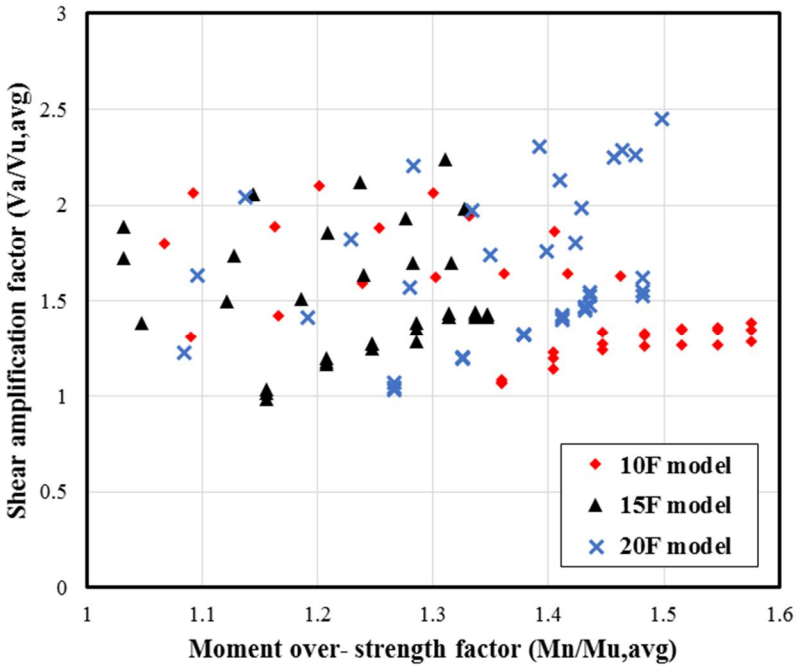

Fig. 3-22 All data corresponding to parameter 1 to 4

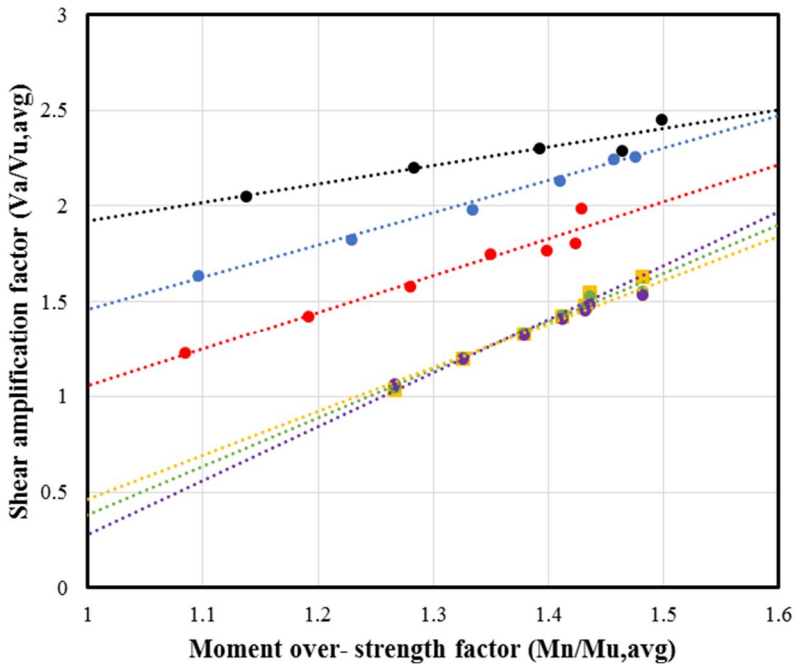

Fig. 3-23 Data of 20 stories modeling in the Fig. 3-22

Fig. 3-24 shows the converted data by normalizing equation. The base shear amplification factor was tend to be increased as the normalized parameter increases. Also, the linear tendency was not related to the number of stories of the modeling.

Therefore, the design equation for predicting the base shear amplification factor was assumed to be form of linear function, which is shown in the Fig. 3-24. The y-intercept of the linear function, which means that Mn,x is equal to Mn,0, was assumed to be one. Based on the results of 173 modeling, regression analysis was carried out in order to derive the following design equation for the base shear amplification factor.

$$y = 1.111x + 1.0 \qquad (3\text{-}2)$$

$$\frac{\mathrm{V}_a}{V_{u,avg}} = 1.111\left(\frac{M_{n,x} - M_{n,0}}{M_{u,avg}}\right) + 1.0 \quad (3\text{-}3)$$

$$\frac{\mathrm{V}_a}{V_{u,avg}} = 1.111\left(\frac{\mathrm{M}_{n,x}}{M_{u,avg}} - \frac{\mathrm{M}_{\mathrm{n},0}}{M_{u,avg}}\right) + 1.0 \quad (3\text{-}4)$$

$$w_v = 1.111\,\Omega - 1.111\Omega_0 + 1.0 \quad (3\text{-}5)$$

Where the V_a is the base shear demand by nonlinear the dynamic analysis, the $V_{u,avg}$ is the base average shear demand by the average response spectrum, w_v is the base shear amplification factor, the Ω is the base over-strength factor and the Ω_0 is the pure base over-strength factor calculated by dividing the pure moment capacity by the average moment demand.

Fig. 3-25 shows comparison of the predicted value and actual value of base shear amplification factor. Error of predicted value and the actual value was within 20%.

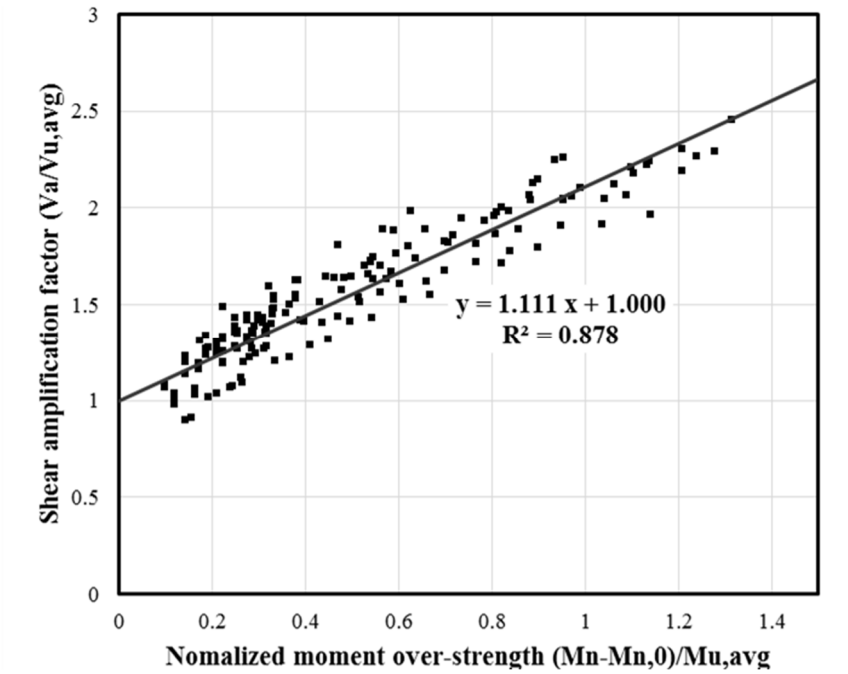

Fig. 3-24 Converted data by normalizing equation

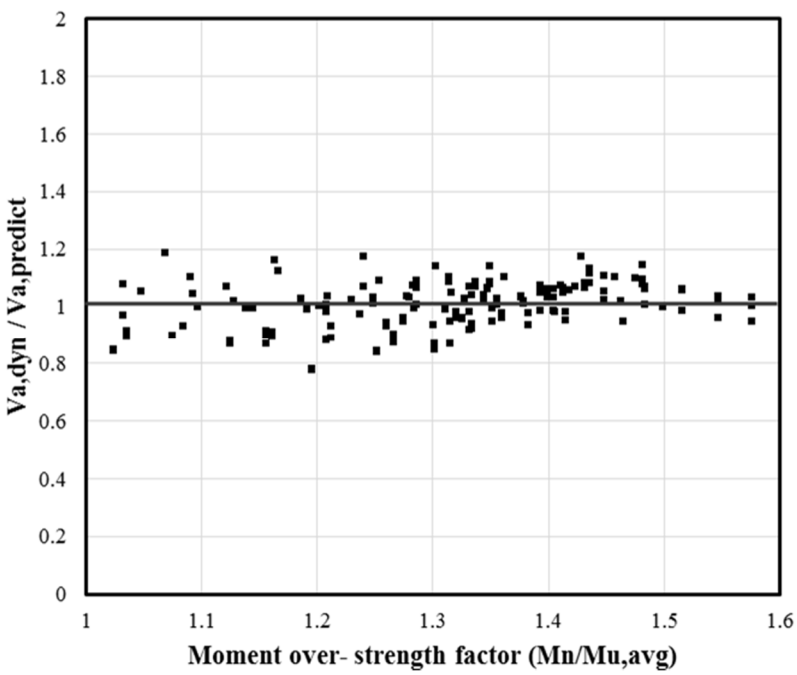

Fig. 3-25 Comparison of the predicted value and actual value

3.5.2 Story shear distribution model

Fig. 3-26 (a), (b) and (c) shows the story shear distribution of modeling with 10, 15 and 20 stories. X axis represents the relative story shear which was calculated by dividing the story shear by the base shear. Y axis represents the relative height. In the each graph, a red line represents the average value of story shear.

Fig. 3-26 (d) shows the comparison of the average story shear distribution of modeling with 10, 15 and 20 stories. X axis represents the relative story shear and Y axis represents the relative height. When the relative height was smaller than 0.5, the relative story shear of 10 stories modeling was greater than the others in the same relative height. On the other hand, when the relative height was larger than 0.5 the relative story shear showed similar distribution. Through these results, the story shear distribution model was proposed.

Fig. 3-27 shows the proposed story shear distribution model. The base shear was able to be calculated by multiplying the base average shear demand and the base shear amplification factor. When the relative height was lower than 0.5, the model was assumed to be linear shape in order to design conservatively. Through the average story shear distribution, the story shear corresponding to relative height of 0.5 was determined to be 40% of the amplified base shear. When the relative height was greater than 0.5, the story shear was mostly smaller than the story shear at the relative height of 0.5. However, since it is possible that the story shear is amplified radically in the higher stories, the model was assumed to be uniform shape in order to design conservatively. Compared with the story shear distribution model provided in Eurocode 8, the proposed model predicts more economically.

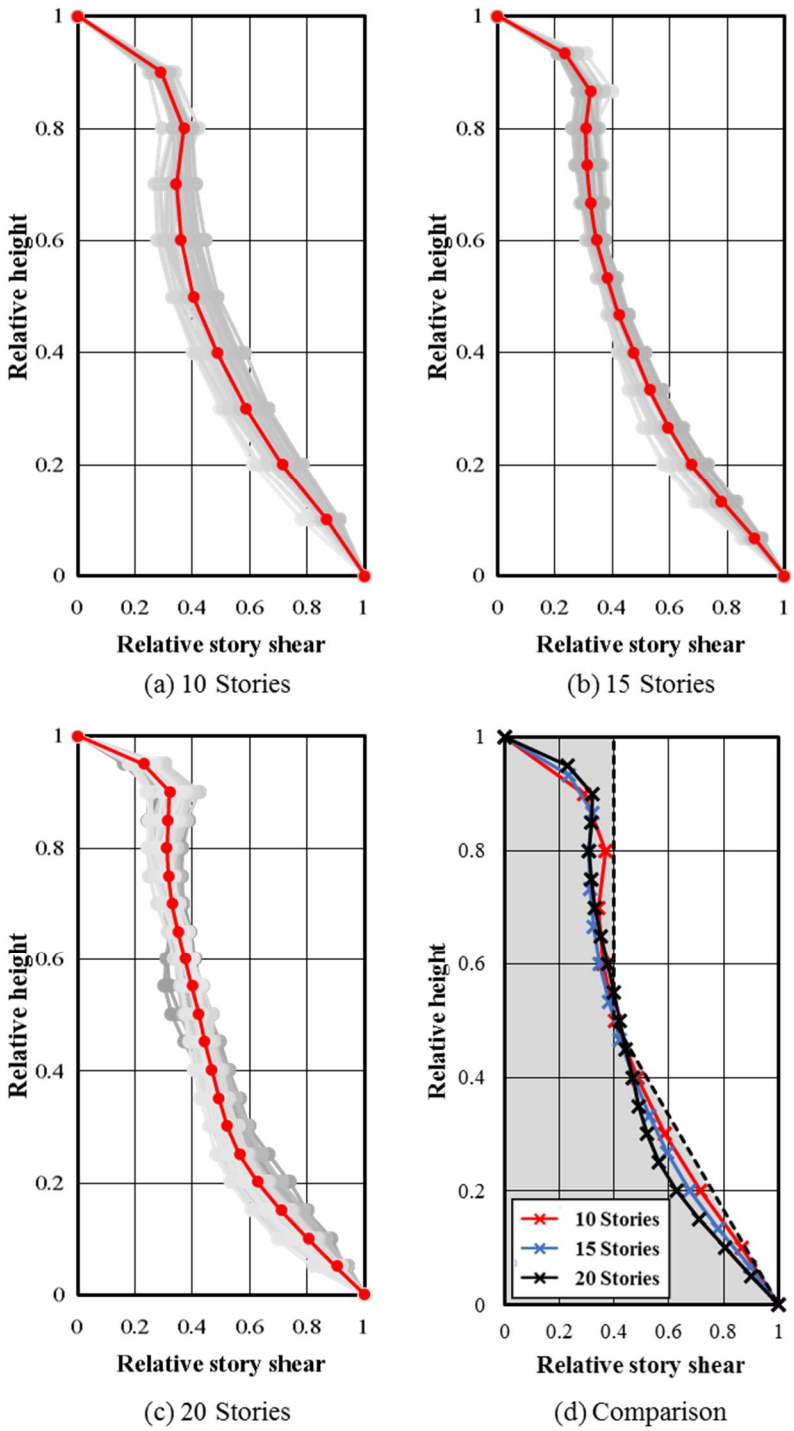

(a) 10 Stories (b) 15 Stories

(c) 20 Stories (d) Comparison

Fig. 3-26 Story shear distribution of modeling

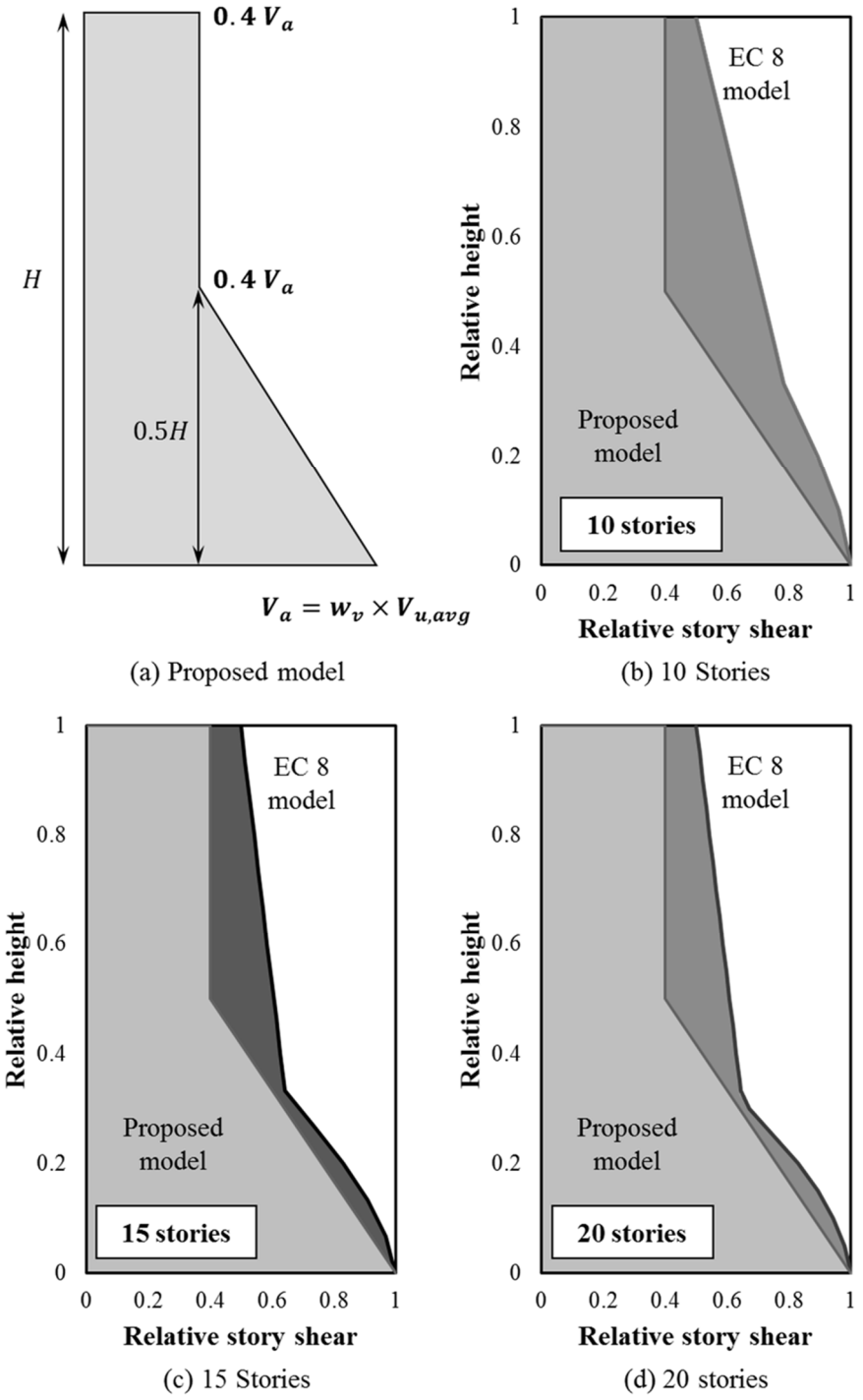

Fig. 3-27 Proposed story shear distribution model

Chapter 4. Capacity Design of Pilotis-Wall System without Transfer Girder

4.1 Introduction

Recently, in Korean apartments, the pilotis-wall system is frequently used. It can be a solution for the invasion of privacy and unfavorable condition problem in the lower stories of the building. Additionally, it is possible to provide resting place for residents. In spite of these advantages, current pilotis-wall system has limitations. In the current system, transfer girder between pilotis and wall is used to transfer gravity and lateral loads. However, use of the transfer girder causes some problems: 1) over 1.8 m depth of the transfer girder decreases the efficiency of space; and 2) large size of the transfer girder reduces constructability, which increases construction period.

Additionally, in the structural perspective, in the current system, the concentration of the stress was generated in the connection between the transfer girder and the wall due to the rigidity difference and the geometric discontinuity. By this stress distribution, entire behavior and failure mode of structure is determined. Therefore, careful consideration of this part is required when designing this system.

For these reasons, in the present study, new pilotis-wall system without transfer girders, in which upper wall was directly connected with pilotis, was proposed. On the basis of the capacity design concept, without applying special earthquake load, a design method for the wall in the transfer zone was discussed. To evaluate the

structural performance of the proposed system and verify the design method, both the compression loading and cyclic loading tests were performed.

4.2 Test program

4.2.1 Design concept

In the case of the pilotis-wall system, the gravity and lateral loads from above walls are transferred to pilotis through the transfer zone. At the wall-pilotis connection, stress is concentrated due to the significant decrease of cross-sectional area. Thus, to avoid the premature brittle failure at the connection, the capacity design method based on the actual performance of the structure was used. In this method, each structural member is designed on the basis of the assumed failure mode. Fig. 4-1 shows two failure modes of the pilotis-wall system. Brittle failure at the connection is not recommended for seismic design of the structure Fig. 4-1 (a). In this study, pilotis and wall in transfer zone were designed to resist the required load greater than the load capacity of the upper wall. As a result, plastic hinge occurs at the upper wall, which causes the ductile failure mode Fig. 4-1 (b).

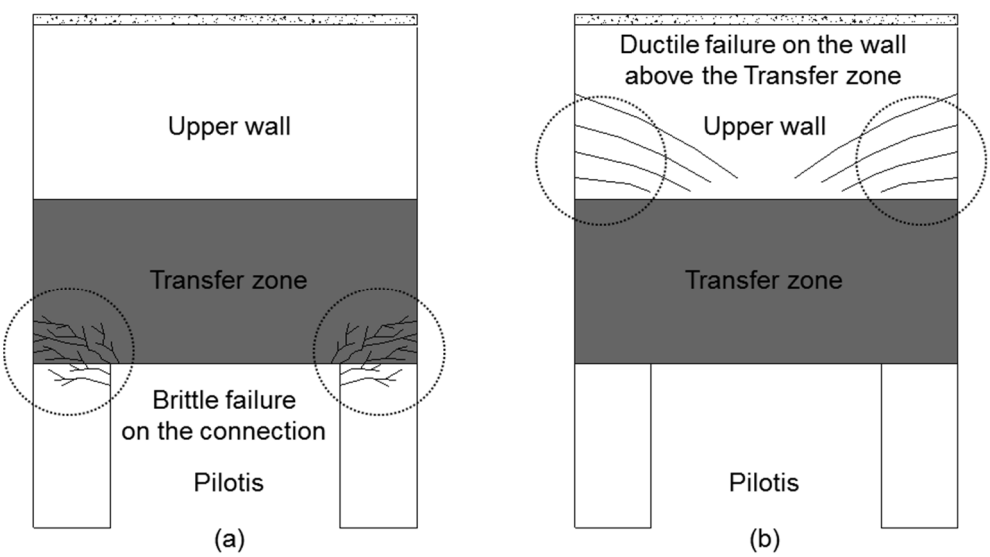

Fig. 4-1 Failure modes of the pilotis-wall system

4.2.2 Design procedure

Fig. 4-2 shows the two different design methods for the design of the reinforcement. The critical section was defined as the area where the wall and the pilotis are connected. Thus, the nominal strength of each critical section was calculated by following equation.

$$P_n = 0.85 f_c' bh \tag{4-1}$$

Where f_c' is concrete strength, b is breadth of the pilotis and h is thickness of the wall. When the compression load and the lateral load are applied, the two kinds of axial forces occur in the critical section Fig. 4-2 (a). The P_g which is relative with the compression load was half of the compression load and the the P_v which is relative with the lateral load was calculated by the moment equilibrium.

$$P_g = P_u/2 \tag{4-2}$$

$$P_v = V_u H/L \tag{4-3}$$

Critical section in compression side, resultant force of the two axial forces is applied as compression force. From this, the design lateral load V_u was evaluated by following equation.

$$P_n = P_v + P_g = P_u/2 + V_u H/L \tag{4-4}$$

$$V_u = L/H(P_n - P_u/2) \tag{4-5}$$

Critical section in tension side, resultant force is applied as tensile force T_{u1}. To resist tensile force, required vertical reinforcement was placed. To prevent premature failure in transfer zone, amount of vertical reinforcement in this area

was increased.

By using a strut-tie model, the tensile force in the transfer zone T_{u2} was evaluated. For a conservative design, the required lateral reinforcement in this area was increased by 25%.

$$T_{u2} = P_u/4 + V_u \tag{4-6}$$

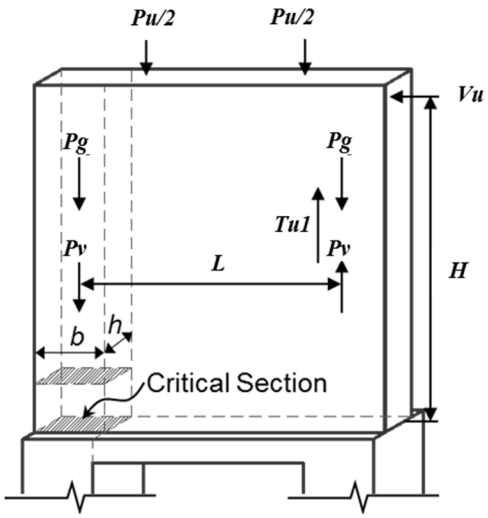

(a) Vertical reinforcement

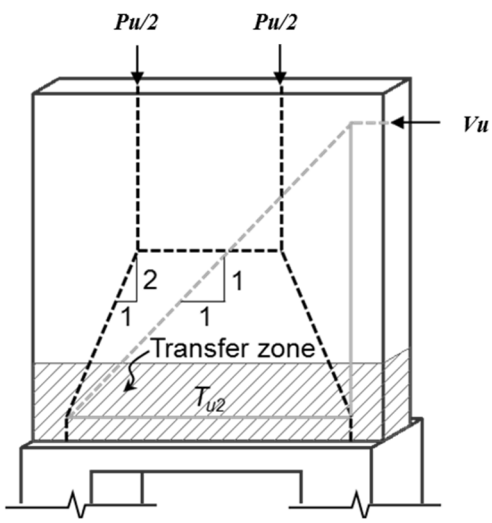

(b) Lateral reinforcement

Fig. 4-2 Design of the reinforcement

4.2.3 Test parameters

Table. 4-1 lists the test parameters of four wall specimens. Three cyclic loading tests were performed on the specimens C1, C2, and C3, and a compression test was performed on the specimen G1. The ρ_v is vertical reinforcement ratio calculated in the critical section, the A_{st} is lateral reinforcements in the transfer zone, the P_n is nominal axial capacity of the critical section, the P_u is design compression load, and the V_u is design lateral load. As main test parameters, parameter1 indicates the contribution ratio of the compressive load to lateral load at the critical section, which evaluates the effect of the magnitude of the earthquake load. Parameter2 evaluates the effect of the pilotis depth (360 mm and 450 mm).

Table. 4-1 Test parameters of test specimens

Specimens		ρ_v (%)		A_{st}	P_n (kN)	P_u (kN)	V_u (kN)	Parameter1 $P:V$	Parameter2 $B_{pilotti}$ (mm)
		Wall	Pilotis						
Compression	G1	0.37	2.98	12 - D16	3,428	3,428	-	100 : 0	360(40%)
Cyclic Loading	C1	1.32	2.98	16 - D16	3,594	1,334	801	37 : 63	360(40%)
	C2	3.13	5.38	16 - D16	3,819	860	1049	23 : 77	360(40%)
	C3	3.05	5.38	18 - D16	4,284	980	1099	23 : 77	450(50%)

4.2.4 Test specimens

Fig. 4-3 Detail of specimen C1, Fig. 4-4, Fig. 4-5 and Fig. 4-6 show the details of the each specimen. All of the specimens consisted of the wall supported by the two pilotis. The dimension of the cross-section of the wall was 1800 x 160 mm. In the case of the specimens G1, C1 and C2, the dimension of the cross-section of the pilotis was 360 x 300 mm. On the other hand, in the case of the specimen C3, the breadth of the piltois was increased from 360 mm to 450 mm.

Fig. 4-3 shows details of the specimen C1. The load contribution ratio which was referred to Parameter1 was designed by $P : V = 37 : 63$. In the critical section of the upper wall, 6-D13 were placed as vertical reinforcement. In the same area of the pilotis, as the vertical reinforcement, 6-D19 were placed. From this design results, the load carrying capacity of the pilotis and transfer zone were greater than that of the upper wall. In the transfer zone, as the lateral reinforcement, pairs of D16 U-shaped stirrups were inserted on both side and welded in the middle of the wall to make fully closed-hoop. Additionally, D10 hooks were placed alternately in order to prevent the buckling of the vertical reinforcement in the transfer zone.

Fig. 4-4 shows details of the specimen C2. The load contribution ratio was designed by $P : V = 23 : 77$. In the critical section of upper wall, 2-D13 and 4-D22 were placed as vertical reinforcement. In the same area of the pilotis, as the vertical reinforcement, 4-D22 came from the upper wall and additional 4-D22 were placed in the transfer zone. The details of lateral reinforcement were same with those of C1.

Fig. 4-5 shows details of the specimen C3. The load contribution ratio which was referred to Parameter1 was designed by $P : V = 23 : 77$. Additionally, the breadth of the pilotis was increased to 450 mm. In the critical section of the upper wall, 2-D13, 2-D16 and 4-D22 were placed as vertical reinforcement. In the same area of the pilotis, as the vertical reinforcement, 4-D22 came from the upper wall and additional 6-D22 were placed in the transfer zone.

Fig. 4-6 shows details of the specimen G1. In the upper wall, 9-D10 were placed as the vertical reinforcement, which was satisfying the reinforcement ratio limit ($\rho = 0.25\%$). In the pilotis, as the vertical reinforcement, 6-D19 were placed and they

were embedded in the transfer zone.

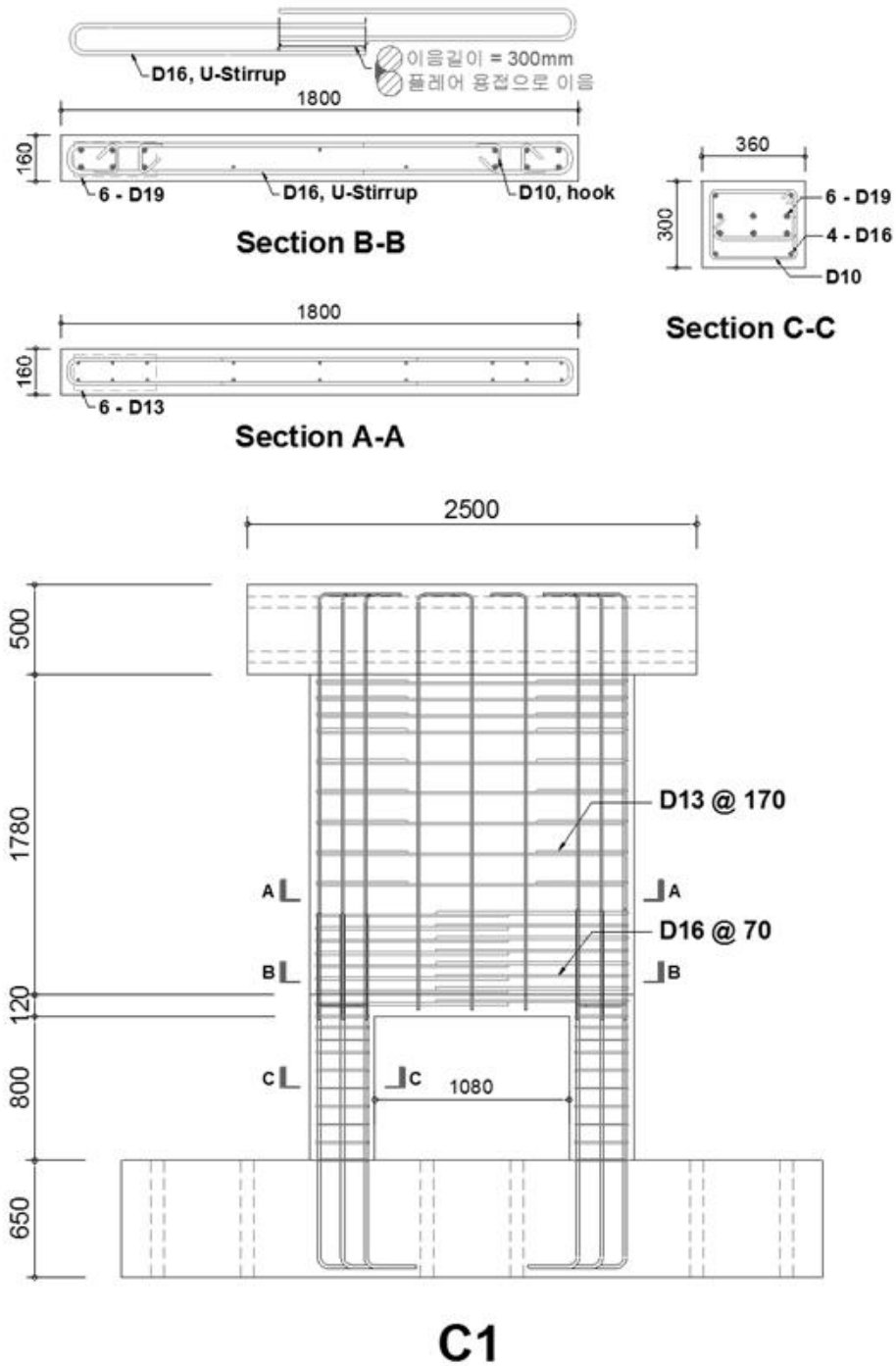

Fig. 4-3 Detail of specimen C1

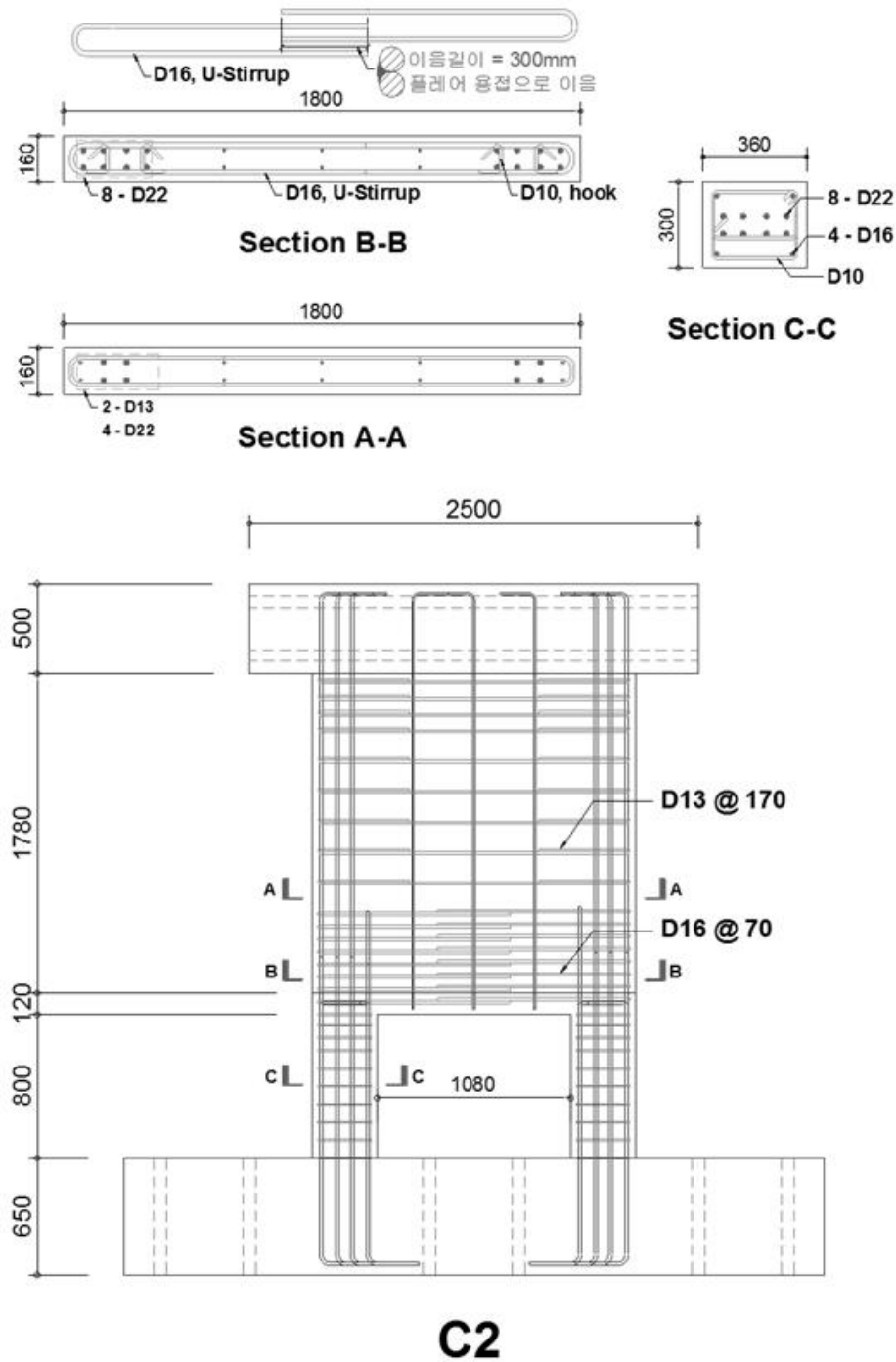

Fig. 4-4 Detail of specimen C2

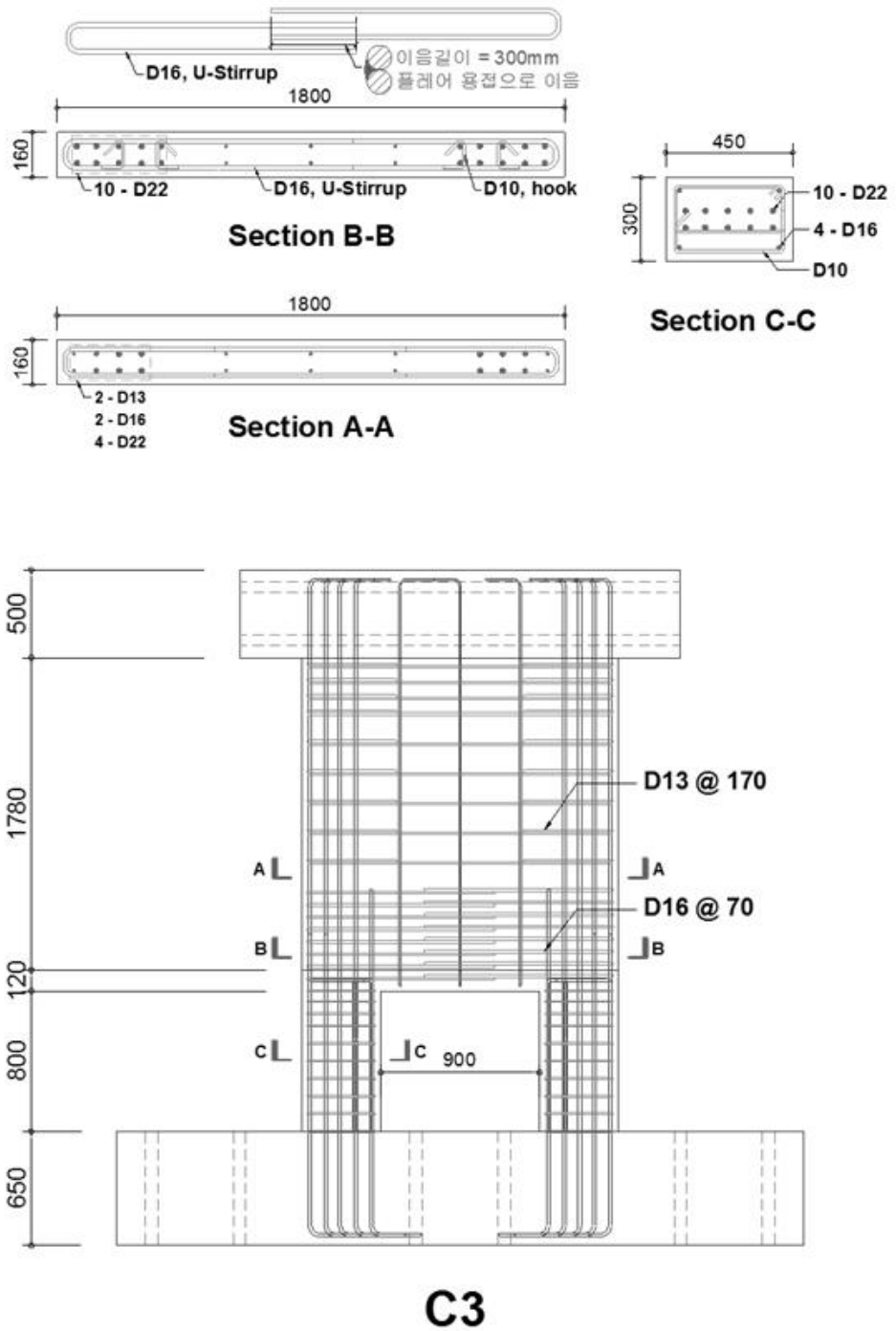

Fig. 4-5 Detail of specimen C3

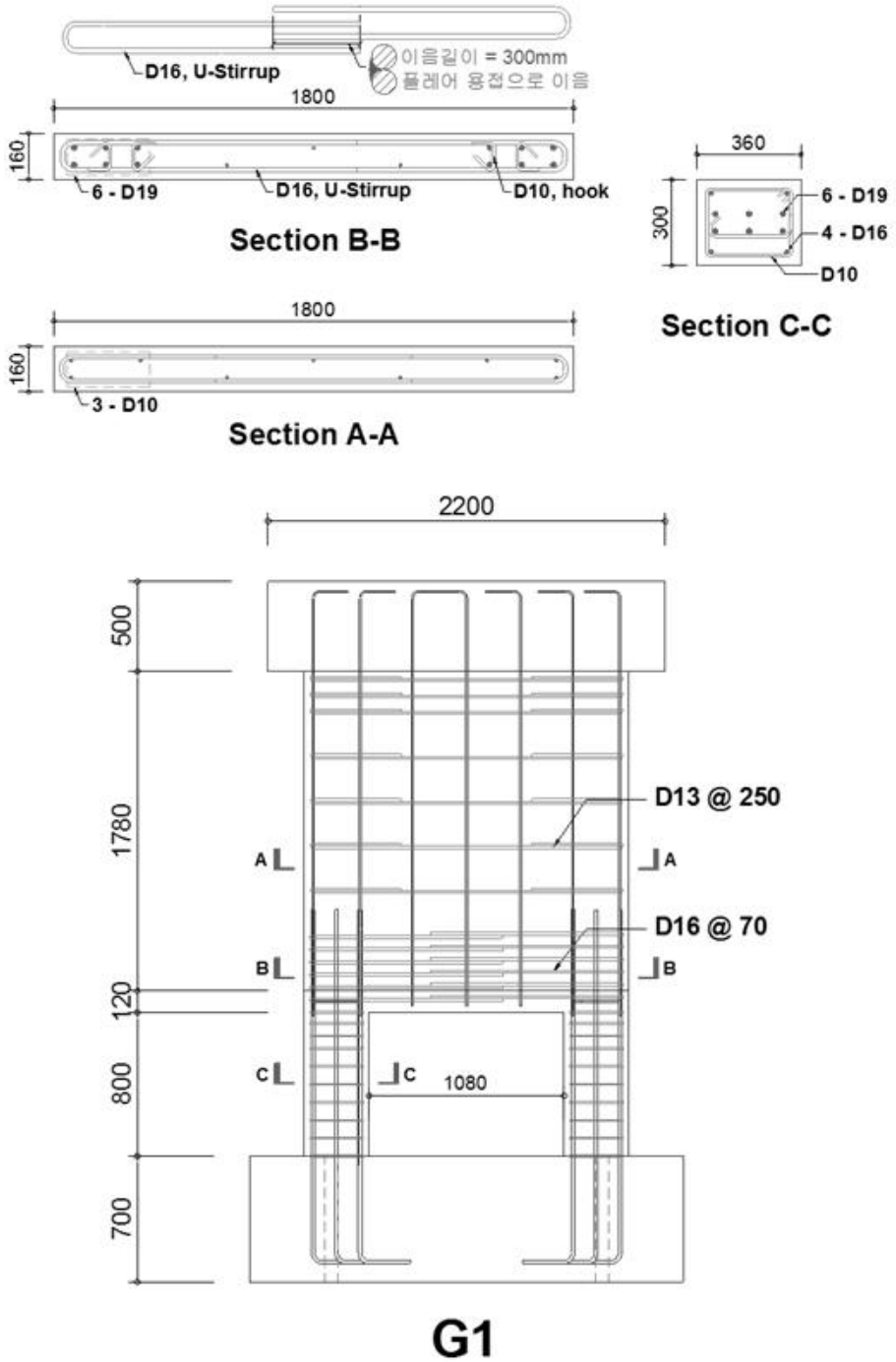

Fig. 4-6 Detail of specimen G1

Fig. 4-7 shows procedures for manufacture of the specimens. The each specimen had a lot of cross-sectional changes. For this reason, it was produced while lying down in order to reduce the number of concrete pouring and to ensure the same concrete strength in the whole specimen.

First the reinforcement was arranged according to the design drawings. The fully closed-hoops which were placed in the transfer zone were formed by inserting pairs of the U-shaped stirrups and welding. After the arrangement of reinforcement, strain gauges which were used to measure the longitudinal strain of re-bars were installed in the surface of the re-bars.

After completing the form work, concrete was poured. The target strength of the concrete was 35MPa. In order to confirm the concrete strength, standard specimens of concrete were made. The surface of the concrete was carefully treated since the specimen was lying. The bolts which were used to install LVDTs were inserted before curing the concrete. After finishing the concrete curing, each specimen was lifted by crane and transported.

(a) Arrangement re-bar

(b) U-shaped stirrups welding

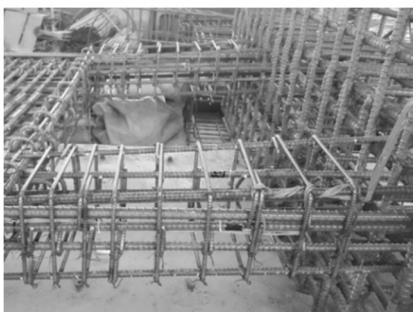

(c) Strain gauge installation

(d) Concrete pouring

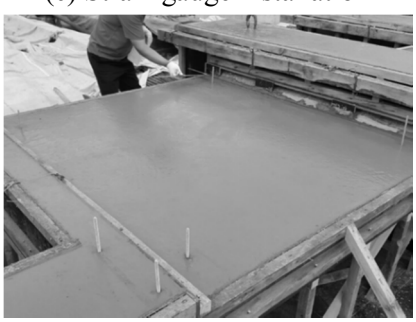

(e) Surface treatment

(f) Specimens lifting

(g) Completed specimen

Fig. 4-7 Procedures for manufacture of the specimens

4.2.5 Test setups

Fig. 4-8 (a) shows the test setups for cyclic loading tests. The pilotis-wall framing system is subjected to earthquake loads while gravity loads are loaded. In order to simulate this situation, by using two 300t actuators, cyclic lateral loading was applied to the test specimens subjected to uniform compression load. Table. 4-2 shows the concrete strength and the uniform compression load for each specimens.

The cyclic loading protocol was planned according to ACI 374.2R-13 (ACI 2013). Fig. 4-9 shows loading pattern of the cyclic loading and Table. 4-3 shows numerical value of lateral displacement and drift ratio of each step. Uniform compression load was calculated according to the concrete strength of the day of test.

In the case of actual apartment building system, by diaphragm action of second floor slab, pilotis behave with other walls in the first floor. As a result, the lateral deformation of pilotis can be limited. In fact, as shown in Fig. 4-10, it was confirmed from the preliminary analysis results that the lateral drift ratio of the pilotis is considerably smaller than that of the wall in the upper stories. To simulate this behavior, on the second floor slab of the specimens, soft lateral supports were applied. These supports were able to move slightly due to load cells which were installed on the tip of the supports and remained elastic state during applying loads. In order to measure the lateral deformation, LVDT was set in the center of loading point.

Table. 4-2 Concrete strength and uniform compression load

Specimen	f_{ck} (N/mm^2)	P_u (kN)
C1	36.7	1334
C2	39	860
C3	35	980

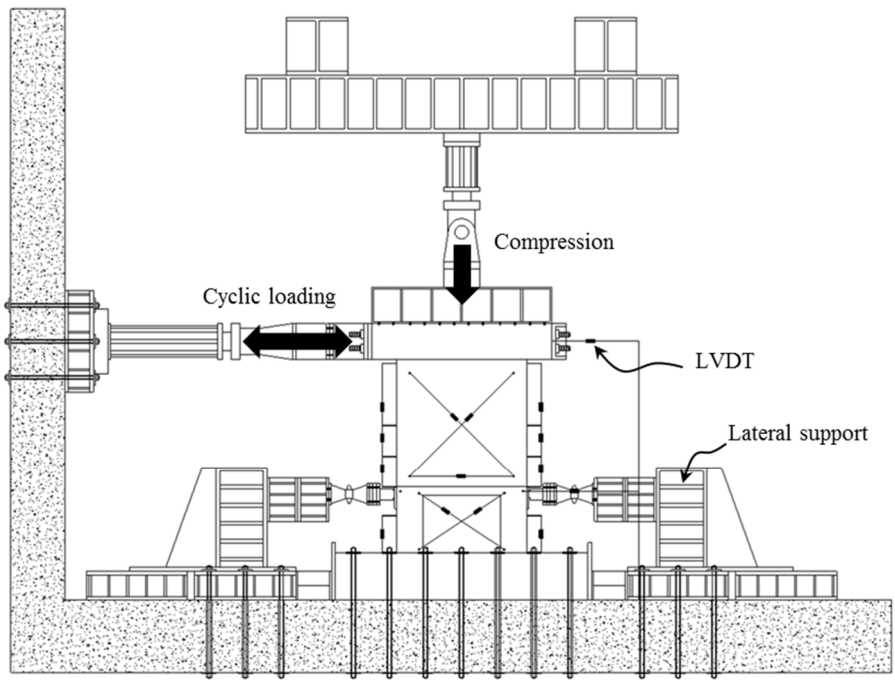

(a) Cyclic loading test setup

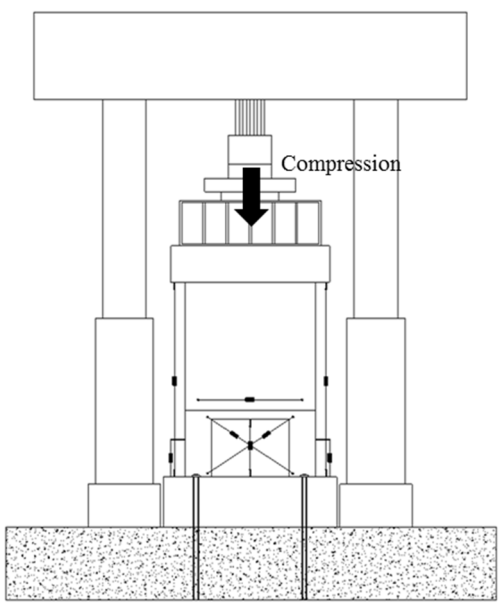

(b) Compression test setup

Fig. 4-8 Test setup

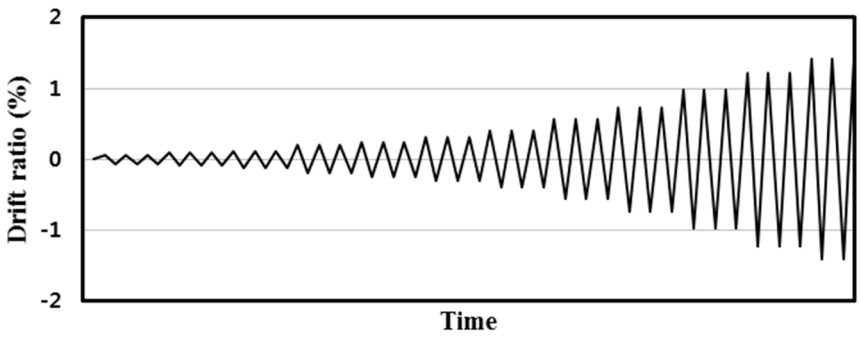

Fig. 4-9 Loading protocol

Table. 4-3 Value of cyclic loading protocol

Load Step	Lateral Deformation (mm)	Lateral Drift ratio (%)
STEP1	±1.76	±0.06
STEP2	±2.74	±0.09
STEP3	±3.52	±0.12
STEP4	±4.69	±0.16
STEP5	±5.87	±0.20
STEP6	±7.24	±0.25
STEP7	±9.19	±0.31
STEP8	±11.93	±0.40
STEP9	±16.43	±0.56
STEP10	±21.52	±0.73
STEP11	±28.95	±0.98
STEP12	±35.99	±1.22
STEP13	±41.47	±1.41

Fig. 4-8 (b) shows the test setup for compression test. To evaluate the axial load carrying capacity of the specimen, by using 1000t UTM(Universal Test Machine), the uniform compression load was applied until failure.

By using roller guide, the lateral support was applied on the center of the wall in order to prevent strength reduction due to the out-plane buckling. Fig. 4-11 shows the completed setups in the laboratory.

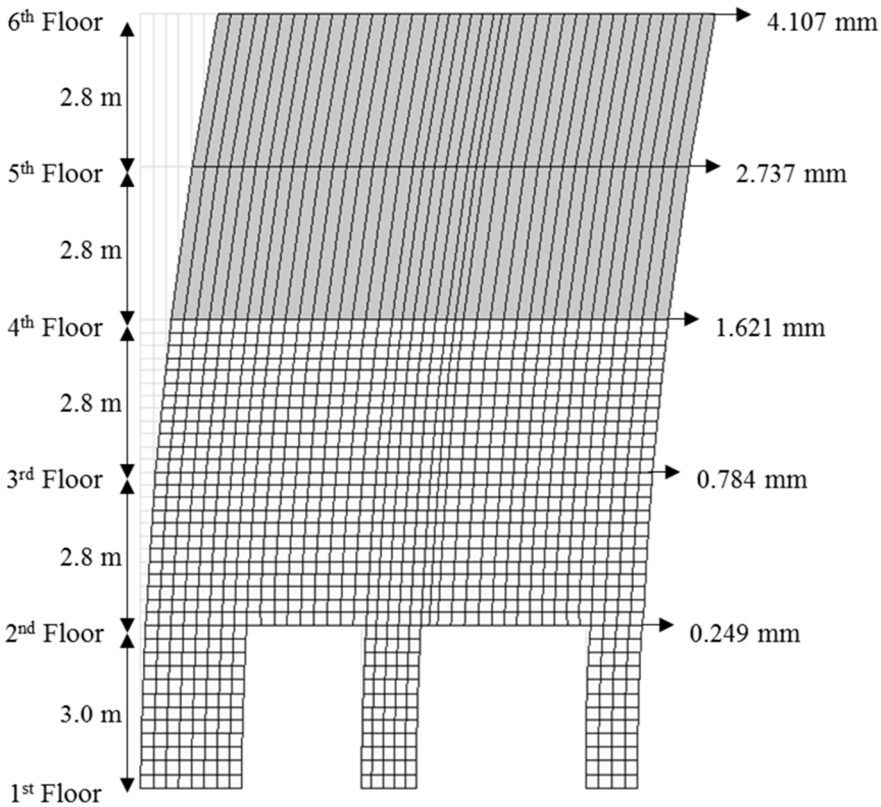

(a) Lateral displacement

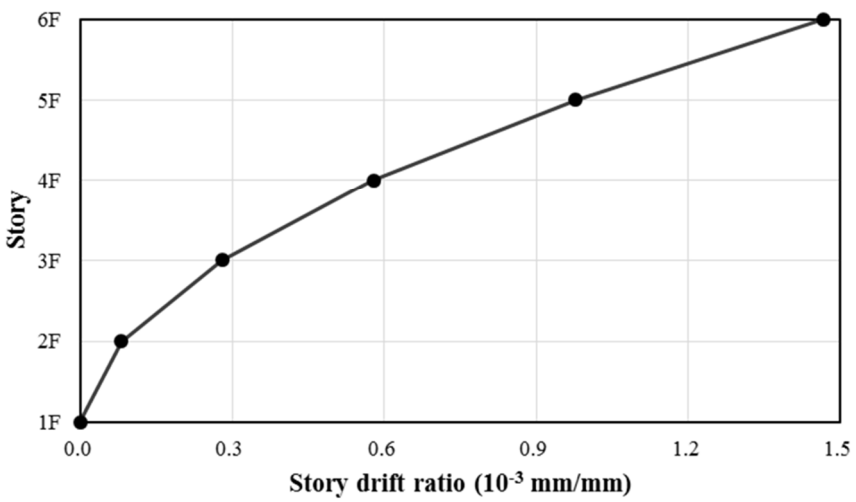

(b) Story drift ratio

Fig. 4-10 Lateral displacement and story drift ratio of pilotis-wall system

(a) Cyclic loading test setup

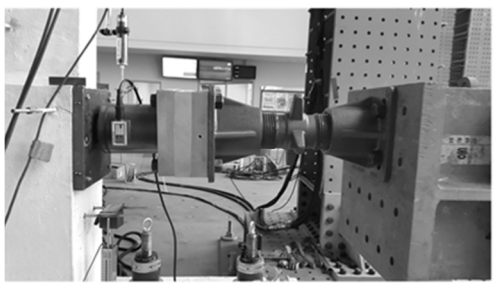

(b) Lateral support

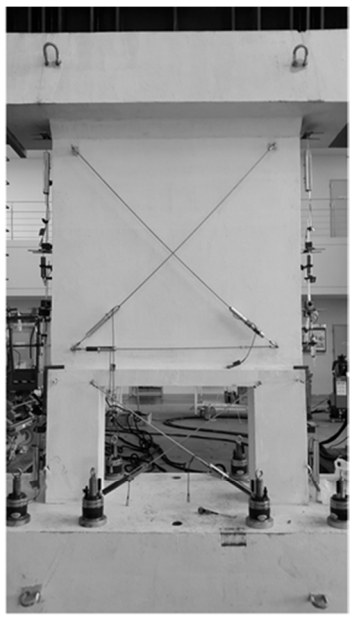

(c) Installation of LVDT

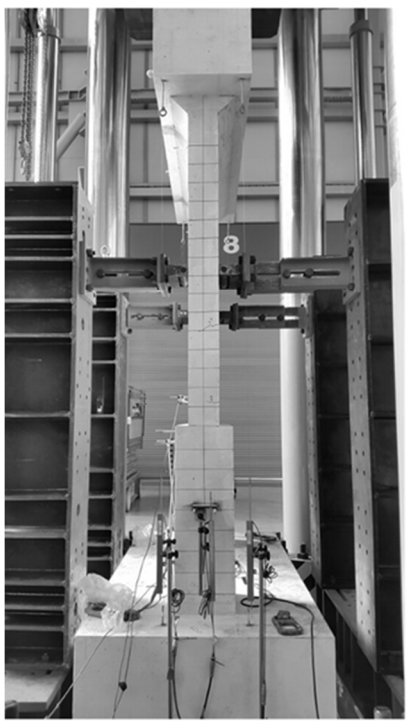

(d) Lateral support

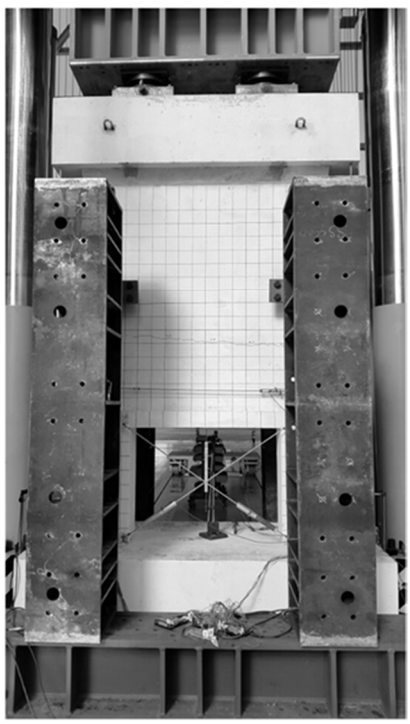

(e) Compression test setup

Fig. 4-11 Setups in the laboratory

4.3 Test results

4.3.1 Cyclic loading tests

(a) Lateral load – drift ratio relationships

Fig. 4-12 shows the lateral load – drift ratio relationships. The lateral drift ratio was calculated from the lateral drift at the loading point and net height of the wall (=2150 mm). The peak strengths V_{exp} of all specimens were greater than the design strength V_u. All of the specimens showed ductile behavior after yielding, and concrete crushing occurred at δ = 1.0 to 1.5% in the compression region.

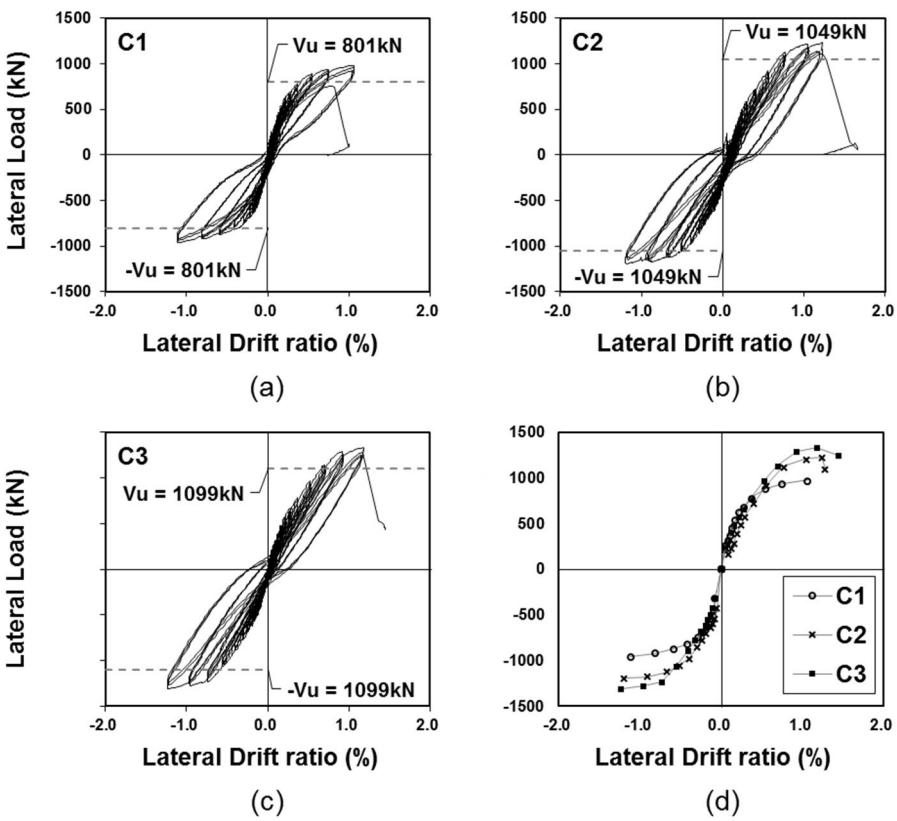

Fig. 4-12 Lateral load – drift ratio relationships of specimens

In the case of specimen C1, the average concrete strength of the day of the test was 36.7MPa. From this, the uniform compression load was calculated as 1,334kN. Fig. 4-12 (a) shows the lateral load - drift ratio relationships of specimen C1. In the early stage of the load steps, the slope of the graph was constant because the specimen was in the elastic state. However, after the horizontal cracks started to occur at δ = 0.25%, the amount of the energy dissipation was increased and the slope of the graph became gradually gentle.

In the positive direction, the peak strength V_{exp} of specimen C1 was 979kN, which was 22% larger than the design strength $V_{u.}$ = 801kN. In the negative direction, the peak strength V_{exp} was -962kN, which was 20% larger than the design strength. The ultimate drift ratio was 1.12% and the test was terminated at the fist cycle of the 12th load step due to the concrete crushing at the compression side.

In the case of specimen C2, the average concrete strength of the day of the test was 39MPa. From this, the uniform compression load was calculated as 860kN. Fig. 4-12 (b) shows the lateral load - drift ratio relationships of specimen C2. Similarly, the slope of the graph was constant in the early stage of the load steps, however, after the horizontal cracks started to occur at δ = 0.09%, the amount of the energy dissipation was increased and the slope of the graph became gradually gentle.

In the positive direction, the peak strength V_{exp} of specimen C2 was 1,231kN, which was 17% larger than the design strength $V_{u.}$ = 1049kN. In the negative direction, the peak strength V_{exp} was -1193kN, which was 14% larger than the design strength. The ultimate drift ratio was 1.29% and the test was terminated at the fist cycle of the 13th load step due to the concrete crushing at the compression

side.

In the case of specimen C3, the average concrete strength of the day of the test was 35MPa. From this, the uniform compression load was calculated as 980kN. Fig. 4-12 (c) shows the lateral load - drift ratio relationships of specimen C3. Similarly, the slope of the graph was constant in the early stage of the load steps, however, after the horizontal cracks started to occur at δ = 0.06%, the amount of the energy dissipation was increased and the slope of the graph became gradually gentle.

In the positive direction, the peak strength V_{exp} of specimen C2 was 1,334kN, which was 21% larger than the design strength V_u. = 1099kN. In the negative direction, the peak strength V_{exp} was -1310kN, which was 19% larger than the design strength. The ultimate drift ratio was 1.44% and the test was terminated at the fist cycle of the 13th load step due to concrete crushing at the compression side. Table. 4-4 shows the comparison of the test results and predictions.

Fig. 4-12 (d) shows the envelop curves of the each specimen. The envelope curve was plotted from the lateral load – drift ratio relationships by connecting the maximum drift ratio point of first cycle of each load step. By using these curve, the ductility of each specimen was evaluated. The maximum drift ratio δ_u was defined at the failure. The yield drift ratio δ_y was calculated based on equivalent elasto – plastic energy absorption model (Park 1988). According to this model, by the assumption that total energy dissipation should be constant, the lower area of envelop curve and that of the equivalent elasto-plastic curve were same. Thus, the yield drift ratio was able to be calculated as follows:

$$A_{envelop} = \sum_{i=1}^{n}(P_i - P_{i-1})\delta_i \quad (4\text{-}7)$$

$$A_{e-p} = P_u\delta_u - 1/2P_u\delta_y \quad (4\text{-}8)$$

$$\therefore\ \delta_y = 2\delta_u - \frac{2}{P_u}\sum_{i=1}^{n}(P_i - P_{i-1})\delta_i \quad (4\text{-}9)$$

Where the $A_{envelop}$ is lower area of the envelop curve, the $A_{e\text{-}p}$ is lower area of the elasto-plastic curve, the P_i is lateral load of ith load step, the $P_{i\text{-}1}$ is lateral load of i-1th load step, the P_u is peak load, the δ_i is drift ratio of ith load step, the δ_y is yield drift ratio and the δ_u is maximum drift ratio.

Table. 4-5 shows the yield drift ratio, the maximum drift ratio, the ductility and the yield stiffness of the specimens. The ductility was calculated by dividing the maximum drift ratio by the yield drift ratio. In the case of the specimen C1 which had a greater axial force ratio, the ductility was greater than that of the others due to the greater yield stiffness. In the case of the specimen C3 which had a larger breadth of pilotis, the ductility was less than that of the others. However, it carried a greater ultimate strength than the others.

Table. 4-4 Comparison of the test results and predictions

Specimen	Test Results		Predictions	Ratio	
	V_{peak} (kN)		V_u (kN)	V_{peak} / V_u	
	Positive	Negative.		Positive	Negative
C1	978.68	-961.48	801	1.22	1.20

C2	1230.94	-1193.03	1049	1.17	1.14
C3	1334.32	-1309.91	1099	1.21	1.19

Table. 4-5 Summary of the yield drift ratio and ductility

Specimen	Yield Drift (mm)		Maximum Drift (mm)		Ductility		Yield Stiffness
	Δ_y (δ_y)		Δ_u (δ_u)		μ ($=\delta_y/\delta_u$)		k_y ($=V_u/\Delta_y$)
	Positive	Negative	Positive	Negative	Positive	Negative	
C1	9.6 (0.44)	8.8 (0.41)	22.8 (1.06)	24.0 (1.12)	2.4	2.7	102.3
C2	16.1 (0.75)	9.2 (0.43)	27.5 (1.29)	25.7 (1.20)	1.7	2.8	76.4
C3	15.4 (0.72)	12.9 (0.60)	31.0 (1.44)	26.5 (1.22)	2.0	2.1	86.5

(b) Failure modes and crack patterns

Fig. 4-13, Fig. 4-14, Fig. 4-15 and Fig. 4-16 show failure modes and crack patterns of the specimens. In the case of all of the specimens, concrete cracks occurred at the upper wall rather than the pilotis, which was intended in the capacity design. At the final stage of load step, after the concrete cover was eliminated, the concrete crushing occurred with buckling of re-bars at the compression side.

Fig. 4-14 shows crack patterns of specimen C1. At the early stage of the load step, concrete cracks were not observed since the tensile force due to the lateral load was smaller than the compression force. The first horizontal cracks were observed at δ = 0.25% at the tension side of the upper wall. Diagonal cracks were

developed from the horizontal cracks and they were observed over the entire wall surface.

Eventually, concrete crushing occurred at the height of 400mm from the bottom face of the wall. On the other hand, damages in the pilotis were limited. After the end of the test, the concrete cover was removed to observe the state of re-bars in the failure part. All of the re-bars which were in the critical section of the upper wall were buckled, however, damages on the re-bars which were in the critical section of the transfer zone were not observed.

Fig. 4-15 shows the crack patterns of specimen C2. Concrete cracks were able to be observed at the early stage of the load step since the compression force was smaller than that of the specimen C1. The first horizontal cracks were observed at δ = 0.09% at the tension side of the upper wall. Diagonal cracks were developed from horizontal cracks and they were observed over the entire wall surface.

Finally, concrete crushing occurred at the height of 400mm from the bottom face of the wall. On the other hand, damages in the pilotis were limited. Additionally, all of the re-bars which were in the critical section of the upper wall were buckled.

However, the degree of damages due to buckling was less than that of the specimen C1 because of the smaller compression load. Damages on the re-bars which were in the critical section of the transfer zone were not observed.

Fig. 4-16 shows crack patterns of specimen C3. The first horizontal cracks were observed at δ = 0.06% at the tension side of the upper wall. Diagonal cracks were observed over the entire wall surface.

Finally, concrete crushing occurred at the height of 600mm from the bottom face of the wall. On the other hand, damages in the pilotis were limited. Damages on the re-bars were not able to be observed since the degree of concrete crushing was little.

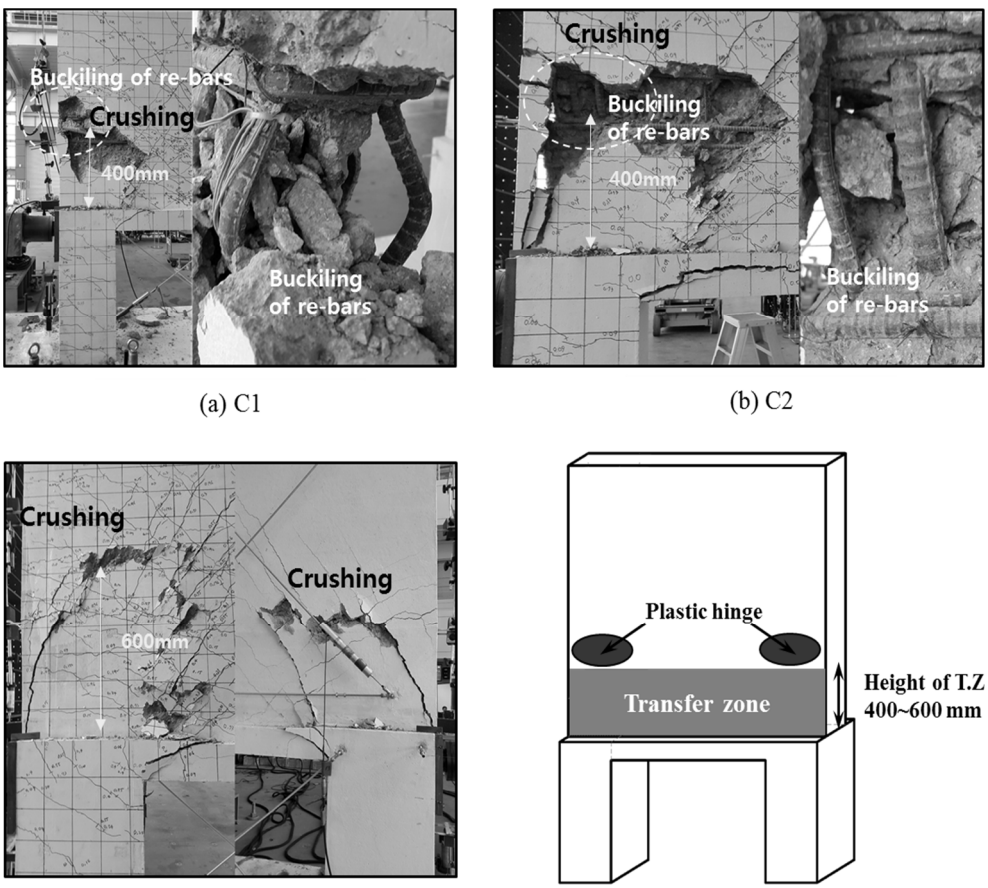

(a) C1

(b) C2

(c) C3

Fig. 4-13 Failure modes at the end of the tests

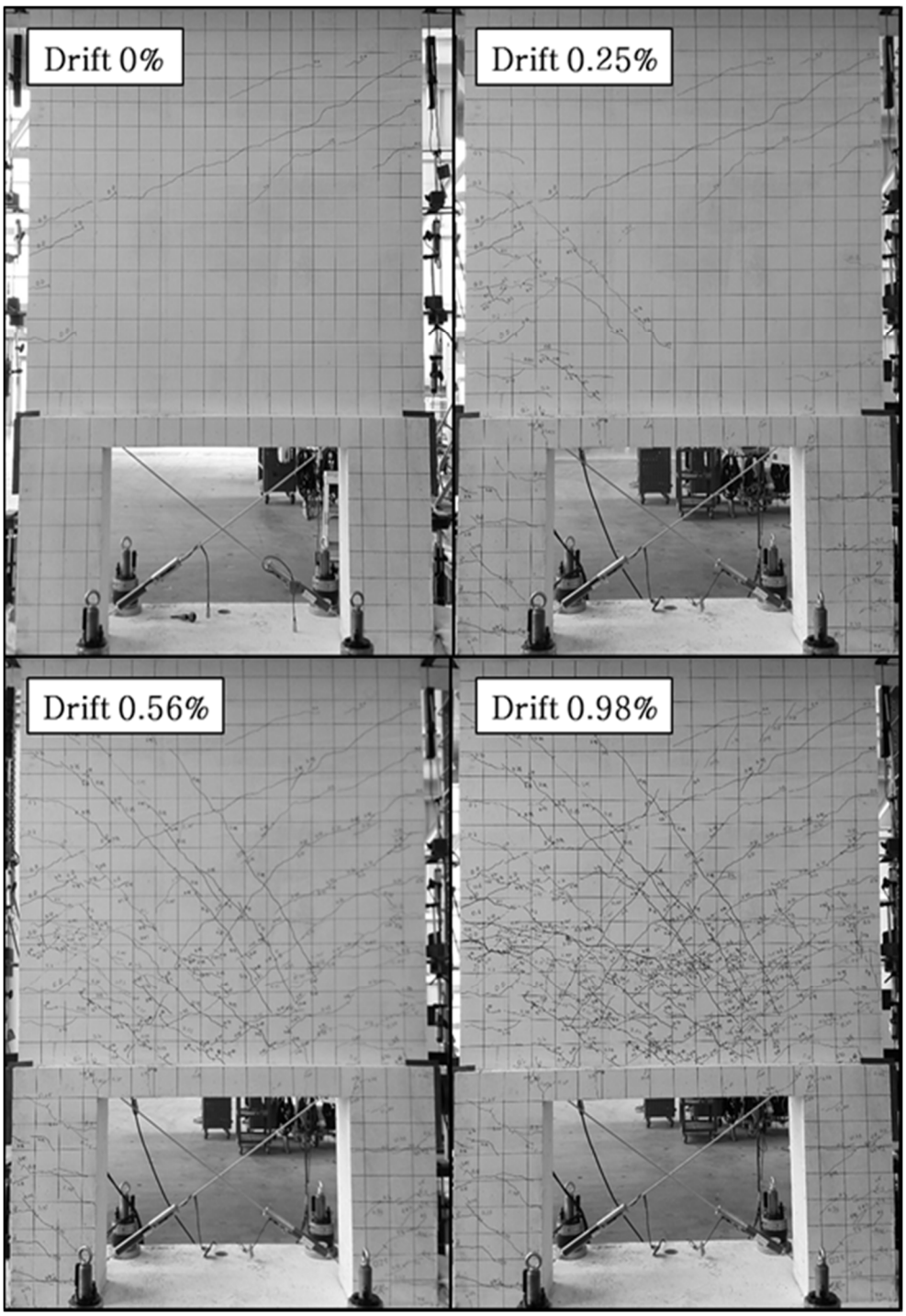

Fig. 4-14 Crack patterns of C1

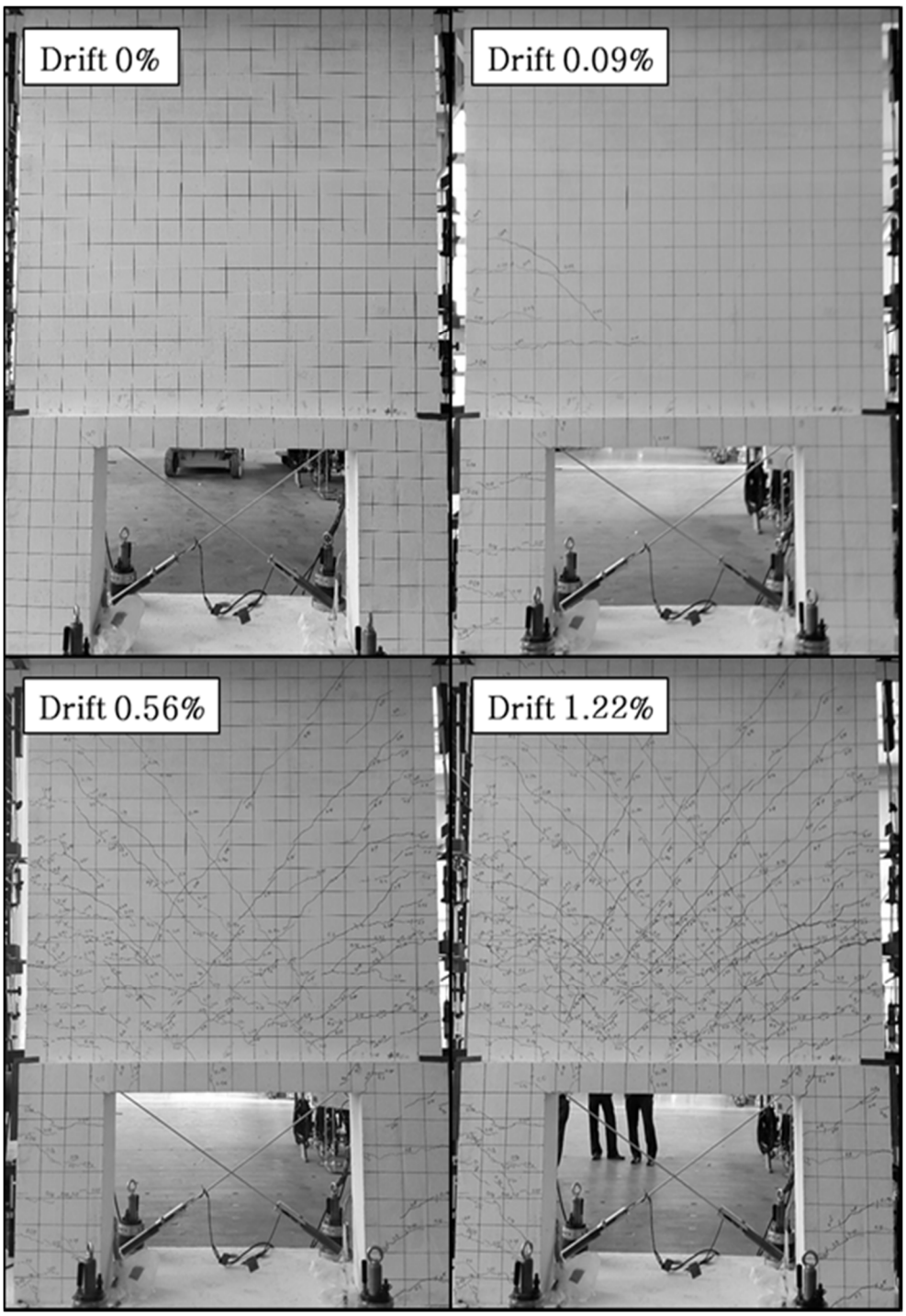

Fig. 4-15 Crack patterns of C2

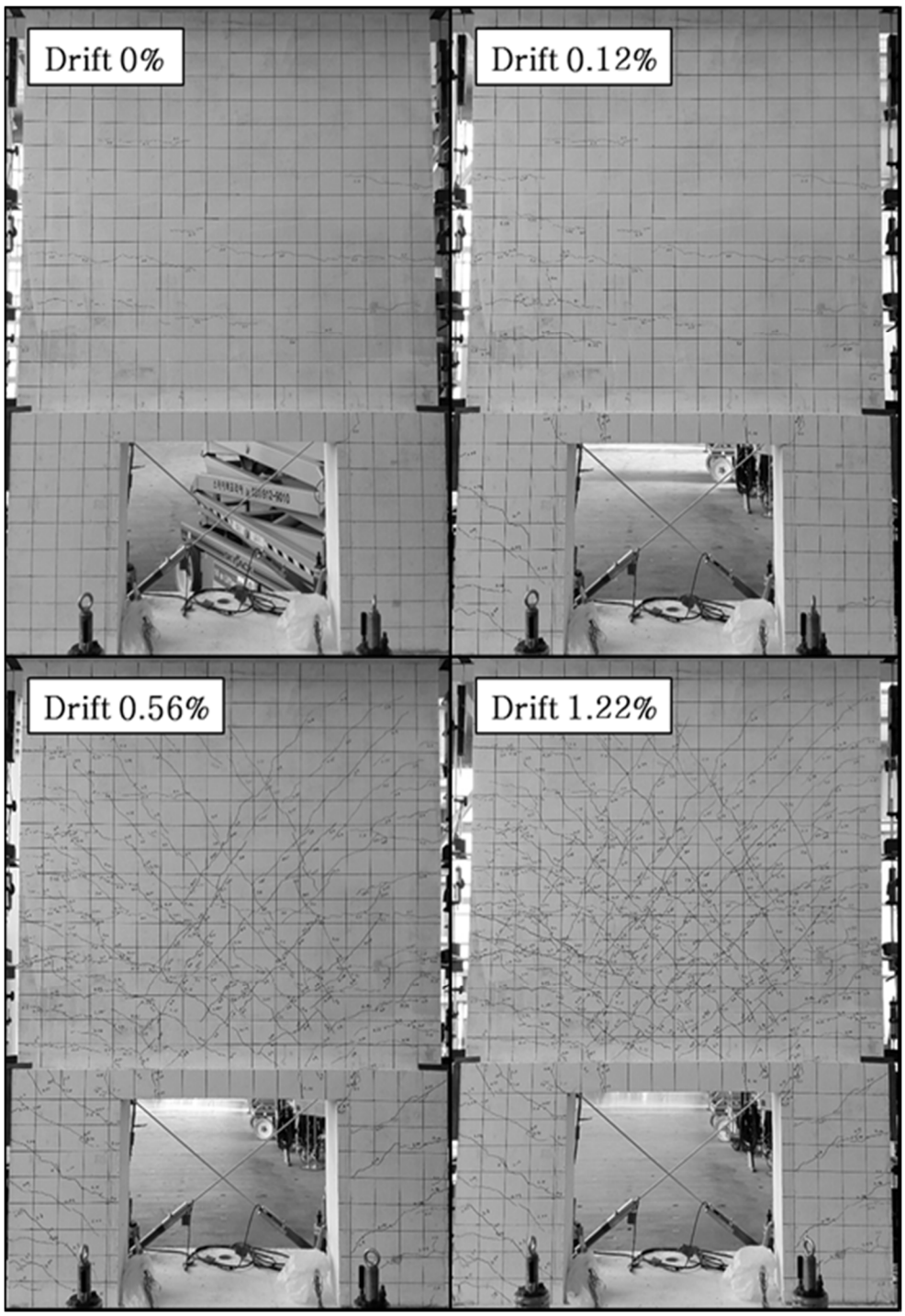

Fig. 4-16 Crack patterns of C3

(c) Strain of the re-bars

Fig. 4-17 shows the re-bar strains. In the pilotis and transfer zone, rebar strains were less than the yield strain Fig. 4-17 (a) to (c). In the upper wall, however, rebar strains exceeded the yield strain as the load increases. This is because the damage was concentrated and the rebar buckling occurred in the upper wall.

Table. 4-6 shows the summary of the maximum values of the re-bar strains. In the case of each specimen, the maximum strain values of vertical re-bars in the pilotis were 0.0014, 0.0029 and 0.0022, which means that all of them were in elastic state during the tests. Furthermore, the maximum strain values of re-bars in the transfer zone were 0.0015, 0.0012 and 0.0012 for vertical re-bars and 0.0028, 0.0027, 0.0030 for lateral re-bars. This means that they were also in the elastic state during the test. In the case of vertical re-bars in the upper wall, however, the maximum strain values were much greater than the yield strain due to reaching plastic state. Therefore, from the test results, it was determined that the plastic hinge occurred in the upper wall as it intended in the design. As a result, the damages on the pilotis and transfer zone were limited.

Table. 4-6 Maximum strain value of re-bars

Strain (mm/mm)	Vertical re-bars			Lateral re-bars
	Pilotis	Upper wall	Transfer zone vertical	Transfer zone lateral
C1	0.0014	1.0000	0.0015	0.0028
C2	0.0029	1.0000	0.0012	0.0027
C3	0.0022	0.0269	0.0012	0.0030

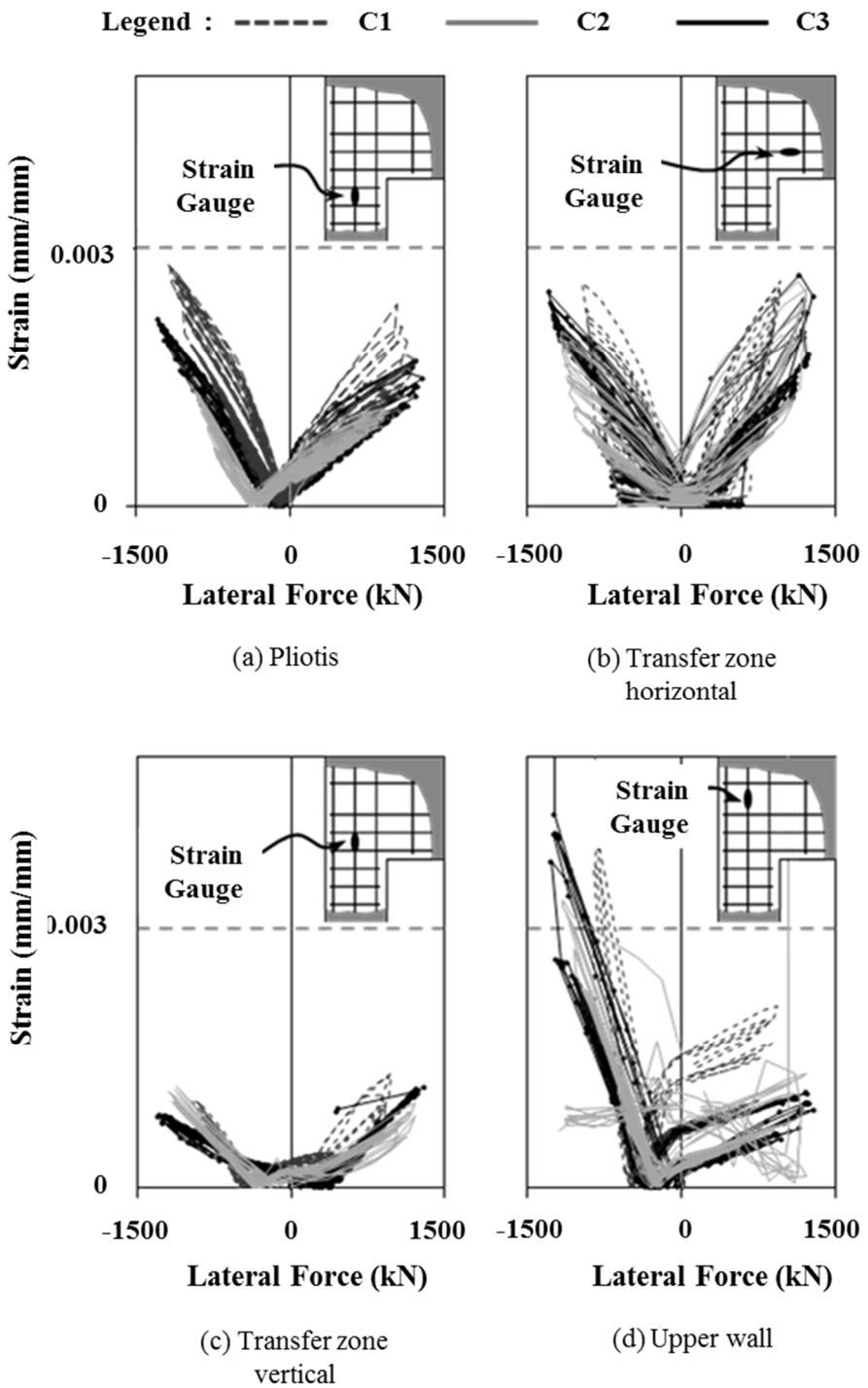

Fig. 4-17 Rebar strains of the specimens under cyclic loading

4.3.2 Compression Test

(a) Lateral load – drift ratio relationships

Fig. 4-18 shows the axial load – strain relationships. The axial strain was calculated from the average axial shortening at the four corner and net height of the specimen (=2700 mm). In the case of specimen G1, the average concrete strength of the day of the test was 35MPa. From this, the expected nominal strength P_n was calculated as 3,748kN. The peak strength P_u was 5,414kN which was 1.44 times the nominal strength. The crushing of the concrete occurred at P_{cr} = 5,342kN in the compression region. Table. 4-7 Summary of the compression test shows the summary of the compression test.

Table. 4-7 Summary of the compression test

Specimen	Pu (kN)	εu (mm/mm)	εcr (mm/mm)	Ki (kN/mm)	Pn (kN)	Pu/Pn (ratio)
G1	5414	0.00190	0.00195	1128	3748	1.44

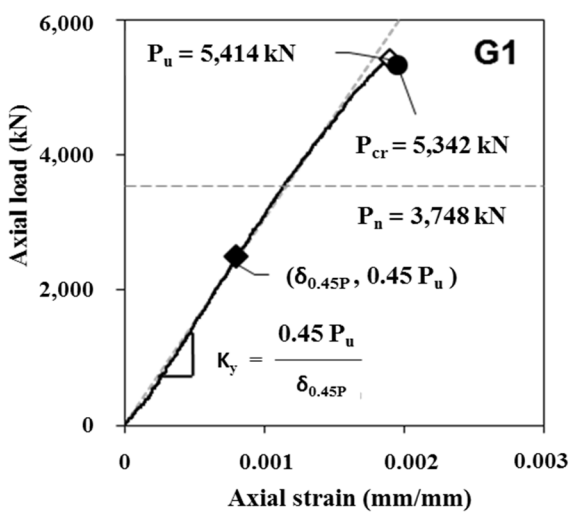

Fig. 4-18 Axial load – strain relationships

(b) Failure mode and crack pattern

Fig. 4-20 shows the crack patterns of specimen G1. At P = 900kN, the vertical cracks were observed at the bottom of the slab. And the diagonal cracks were developed from the vertical cracks.

Eventually, concrete crushing occurred at the height of 300mm from the bottom face of the wall. On the other hand, the damages in the pilotis were limited. After the end of the test, the concrete cover was removed to observe the state of re-bars in the failure part. All of the re-bars which were in the critical section of the upper wall were buckled, however, the damages on the re-bars which were in the critical section of the transfer zone were not observed. Fig. 4-19 shows damages in the specimen.

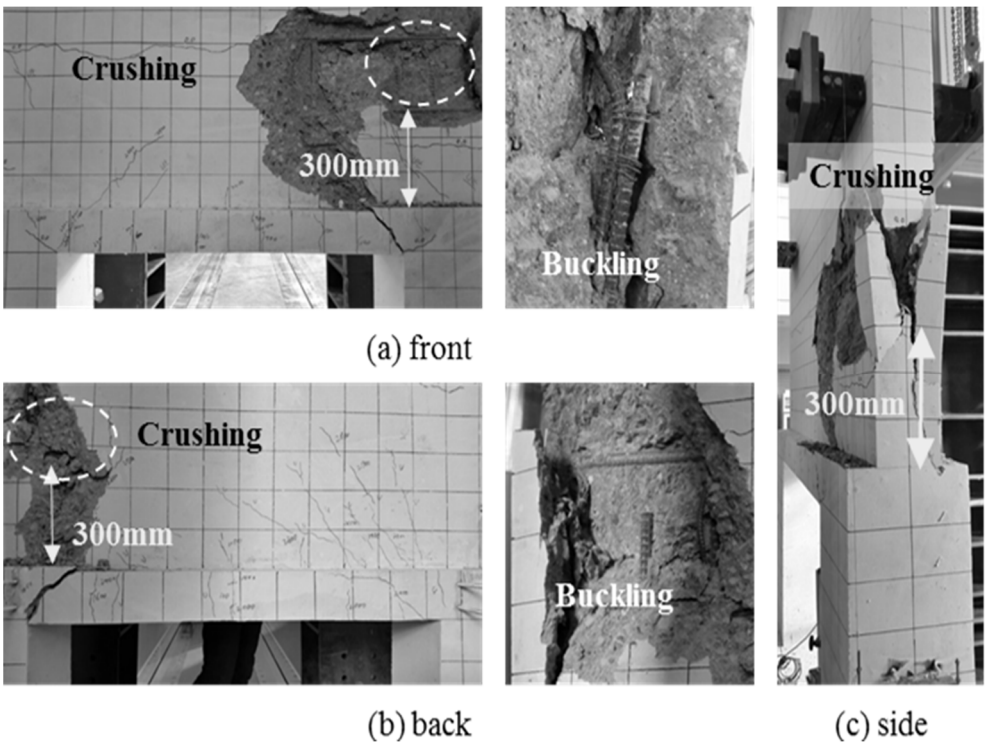

Fig. 4-19 Failure modes at the end of the test

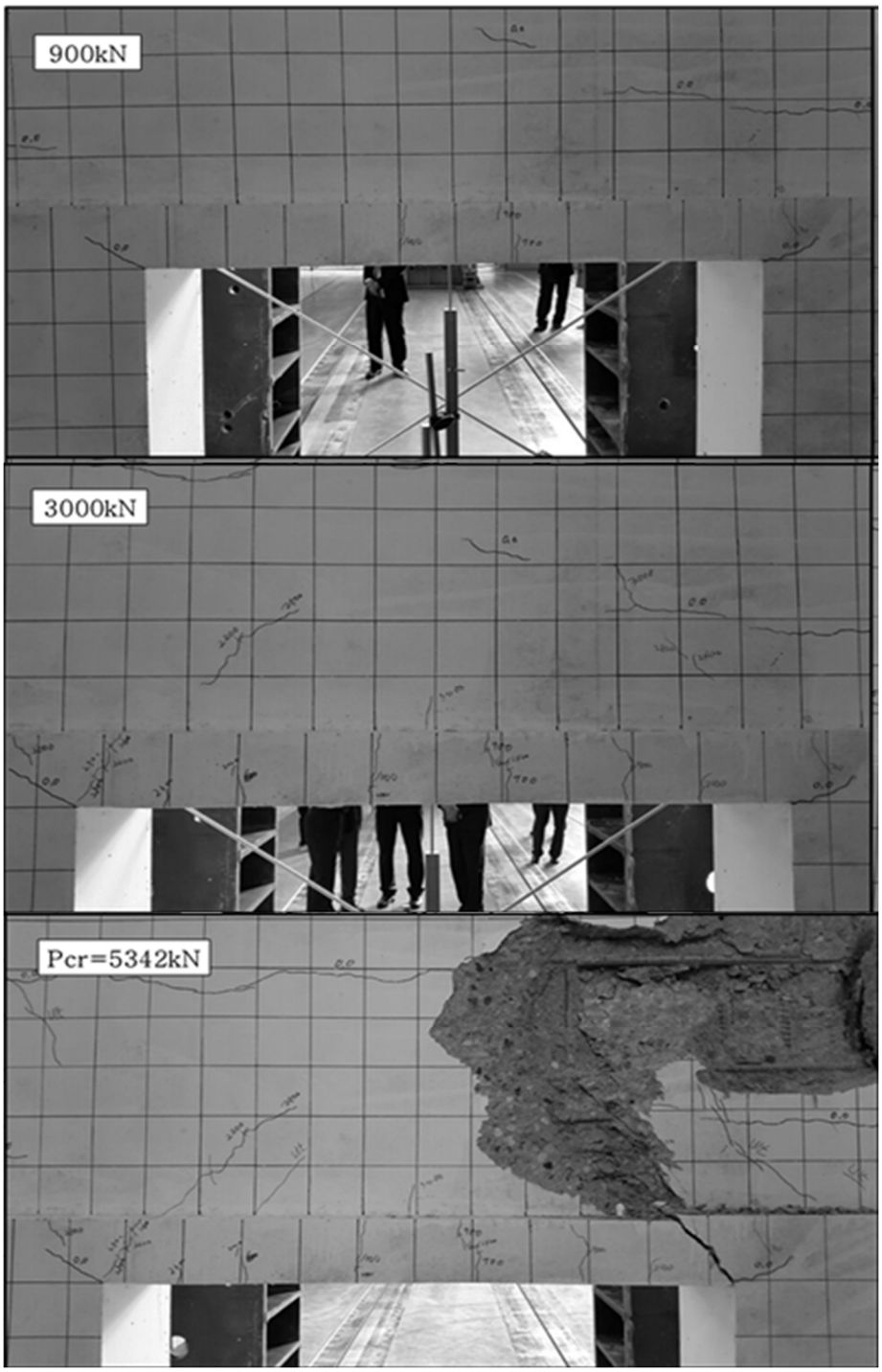

Fig. 4-20 Crack patterns in specimen G1

(c) Strain of the re-bars

Fig. 4-21 shows the re-bar strains. In the pilotis and transfer zone, rebar strains were less than the yield strain [Figs. 7(a) to (c)]. In the upper wall, however, rebar strains exceeded the yield strain as the load increases. This is because the damage was concentrated and the rebar buckling occurred in the upper wall.

Table. 4-8 shows the summary of the maximum values of the re-bar strains. The maximum strain values of vertical re-bars in the pilotis and rebars in the transfer zone were 0.0011, 0.0015 and 0.0013, which means that all of them were in elastic state during the tests. In the case of vertical re-bars in the upper wall, however, the maximum strain values were greater than the yield strain due to reaching compressive plastic state. Therefore, from the test results, it was determined that the system was able to transfer the axial load until failure of the upper wall while the damages on the pilotis and transfer zone were limited.

Table. 4-8 Maximum strain value of re-bar

Strain (mm/mm)	Vertical re-bars			Lateral re-bars
	Pilotis	Upper wall	Transfer zone vertical	Transfer zone lateral
G1	0.0011	0.0024	0.0015	0.0013

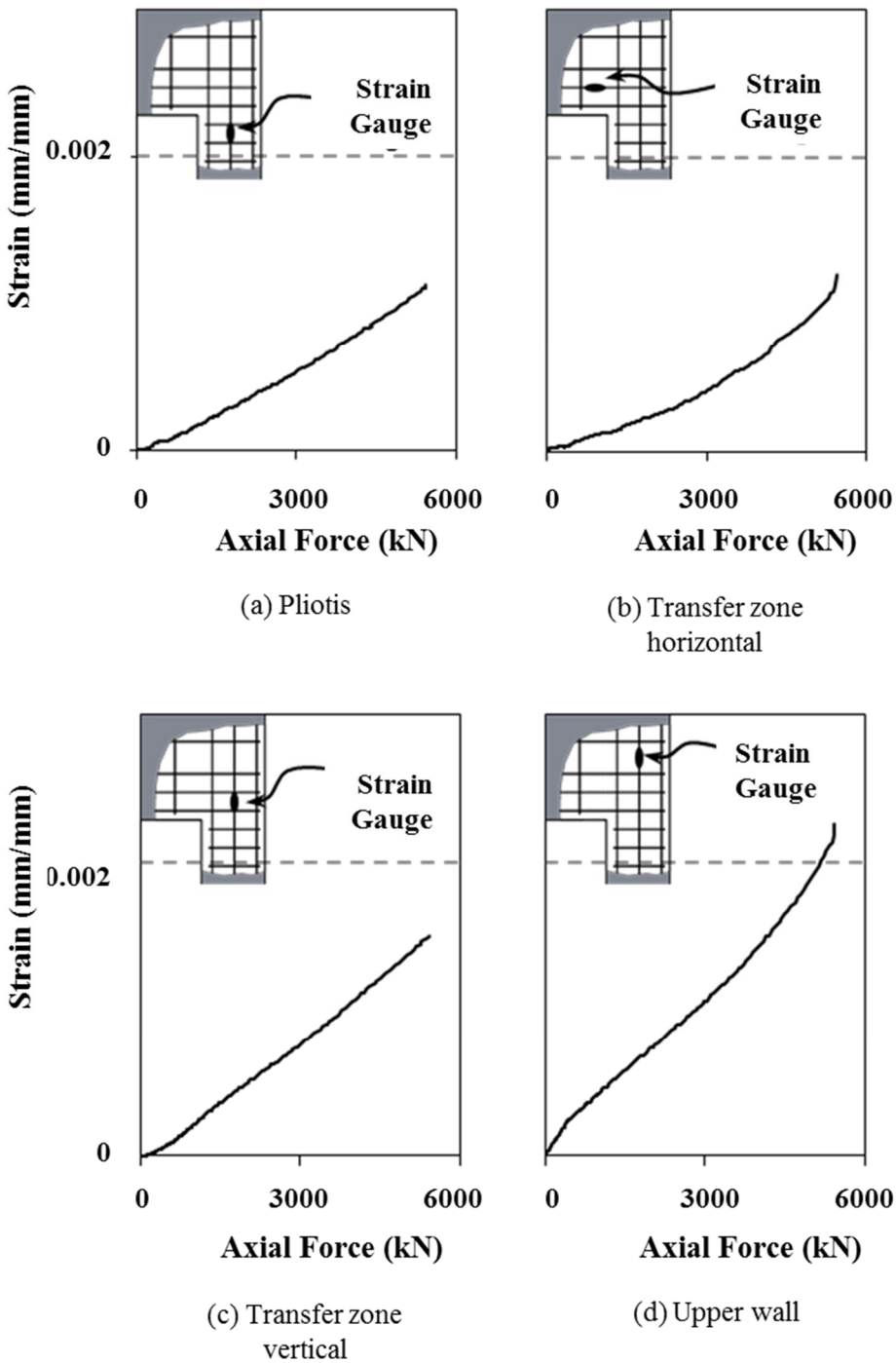

Fig. 4-21 Rebar strains of the specimens under compression

Chapter 5. Conclusion

In this study, for application of capacity design of high-rise residential buildings, following studies were conducted on the issues to be considered.

[1] In the case of capacity design of slender shear wall, to accurately evaluate nonlinear shear demand, shear amplification effect was investigated. Nonlinear analysis modeling were established and nonlinear dynamic analysis was carried out for each modeling. Total five parameters affecting to shear amplification were considered. Parameter 1 was axial force ratio, changing moment capacity of the wall. Parameter 2 was response modification factor, changing shear and moment demand. Parameter 3 was the number of stories designed identically, making the wall in some area over-designed. Parameter 4 was characteristics of selected ground motions, changing effect of higher-order mode. Lastly, parameter 5 was detail of the connection beam, changing transferred load between both walls.

Total 173 data were obtained by analysis. Through the analysis results, the base shear amplification factor was proposed. For normalized data with moment over-strength factor, the linear tendency was obtained. From this tendency, the linear equation for predicting the base shear amplification factor was derived and the regression analysis was carried out to determine the coefficient of the equation. The proposed design equation was able to predict the amplification factor within the error of 20%.

Also, by analyzing the results, story shear distribution model was proposed. Conservative model was determined by average story shear distribution of modeling of 10, 15 and 20 stories. In the proposed model, amplified base shear

should be calculated by the proposed equation. Also, it assumed to have linearly increased shape below relative height of 0.5 and uniform shape above relative height of 0.5.

Both the proposed equation for base shear amplification factor and the model for the story shear distribution are able to be used in process of the capacity design. By the design results of elastic analysis, it is possible to evaluate shear demand with considering nonlinear dynamic behavior of the wall. Through this, the difference between elastic shear demand and dynamic shear demand can be minimized and structural safety of high-rise residential building can be secured for large earthquakes.

[2] In the case of capacity design of pilotis-wall system, to design pilotis and transfer zone economically and safely, a new system without transfer girder and design method based on concept of capacity design was proposed. The structural behavior of the proposed system and the design method for the system were verified by cyclic loading tests and compression test.

Proposed system was designed to prevent premature brittle failure in the transfer zone and to be governed by ductile failure of upper wall above the transfer zone. To prevent premature brittle failure of connection joint, the wall and the pilotis were designed to resist more loads than the upper wall.

Assumed that upper wall yields, coupled force, generated in both edge of the wall, was able to be calculated by flexural capacity of the wall. By net force of coupled force and vertical force by gravity load, compressive force was generated in one edge of the wall. To resist this force, critical section was designed. Otherwise, in the other edge, by the net force, tensile force was generated. The

upper wall was designed to resist the tensile force. In the case of the wall in the transfer zone, more vertical re-bars were placed to have more flexural capacity than the upper wall.

In the transfer zone, tie force was generated by the gravity load and lateral load. By using strut-tie model, the tie force was evaluated conservatively. To resist the tie force, horizontal re-bars were placed in this zone.

Three cyclic loading tests and one compression test were conducted for four specimens designed by proposed design method. All of specimens showed greater maximum strength than predicted strength. In the case of all specimens, concrete crushing and buckling of re-bars occurred at the upper wall. On the other hand, in the transfer zone and pilotis, damages were relatively limited. Also, re-bars in the transfer zone and pilotis were in elastic state but those in the upper wall were yielded.

Through these results, in the proposed pilotis-wall system without the transfer girder, it was possible to predict accurately the actual seismic loads. Moreover, by the failure mode intended in the design, the premature failure in the connection joint was able to be prevented for both the gravity load and the lateral load. Through this, proposed system and design method was verified to be able to predict the seismic loads more accurately and secure the structural safety.

In this study, for the capacity design of high-rise residential buildings, studies on the nonlinear shear demand distribution of the slender shear wall and the design of the transfer zone of pilotis-wall system are focused. However, further studies are needed besides the issues included in this study. In addition to the nonlinear shear demand distribution of the slender shear wall, that of the pilotis-wall system should

be determined. Furthermore, from the aspect of overall structural system, change of the nonlinear shear demand distribution due to interaction between two systems should be considered. These issues are expected to be addressed in future studies.

References

[1] ACI Committee 374. (2013). Guided for testing reinforced concrete structural elements under slowly applied simulated seismic loads. American concrete institute

[2] AIK. (2016). Korean Building Code and Commentary. Architectural Institute of Korea.

[3] Blakeley RWG, Cooney RC, Megget LM (1975) Seismic shear loading at flexural capacity in cantilever wall structures. Bull N Z Nat Soc Earthq Eng 8:278–290

[4] Boivin, Y. (2012). New capacity design methods for seismic design of ductile RC shear walls. Université de Sherbrooke.

[5] Booth, E. D. (1994). Concrete structures in earthquake regions: design and analysis. Longman Scientific & Technical; Copublished in the US with J. Wiley.

[6] CEB (1980, 1983, 1985) Model code for seismic design of concrete structures, Bulletin d'Information, Comite Europeen du Beton, No.133, 160, 165 (respectively). Lausanne, Switzerland.

[7] CEN (1988) Eurocode No 8–structures in seismic regions-Design. Part 1 General and building

[8] Eibl J, Keinzel E (1988) Seismic shear forces in RC cantilever shear walls, vol VI. 9th World Conference on Earthquake Engineering, Tokyo

[9] Kwan, A. K. H., & Zhao, Z. Z. (2002). Cyclic behaviour of deep reinforced concrete coupling beams. Proceedings of the Institution of Civil Engineers: Structures and Buildings.

[10] NZS (1982, 1995, 2006) NZS 3101: Part1, Concrete Structures Standard; Part 2. Commentary on the design of concrete structures, New Zealand Standards, Wellington.

[11] Park, R. (1989). Evaluation of ductility of structures and structural assemblages from laboratory testing. Bulletin of the New Zealand National Society for Earthquake Engineering, 22(3), 155-166.

[12] Park, R., & Paulay, T. (1975). Reinforced concrete structures. John Wiley & Sons.

[13] Rutenberg, A. (2013). Seismic shear forces on RC walls: review and bibliography. Bulletin of Earthquake Engineering, 11(5), 1727-1751.

[14] Rutenberg, A., Nsieri, E. (2006). The seismic shear demand in ductile cantilever wall systems and the EC8 provisions. Bulletin of Earthquake Engineering, 4(1), 1-21.

[15] Jang, S. H., Kim, H. C., Hong, W. K. (2001). An Evalutationand Response Anlaysis of a Hybrid Building System by Introductin Haunch at the Transfer Floor. Jorunal of the Earthquake Engineering Society of Korea, 5(1), 63-72.

[16] Chung, Y. I., Yoon, S. H., Hong, W. K., Kim, H. C. (2002). Evaluation of an Effective Load Transfer System Applied to a Simple Model of a Wall Frame Structural System. Jorunal of the Earthquake Engineering Society of Korea, 6(3), 23-29.

초 록

고층주거용건물의 성능설계 과정에서 세장한 벽체와 필로티가 있는 벽체의 설계

김 성 현

서울대학교 건축학과 대학원

국내 지진발생 위험도가 증가됨에 따라 내진설계에 대한 관심이 증대되고 있으며 관련 내진기준의 적용이 강화되고 있다. 기존의 탄성해석에 기반한 내진설계법은 지진하중을 정확히 예측하는 것이 어렵다. 따라서 보다 정확히 지진하중을 평가하고 최적의 설계 결과를 얻기 위해 고층주거용 건물의 내진설계에 성능설계법을 사용할 수 있다. 그러나 국내 고층 주거용 건물에 성능설계법을 적용하기 위해서는 구조시스템적 특성에 의한 몇몇 주의점이 고려되어야 한다. 따라서 본 연구에서는 고층 주거용 건물의 성능설계 적용을 위해 고려되어야할 사항들 중에서 세장한 전단벽 시스템에 대한 요구 전단력 분포 연구와 필로티 구조의 설계에 대한 연구가 선행 되었다.

먼저 세장한 전단벽 시스템에서 성능설계시 발생하는 문제는 설계시 고려한 요구 전단력에 비해 실제 요구 전단력이 크게 증폭된다는 것이었다. 이러한 요구 전단력의 증폭 현상을 설계시 고려하지 않을

경우 부재가 과소 설계되어 지진에 대한 구조 안전성을 확보하기 어려워진다. 따라서 벽체 전단력 증폭 현상을 분석하고 이를 성능설계과정에 반영할 수 있는 설계 요소가 제안되었다.

비선형 해석 수행 프로그램인 Perform 3D를 활용하여 변수별 비선형 해석 모델링을 수립하고 비선형 동적해석을 수행하였다. 해석 결과를 토대로 요구전단력 증폭현상에 영향을 미치는 요인을 변수별로 분석하고 비선형 요구 밑면전단력을 예측하기 위한 밑면 전단력 증폭계수가 제안되었다. 제안된 밑면전단력 증폭계수는 설계 대상 벽체의 밑면 초과강도계수를 기반으로 결정되며, 비선형 밑면 요구전단력을 오차범위 20% 내에서 예측할 수 있었다. 또한 해석결과의 평균 층 전단력 분포를 바탕으로 비선형 요구전단력의 층 전단력 분포가 제안되었다. 제안된 층 전단력 분포 모델은 기존의 유로코드 분포 모델에 비해 보다 경제적으로 비선형 요구 전단력의 수직 분포를 예측 할 수 있었다. 제안된 밑면전단력 증폭계수와 층 전단력 분포 모델은 세장한 전단벽체의 성능설계 과정에서 벽체 비선형 요구전단력을 보다 합리적으로 예측이 가능하고 과소설계를 방지하여 구조 안전성을 확보할 수 있다.

다음으로 필로티-벽 시스템의 성능설계시 고려되어야할 사항은 필로티와 벽체가 연결되는 전이구간에 대한 경제적인 설계방법이다. 이를 위해서 전이보가 제거된 시스템이 제안되었고 이 시스템에 대한 합리적 성능설계방법이 제안되었다. 제안된 시스템에 대해 구조 성능을 평가하고 설계법에 대해 검증하기 위해서 반복가력 하중실험과 중심압축 실험이 수행되었다.

초 록

제안된 전이보 없는 필로티-벽 시스템은 성능설계법의 원리에 의하여 전이구간 벽체와 필로티 접합부의 조기 취성파괴를 방지하고 전이구간 상부벽체에서 연성파괴가 유도되도록 설계되었다. 실험 결과 의도한 파괴 메커니즘 대로 모든 실험체에서 접합부의 조기 취성파괴가 발생하는 대신, 전이구간 상부벽체에서 인장측 철근은 항복하고 압축측에서 압괴가 발생하며 파괴 되었다. 전이구간 벽체와 필로티의 내외부적 손상은 상대적으로 제한적이었다. 이를 통해 제안된 시스템 및 성능설계법은 필로티-벽 시스템을 보다 경제적으로 구현할 수 있음이 확인되었다.

주요어 : 성능설계, 세장한 전단벽 시스템, 필로티-벽 시스템

학 번 : 2015-21099